IMPINGEMENT HEAT TRANSFER ON A ROTATING CYLINDER - AN EXPERIMENTAL STUDY OF CALENDER COOLING

by

Lorraine Pelletier

A thesis submitted to the Faculty of Graduate Studies and Research in partial fulfilment of the requirements for the degree of Master of Engineering

Chemical Engineering Department
McGill University
Montréal, P.Q.
Canada

© March 1984

to Addie

ABSTRACT

The effect of air nozzle position on local and average heat transfer rates for a row of round jets impinging on a rotating cylinder was investigated experimentally. The cylinder was the middle roll of a vertical stack of three rotating rolls, each 457 mm in diameter, which simulated a paper machine calender stack. Industrial calender cooling nozzles, having an inside diameter d = 25 mm were used. Air was blown from these nozzles at a velocity of 70 m/s, equivalent to a Reynolds number of 110,000 ± 10,000. Both heating ($21 \leq \Delta T \leq 25$) and cooling ($10 \leq \Delta T \leq 15$) were studied.

Circumferential Nusselt number profiles passing through the stagnation point were obtained with a nozzle-to-nozzle spacing of 8d, for nozzle-to-roll spacing ranging from 1 to 8d, for various nozzle locations around the circumference of the roll, and for nozzles inclined -45° to 45° from the normal to the roll surface. Circumferential profiles at axial positions away from the stagnation point were measured with nozzle-to-roll spacing of 4d, for nozzle-to-nozzle spacings of 4 and 8d.

Local heat flux values were obtained by measuring the local roll surface temperature and solving the one-dimensional unsteady state heat conduction equation.

The major influences on the heat transfer coefficients were the temperature of the ambient air, the nozzle-to-roll spacing and the nozzle-to-nozzle spacing. Location of the

nozzles around the circumference of the roll and inclination of the nozzles with respect to the roll surface had only minor influences on the heat transfer coefficients.

RESUME

On a conçu une experience en laboratoire dans le but d'étudier l'effet de la position de jets d'air sur les taux de transfert de chaleur pour une rangée de buses a section circulaire soufflant sur un cylindre en rotation. Ce cylindre occupait la position intermédiaire dans une calandre à trois rouleaux, simulant ainsi une lisse continue. Chaque rouleau avait un diametre de 457 mm. Des buses disponibles commercialement, de diametre interne d = 25 mm, ont été utilisées. L'air était soufflé à une vitesse de 70 m/s, pour un nombre de Reynolds équivalent à 110,000 ± 10,000. Les effets de jets d'air chaud ($21 \leq \Delta T \leq 25$) et froid ($10 \leq \Delta T \leq 15$) ont été etudiés.

Des courbes du nombre de Nusselt passant par le point de stagnation ont été obtenues sur la circonférence avec des distances inter-buses de 8d pour les configurations suivantes: des distances buse-rouleau s'échelonnant de 1d a 8d, diverses positions des buses autour du rouleau, et, des inclinaisons de buses de -45° a 45° par rapport à la normale de la surface du rouleau. Des profils sur la circonférence, mais a l'écart du point de stagnation, ont été mesurés avec des distances buse-rouleau égales à 4d, pour des distances inter-buses de 4d et 8d.

On a obtenu des valeurs de flux localisés de chaleur en mesurant la température de surface du rouleau et en solutionnant l'équation de conduction de chaleur à une dimension en regime transitoire.

Les facteurs qui ont le plus influencé les coefficients de transfert de chaleur sont la température de l'air ambiant, la distance buse-rouleau et la distance inter-buse. La position des buses autour du rouleau ainsi que leur inclinaison par rapport à la surface n'ont eu que peu d'effet sur ces coefficients.

ACKNOWLEDGEMENTS

To begin with, I would like to express my heartfelt thanks to Dr. R.H. Crotogino for his apparently limitless reserves of patience and his continuous encouragement. His friendship made the difficult periods of this study more pleasant.

I would also like to thank Dr. W.J.M. Douglas for his constructive advice and financial support in the course of this work.

I am grateful to Drs. A.S. Mujumdar and A.R.P. van Heiningen for many useful discussions throughout this project.

Special thanks must go to Bing, Osman, and Suna for their friendship and their assistance which made the completion of this work possible.

Furthermore, I would like to express my gratitude to the many individuals who participated in the construction of my equipment; in particular, Messrs. R.J. Stone, D.P.W. Pounds, A. Krish, H. Alexander, A. Gagnon, W. Greenland, N. Habib and J. Dumont.

A special note of appreciation goes to Dr. Shih for the fabrication of the heat flux sensor which was, to a large extent, responsible for the success of this project.

I would like to acknowledge the assistance of the staff of the computer facilities at PPRIC and DATAC. The receipt of a PPRIC scholarship is also gratefully

acknowledged.

To my colleagues in the department of chemical engineering, especially Tony, I extend my thanks for making my days in the department very enjoyable.

TABLE OF CONTENTS

page

CHAPTER 3. EQUIPMENT AND PROCEDURE

CHAPTER 4. RESULTS AND DISCUSSION

LIST OF FIGURES AND TABLES

page

NOMENCLATURE

A	sensitivity, volt/°C
Cp	heat capacity, J/kg K
d	nozzle diameter, mm
d	film thickness, mm (Equation 3.2)
D	roll or cylinder diameter, mm
f	fractional open area
Fo	Fourier number
h	heat transfer coefficient, W/m^2K
H	nozzle-to-roll distance, mm
k	thermal conductivity, W/mK
L	length of gold film pattern, mm
M_{vs}	mass velocity ratio
n	number of finite difference layers
Nu	local Nusselt number
$\overline{Nu}$	average Nusselt number
Nu_{max}	maximum Nusselt number
Nu_o	stagnation point Nusselt number
P_B	barometric pressure, mm of Hg
P_{sj}	static pressure, mm of H_2O
q	heat flux, W/m^2
q_{sm}	maximum self-heating heat flux, W/m^2
r	lateral extent of stagnation region, mm
R_o	resistance of heat flux sensor at 0°C, ohms
R_s	resistance of heat flux at surface temperature, ohms
R_v	variable resistance, ohms

Re	jet Reynolds number
S	nozzle-to-nozzle spacing, mm
Sh	Sherwood number
t	time, s
Δt	time step, s
T	temperature, °C
$\bar{T}$	average temperature, °C
T_A	ambient air temperature, °C
T_j	jet temperature, °C
T_s	surface temperature, °C
ΔT_C	temperature driving force for cooling jets, °C
ΔT_H	temperature driving force for heating jets, °C
ΔT_s	change in surface temperature, °C
u'	velocity fluctuations, m/s
U_{jY}	jet velocity, m/s
U_{jo}	velocity of jet at centreline, m/s
v	voltage drop over the sensor in Wheatstone bridge, volts
V	fluctuating bridge voltage, volts
V_d	digital voltage, volts
V_s	roll or cylinder speed, m/s
ΔV	voltage change, volts
ΔV_d	digitized voltage change, volts
w	width of two-dimensional jet, mm
W	width of gold film strip, mm
x	axial position, mm
z	distance, mm
Δz	thickness of layer, mm

y	circumferential distance from stagnation point, mm
y_o	height of stagnation point region, mm
z	penetration depth, mm

Greek Letters

α	thermal diffusivity, m^2/s
a	coefficient of heat flux sensor calibration (Equation 3.3)
α_t	temperature coefficient of resistance, °C
b	coefficient of heat flux sensor calibration (Equation 3.3)
δ_f	resistivity, ohm-mm
θ	circumferential position or angle, °
μ_j	viscosity of air at jet temperature, kg/ms
ρ	density, kg/m^3
ρ_j	density of air at jet temperature, kg/m^3
ρ_s	density of air at surface temperature, kg/m^3
ϕ	deflection angle, °

subscript

C	cooling jets
H	heating jets
i	interface
s	back of sensor
o	sensor surface
t	time t
1	first layer of substrate

1. INTRODUCTION

1.1 Background

The papermaking process is illustrated in Figure 1.1.1. It consists of 4 basic operations; a) formation and drainage, where the fibre suspension issuing from the headbox is deposited on a moving screen (foudrinier) and the water is removed by gravity and suction b) pressing, to remove further water and to consolidate the sheet c) drying, to evaporate the remaining water and d) calendering, to reduce the paper thickness and roughness, and to produce a sheet of uniform thickness across the width of the paper.

Calendering reduces the thickness of paper by pressing during passage through the nips between cast iron rolls. A calender stack typically consists of 2 to 8 rolls stacked vertically as shown in Figure 1.1.2, with roll diameter ranging from 300 to 800 mm. The paper enters the top nip and proceeds through each nip down the stack. Paper machines may have one or two such calender stacks.

According to Crotogino (1982), the main factors involved in thickness and roughness reduction in a calender stack are nip load, roll diameter, machine speed, and the temperature, moisture content and initial bulk (inverse of apparent density) of the paper. Of these, the two most important parameters are nip load and paper temperature, in that they have the strongest effect on thickness reduction, can be manipulated readily on a modern calender, and can be

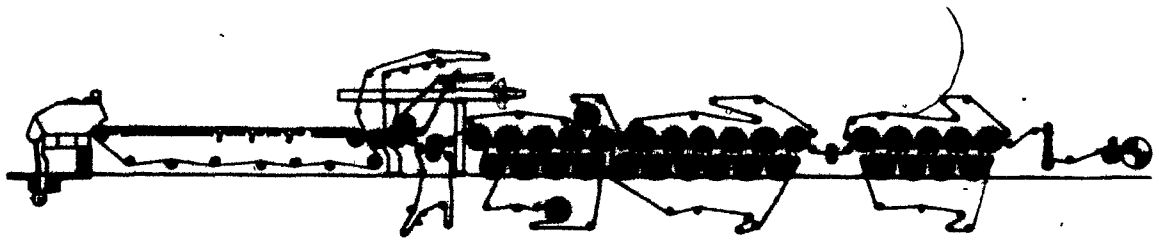

Figure 1.1.1 Schematic of a typical paper machine.

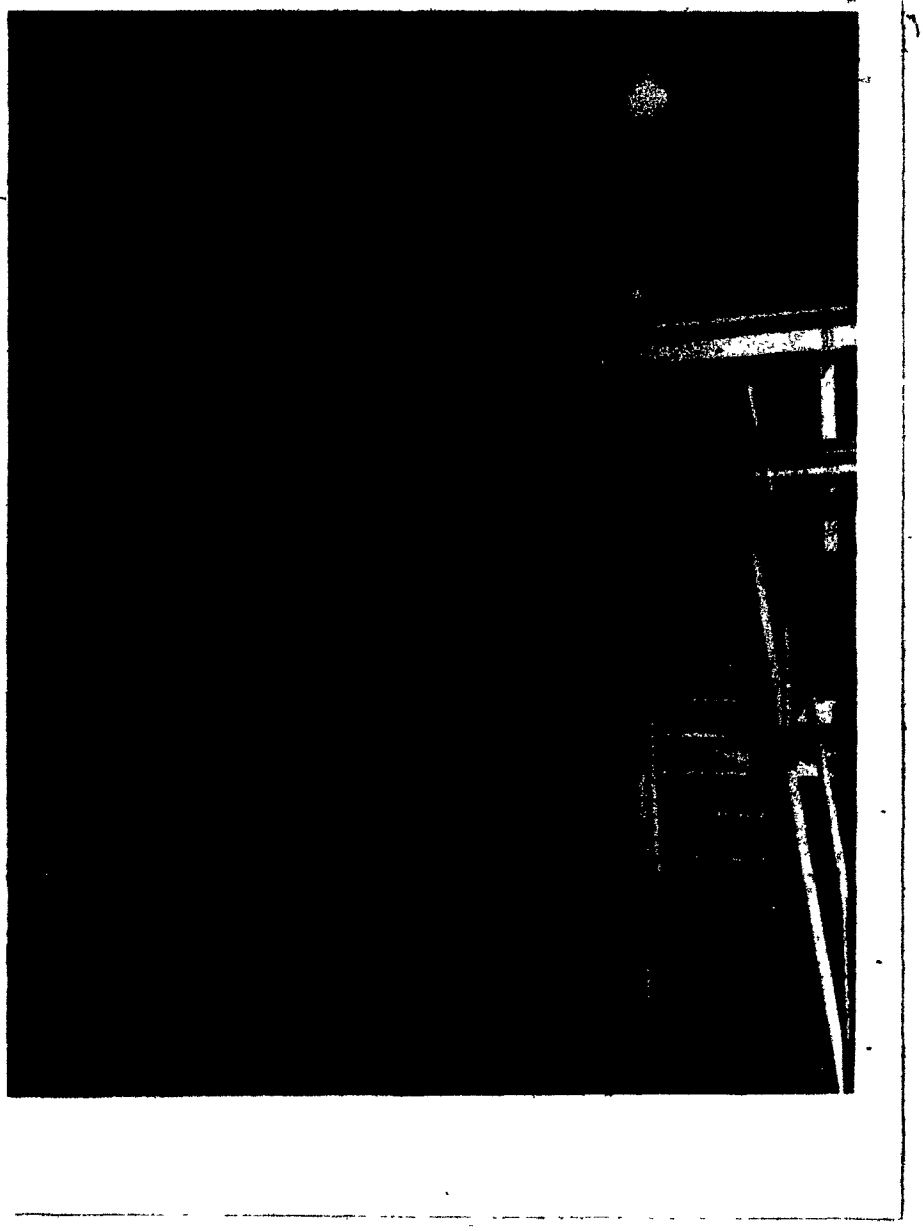

Figure 1.1.2 Calender stack in a paper machine.

used to control the thickness uniformity across the width of the paper machine. When the nip load is increased, the paper is pressed more, thus becoming thinner. When the paper temperature is increased, the paper becomes more plyable, hence easier to calender.

The cross-machine variations in basis weight (weight per unit area), moisture content and temperature of the paper entering the calender will affect the thickness uniformity of the paper across the width of the paper machine. The deflection of the rolls and the grinding tolerance on the roll, i.e. the cross-machine variation in roll diameter will also affect the thickness uniformity of the paper. The roll grinding and external load distribution directly affect the nip load distribution and thus the paper thickness. Paper temperature and paper moisture content affect the cross-machine variation in temperature of the calender rolls, causing small variations in roll diameter, which in turn affects the cross-machine distribution of nip load. For example, a hot streak in the paper entering the calender stack will cause the rolls to heat up and expand over the width of the streak. Consequently the nip pressure in the region of the streak will be increased, causing the paper thickness to be reduced excessively.

To appreciate the order of magnitude of the variations involved, let us consider a typical newsprint machine. The paper entering a newsprint calender may have a thickness of 150 μm. In the last nip of the calender, the paper may have

a thickness of approximately 50 μm, for which the desired tolerance is 1±μm. The calender rolls on the other hand may be 500 mm in diameter or 10,000 times the thickness of the paper and 500,000 times the desired tolerance for the paper. Such tolerances are difficult to maintain when roll temperatures may vary by as much as 10°C along the roll. Hence some means are required to compensate for non-uniformities in the paper and in the calender rolls.

It is customary to control roll temperature and consequently local nip pressure in a paper machine calender with an array of impinging jets of air. Such air showers are generally applied to cool the roll where it is necessary to increase the thickness of the paper. As cold air cools and shrinks the roll, the nip pressure is relieved at that point. At locations where thinner paper is required, the rolls can be heated with hot air showers or by applying friction pads, causing the reverse effects of those just noted.

The air showers used to control calender roll temperature usually consist of a row of nozzles, equidistantly spaced across the width of the calender, as illustrated in Figure 1.1.3. Usually two rows of nozzles, directed at different rolls in the stack, are used. The geometry of the nozzles, nozzle-to-nozzle spacing, nozzle-to-roll spacing, orientation of the nozzles to the rolls and location of the nozzles in the calender vary substantially between machines. Four configurations of

Figure 1.1.3 Industrial calender control air nozzles.
(a) 12 mm nozzle diameter

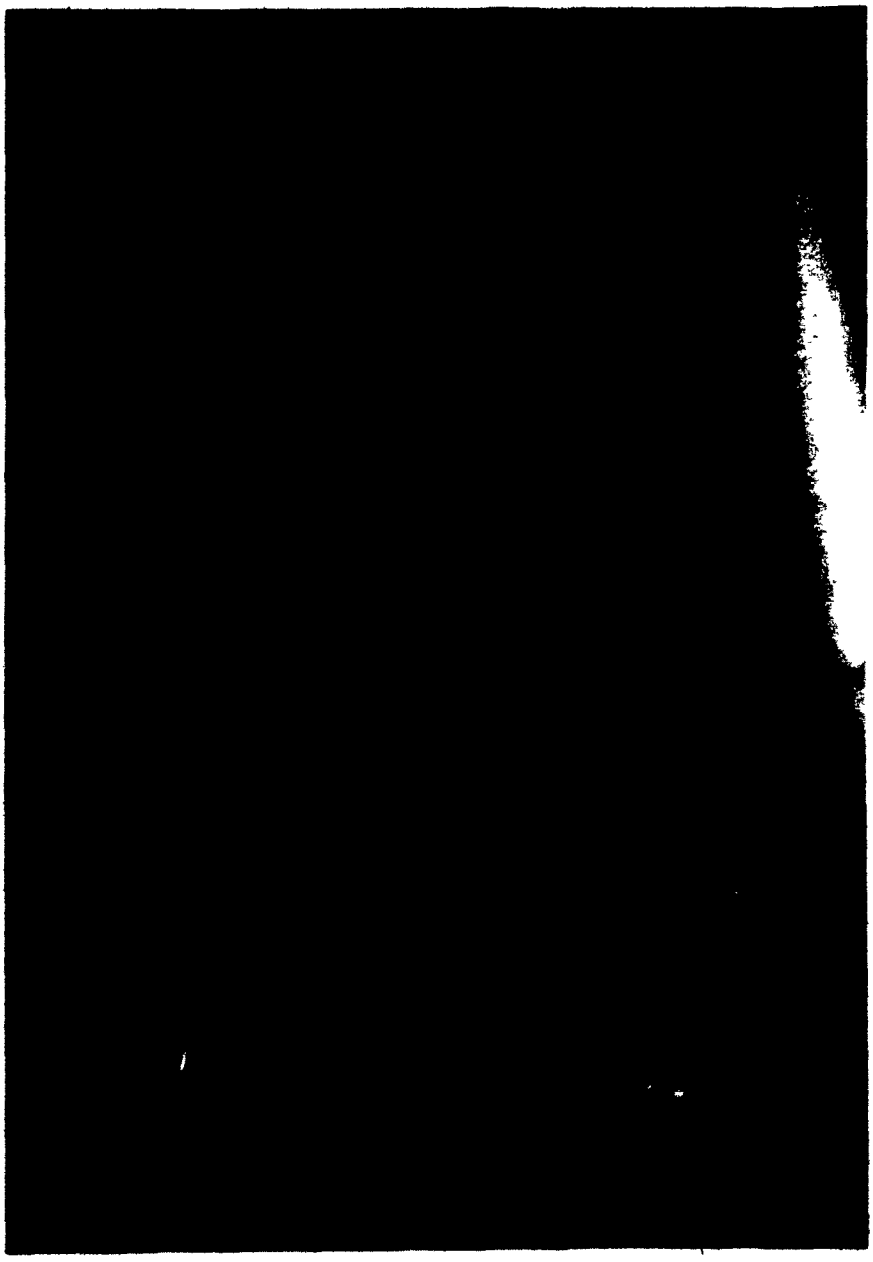

Figure 1.1.3 (b) 25 μm nozzle diameter

Figure 1.1.3 (c) 12 x 50 mm rectangular nozzle

Figure 1.1.3 (d) **Shower-head nozzle**

nozzles currently used industrially are shown in Figure 1.1.3. In Figure 1.1.3a), nozzle diameter is approximately 12 mm and the nozzle-to-nozzle spacing as well as nozzle-to-roll spacing are 100 mm. The nozzles in Figure 1.1.3b) are 25 mm in diameter, are spaced 200 mm apart and 25 mm from the roll. In Figure 1.1.3c), 12 x 50 mm horizontal rectangular slot nozzles are placed with a 25 mm nozzle-to-roll spacing and a 100 mm nozzle-to-nozzle spacing. The nozzles shown in Figure 1.1.3d) are of a shower-head variety, consisting of an array of small orifices.

1.2 Objectives and scope of the study

The heat transfer characteristics of various possible nozzle arrangements is an essential element in the design and choice of an optimum calender cooling system. Unfortunately, however, there are few published data available about the heat transfer characteristics of the nozzle arrangements, which might aid in the design or choice of such systems. The need for a rational design procedure for calender control air showers provided the stimulus for the present study.

The major objectives of this study were a) to construct a facility for the measurement of the heat transfer rates from air jets impinging on a calender roll and b) to investigate how these heat transfer rates are affected by the position of the nozzles relative to the roll and to other nozzles. To achieve these objectives, a major new experimental facility was built, consisting of a model calender stack and calender control air system.

In this exploratory study, measurements were made for one type of nozzle, the type supplied by Midland Ross Canada Ltd. with their calender control systems. These nozzles,shown in Figure 1.1.3b) are essentially long tubes.

Since the main thrust of this study was to investigate the effect of nozzle position on heat transfer rates, the effects of nozzle exit velocity on heat transfer rates were not studied. Only one nozzle exit velocity (70 m/s) was used, corresponding to Reynolds numbers of 100,000 to

120,000.

The position of a nozzle relative to the calender roll is described by three parameters as shown in Figure 1.2.1. These parameters are

θ - circumferential angle

ϕ - deflection angle

H - nozzle-to-roll spacing

The effect of each parameter on the heat transfer rates was determined by varying each parameter independently from a neutral position.

The position of a nozzle relative to other nozzles is described by the nozzle-to-nozzle spacing, S. Two nozzle-to-nozzle spacings were used and the heat transfer rates were measured at several axial locations, x, between adjacent nozzles.

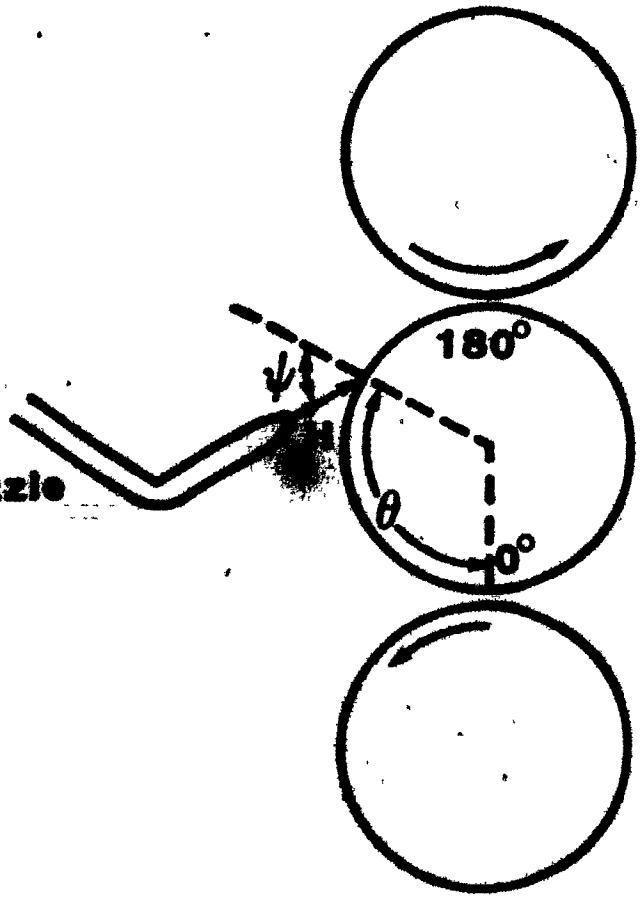

H - nozzle-to-roll spacing

θ - circumferential angle

ψ - deflection angle

Figure 1.2.1 Position of a nozzle relative to a calender roll.

2. LITERATURE REVIEW

2.1 Calender Cooling Literature

Published theoretical or experimental work which relates directly to the calender cooling problem is very limited. Several discussion papers have been published, which speculate about the best position in a calender to place air nozzles. Few measurements made on calenders have been reported in the open literature, and these measurements cannot readily be generalized.

Lyne et al. (1976) performed empirical studies on a pilot machine calender roll to determine the relationship between surface temperature and roll radius changes. For a change in roll surface temperature of 1°C they measured a roll radius change of 1.4 μm on a 0.5 m diameter solid roll. This effect was achieved with two different types of nozzles (a 125 x 8 mm rectangular nozzle and a 15 mm diameter circular nozzle) and with a variety of nozzle-to-roll spacings, air velocities, air temperatures and contact times. Measurements made on the 1000 mm diameter king (bottom) roll of a commercial newsprint calender showed that a 1.5°C change in roll surface temperatues caused a 1.5 μm change in web thickness. Lyne et. al., (1976) concluded, as did Mitchell and Sheahan (1978), that the king roll was the most effective location for the air showers.

Performing experiments on a modern newsprint machine, Mitchell and Sheahan (1978) investigated the effect of

calender stack cooling air showers on calender roll temperature profiles. The effects of nozzle design and position, were measured. They reported that;

a) air showers are more effective as the distance between the jet and the roll is reduced,

b) the effectiveness of air showers applied to the bottom roll was greater than that for air showers on the third roll,

and c) plain nozzles were twice as effective as the multi-orifice nozzles with the same total flow area.

Kaheun et al. (July 1965) found that cooling air applied to the paper web entering the calender is more effective and gives a more rapid response than air applied to the calender rolls. They speculated that the heat transfer efficiency to the web was greater than to the roll and that the cool web was able to change the temperature of several rolls in the calender.

Fjeld et al. (1984) also discussed the optimum location of profiling nozzles in a calender. Based on undisclosed theoretical considerations they recommended that the air should be directed onto calender rolls in the top of the stack, where the greatest thickness reduction takes place.

Bryan (1972) considered the air flows generated by the calender roll as illustrated in Figure 2.1.1. He concluded that in order to get the most effective heat transfer to the

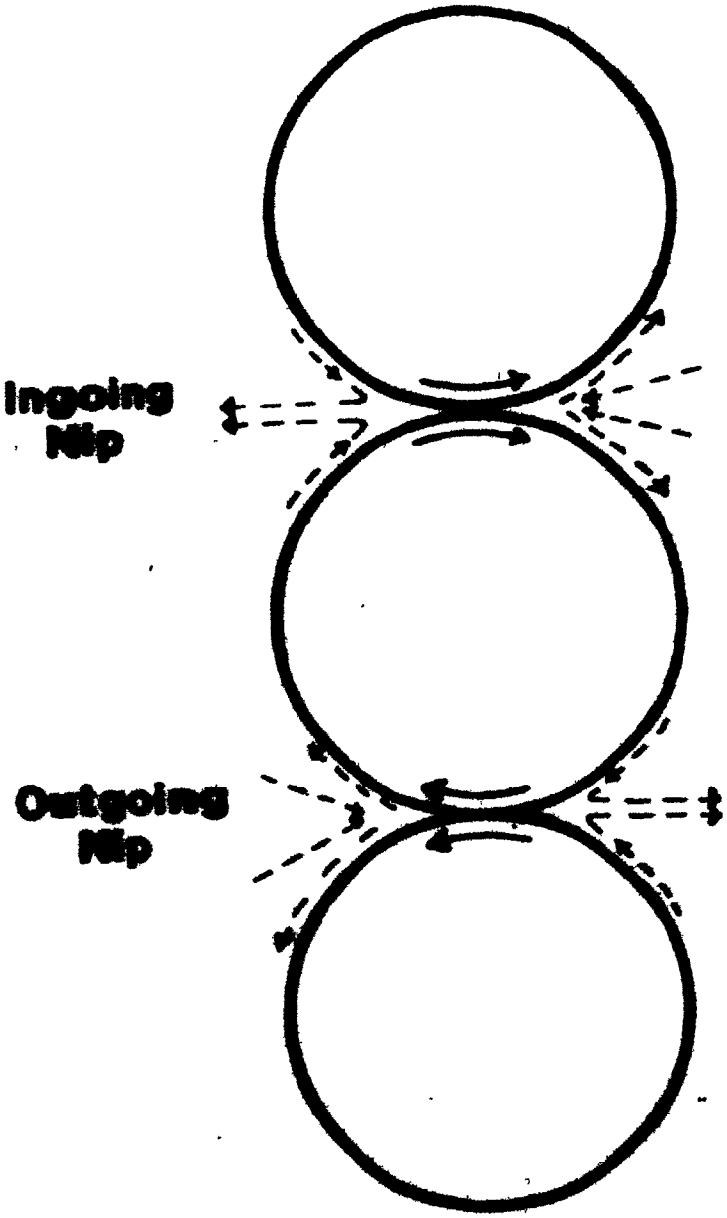

Figure 2.1.1 Air currents around a calender stack.

roll from the air showers, it is necessary to break up the boundary layer carried by the roll. The velocity of the jet necessary to break up this boundary layer depends highly on the position of the nozzle with respect to the roll. The most effective location for the nozzles, according to Bryan, would be to direct them into the low pressure zone at the out-going nip. However, no evidence was presented to support his reasoning.

The limited published work about calender cooling does not provide any consistent information on which one might wish to base the design of a calender control system. The few measurements which have been published, cannot readily be generalized and extrapolated to other calender configurations. The discussions about optimum nozzle position in the calender and relative to the rolls are speculative and contradictory.

2.2 Impinging Jet Literature

Whereas the pulp and paper literature dealing specifically with the calender control problem is very limited, the literature dealing with the more fundamental problem of impingement heat transfer is quite extensive. General reviews of the impingement heat transfer literature have been presented recently by Obot (1980) and Saad (1981). The present review will deal only with the work which is directly relevant to the problem of calender cooling.

Figure 2.2.1 illustrates the flow characteristics of a jet issuing from a circular nozzle and impinging on a flat plate. Poreh and Cermak (1959) divided the flow into three distinct regions, namely the free jet region, the impingement or stagnation region, and the wall jet region.

The free jet region can be subdivided further into the potential core, the developing or transition region, and the region of the developed jet.

The potential core is a region in the jet, where the centreline velocity remains unchanged from that at the nozzle exit. It originates as a core of undisturbed fluid inside the jet, when this flow is not fully developed. Upon leaving the nozzle, this core is not immediately affected by the new boundary conditions. When the flow inside the nozzle is fully developed, there will be no potential core nor a transition region.

The potential core length is an important factor for heat transfer since the stagnation point heat transfer rates tend to reach a maximum when the nozzle-to-surface spacing corresponds to this length. It is affected by the flow conditions and turbulence inside the nozzle, and therefore by the geometry of the nozzle and the flow channel upstream of the nozzle, and by the Reynolds number. Obot (1980) measured potential core lengths ranging from 4 to 7 nozzle diameters for short and long nozzles with and without contoured inlet sections.

The developed flow region exists only for sufficiently

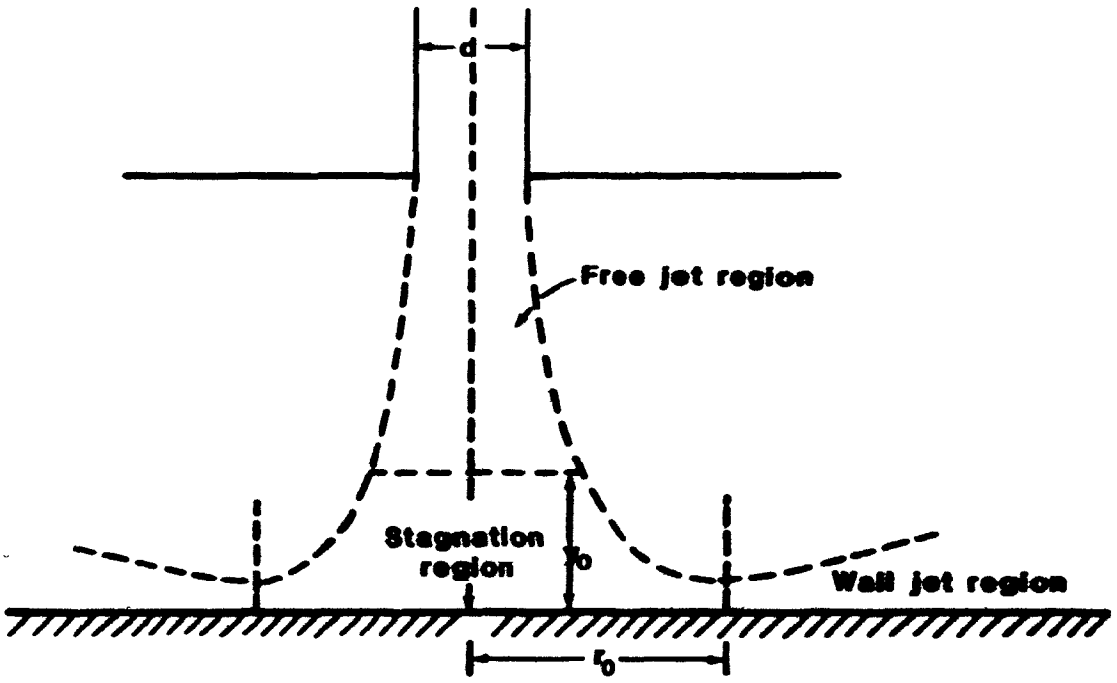

Figure 2.2.1 Axi-symmetric impinging jet.

large nozzle-to-surface spacing. It refers to that part of the free jet in which the centreline velocity is inversely proportional to (z/d). The region beyond the potential core zone where the velocity is no longer constant, but is inversely proportional to (z/d), is referred to as the region of developing flow or the transition region.

At the end of the free jet region, where the flow begins to be affected by the impingement surface, the stagnation region begins. This region extends to the impingement surface and includes the region of diverging flow.

In the stagnation region, the axial velocity decreases sharply, the axial turbulence intensity increases and the pressure increases as the axial velocity component is transformed to a lateral velocity. At the stagnation point, the velocity is zero and the static pressure is at a maximum. The static pressure decreases away from the stagnation point along the lateral direction. This region of strongly negative pressure gradients maintains the boundary layer laminar even for a highly turbulent jet.

The dimensions of the stagnation region were investigated by Obot (1980) and Tani and Komatsu (1966). The height of the stagnation region, y_o, was found by Tani and Komatsu (1966) to be between 1.6 and 2.2 jet diameters, for dimensionless nozzle-to-plate spacings of 4 to 12. The lateral extent of the stagnation region, defined as the distance from the stagnation point where the static pressure

gradients are negligible, has been reported by Tani and Komatsu (1966) to be about 1.6 to 3 jet diameters for the same range of dimensionless nozzle-to-plate spacing.

In the wall jet region, the accelerated stagnation flow transforms to a decelerated wall jet flow with a negligible lateral pressure gradients. The lateral velocity developed in the stagnation region passes through a maximum at the end of the stagnation region. The transition of the boundary layer from laminar to turbulent occurs in the wall jet region. Extensive characterization of the stagnation and wall jet region for an impinging round jet has been given by Obot (1980).

The heat transfer rates for a row of jets impinging on a rotating cylinder can be affected by many geometric and flow parameters such as the nozzle-to-roll spacing, the nozzle-to-nozzle spacing, the jet Reynolds number, the angle of the jets to the roll, the motion of the roll, the curvature of the roll and the streamwise and spanwise distance from the stagnation point. Since a row of round jets consists of several single jets, which may or may not interact, the heat transfer rates of a single round jet are of importance. The factors influencing the heat transfer rates of a single round jet impinging on a flat stationary plate such as the jet Reynolds number, the nozzle-to-plate spacing, the distance away from the stagnation point and the angle of impingement will be investigated.

The effect of nozzle-to-plate spacing on the

stagnation point Nusselt number at two different Reynolds numbers for a turbulent single round jet is illustrated on Figure 2.2.2 with data from Obot (1980). The stagnation point Nusselt number passes through a maximum at a nozzle-to plate spacing of about 7 to 8 diameters. The existence of a maximum stagnation point heat transfer coefficient as a function of H/d has previously been noted by Gardon and coworkers (1962, 1965 and 1966), Nakatogawa et al. (1970), Koopman and Sparrow (1976), amongst others.

Gardon and Akfirat (1965) reported that the maximum in Nu_o as a function of H/d was a result of the velocity profile of the jet and the turbulence level of the jet. The velocity of the jet remains constant throughout the potential core zone but begins to decrease at the end of the potential core zone. The turbulence intensity, on the other hand, increases from the exit of the nozzle to the end of the transition region after which it remains fairly constant. The location at which the decreasing effects of velocity balance the increasing effect of turbulence intensity results in the maximum stagnation Nusselt number. Thus the peak Nu_o coincides with the peak in the absolute magnitude of axial velocity fluctuations, u'/U_{jo}.

The intensity of turbulence at the nozzle exit has a very large effect on Nu_o. By artificially increasing the level of turbulence in the nozzle, Gardon and Akfirat (1965) showed that the stagnation point Nusselt number could be increased almost 100%. This was also shown by Polat et al.

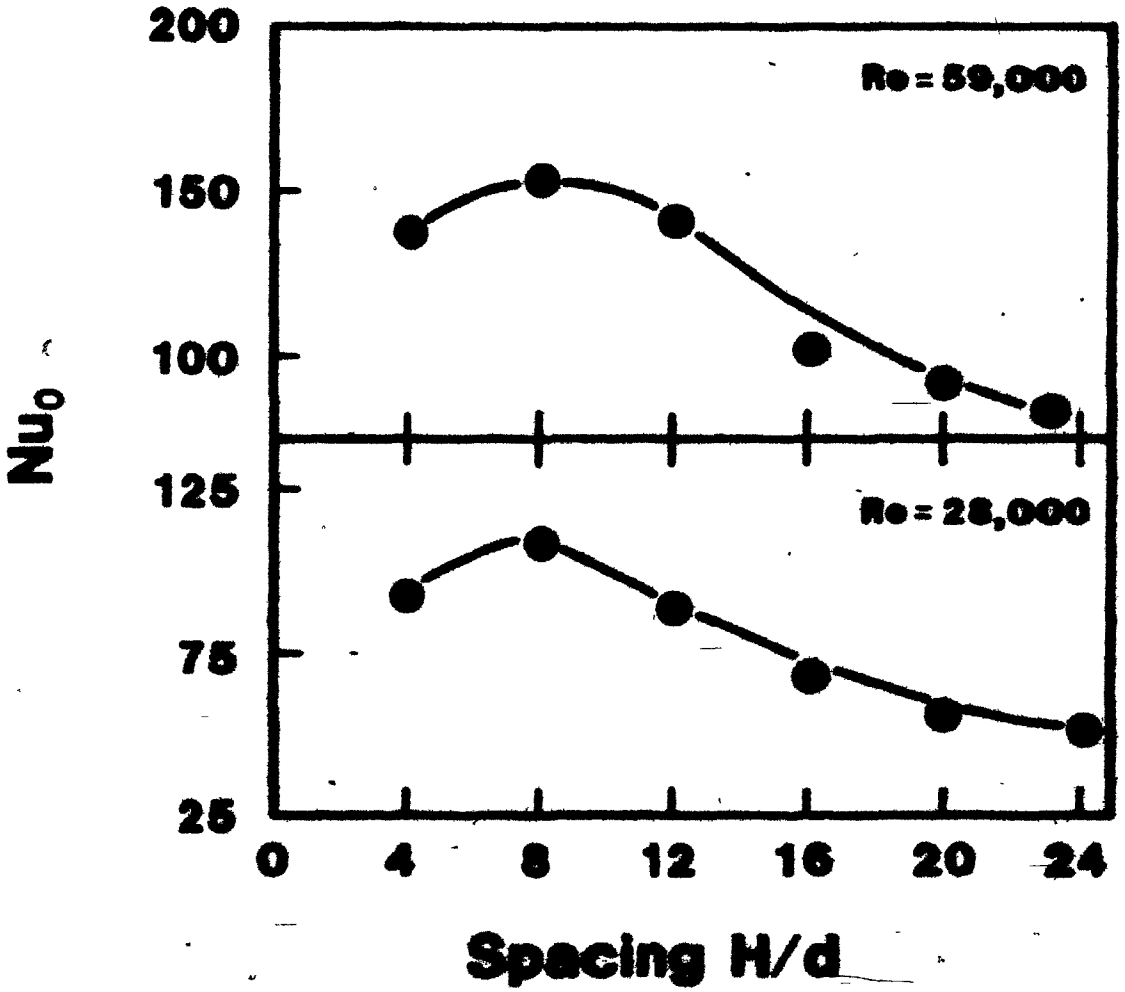

Figure 2.2.2 Effect of nozzle-to-plate spacing on stagnation Nusselt numbers.

(1984). The variation of Nu with H/d at large turbulence levels becomes almost linear, with no evidence of a maximum, because the turbulence increases the Nu_o preferentially at small H/d.

The different levels of turbulence in the jet at the exit of the nozzle may explain the large variations in Nu_o found in literature.

The variation of local Sherwood numbers with distance from the stagnation point is illustrated for a single round jet in Figure 2.2.3 with the data of Schlünder and Gnielinski (1967) for H/d=1.25, 5 and 10. The mass transfer distributions of H/d=1.25 and 5 exhibit a minimum at y/d=1.2 and a secondary maximum at y/d=1.6. These minima and maxima at low nozzle-to-plate spacings are associated with the onset of and the completing of transition from a laminar to a turbulent boundary layer. The combination of a high jet Reynolds number and a low jet spacing produces a negative pressure gradient in the stagnation region, which is sufficiently strong to maintain the boundary layer laminar even for a highly turbulent jet. Beyond the region of steep negative pressure gradient, the onset of boundary layer transition is marked by the minimum at y/d=1.2 while the completion of this transition is marked by the maximum at y/d=1.6.

The effects of Reynolds number on stagnation point Nusselt number and average Nusselt number are illustrated on Figures 2.2.4 and 2.2.5 using the results of various

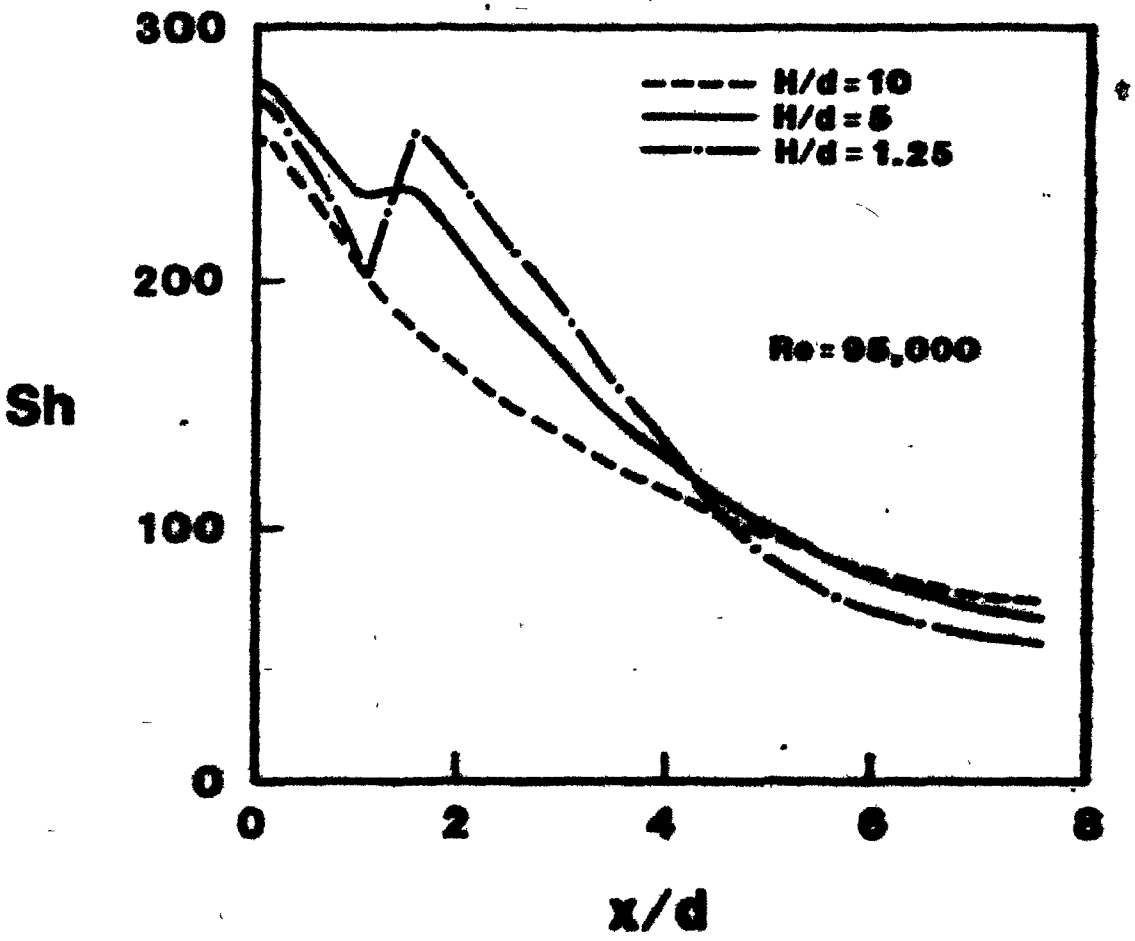

Figure 2.2.3 Effect of nozzle-to-plate spacing on local Sherwood numbers.

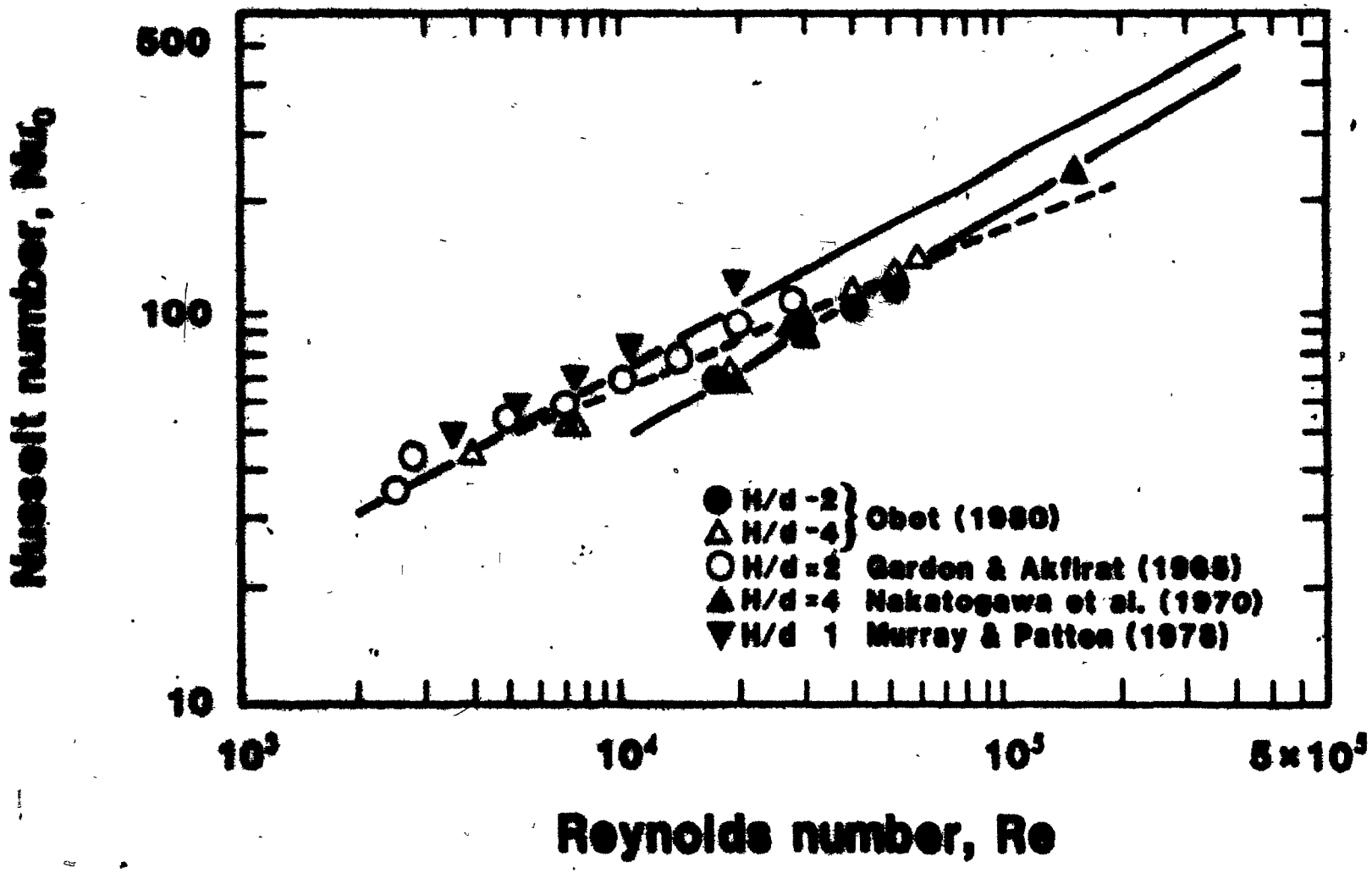

Figure 2.2.4 Effect of Reynolds number on stagnation Nusselt numbers.

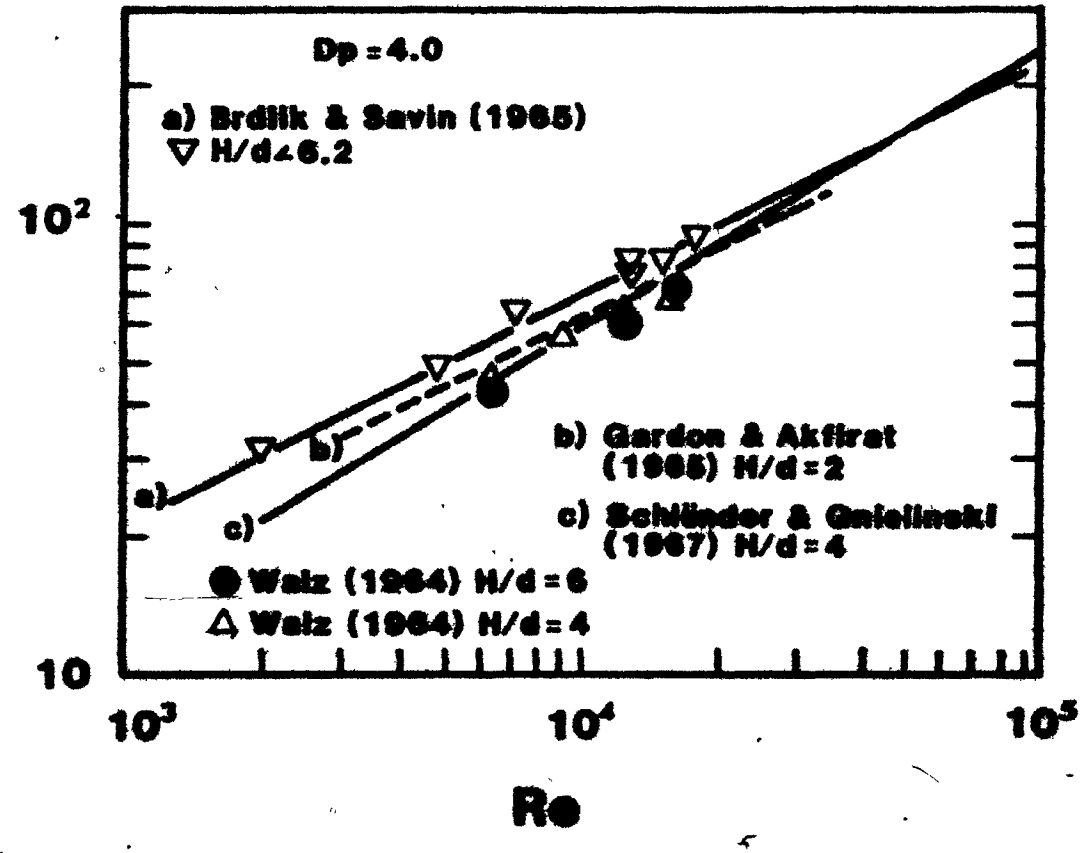

Figure 2.2.5 Effect of Reynolds number on average Nusselt numbers.

workers. The slopes of 0.4 to 0.6 on Figure 2.2.4 are an indication of the laminar character of the boundary layer in the stagnation region even for turbulent jets. The higher slopes of 0.7 to 0.8 for the relationships between the $\overline{Nu}$ and Re on Figure 2.2.5 reflect the fact that beyond some distance from the stagnation point the boundary layer is turbulent, hence in that region the effects of jet Reynolds number on Nusselt number is that normally found for turbulent jets.

Obot (1980) found that the nozzle geometry and length can have significant effects on the local and the average Nusselt numbers. The large differences among the values of heat transfer coefficients found in the literature is attributed by Obot (1980) to be due to the different levels of turbulence arising from the use of different nozzle geometry and inlet configuration.

The influence of the angle between the jet axis and the impingement surface on heat transfer coefficients was studied by Perry (1954) for a single round jet (Figure 2.2.6). The heat transfer coefficients were determined only at the point of intersection between the jet axis and the impingement surface. The impact angle was varied while keeping the nozzle-to-plate spacing constant. The heat transfer coefficients were found to decrease strongly with decreasing impact angle. As the impact angle is decreased from 90° (normal impingement) to 15°, the heat transfer coefficients decreased by 43%.

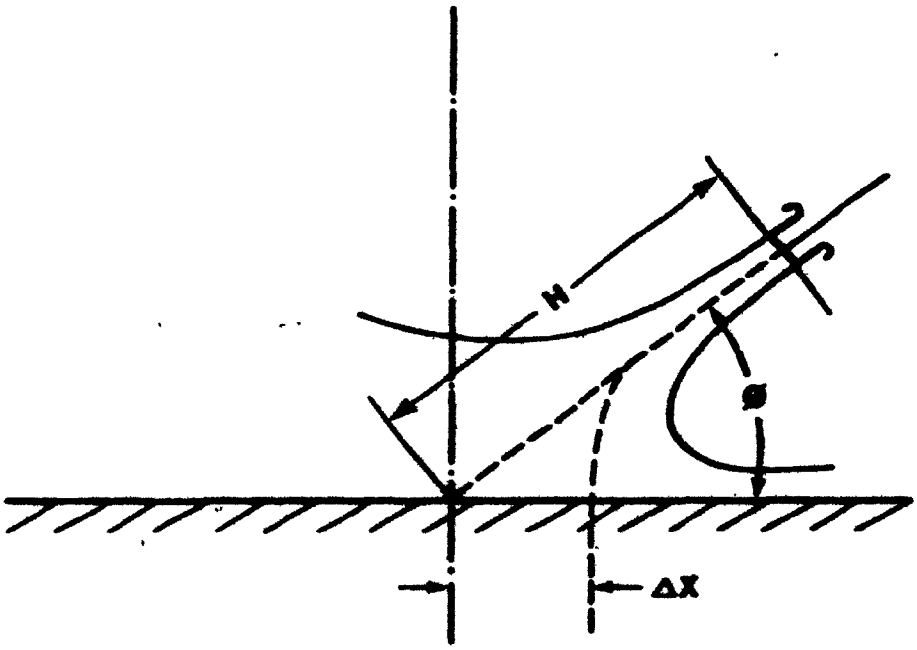

Figure 2.2.6 Inclined impinging jet (schematic).

Korger and Krizek (1972) noted that the stagnation point does not coincide with the point of intersection between the jet axis and the impingement surface but is shifted toward that part of the jet being deflected in the acute angle. The degree by which the stagnation point was shifted is proportional to the nozzle-to-plate spacing and the cosine of the impact angle. The average mass transfer coefficients were found to be practically independent of impact angle for constant nozzle-to-plate spacing for impact angle of 30° to 90°.

Two aspects of the impingement surface are important for industrial applications; the surface motion and the surface curvature. The influence of cylindrical curvature on the impingement characteristics has been studied by Kumada et al. (1972) and Kumada et al. (1976) for a slot jet with a nozzle-to-plate spacing of 2, 8 and 40. The ratio of impingement cylinder diameter, D, to nozzle width, w, was varied from 3.75 to 25. They reported that the stagnation point Nusselt number, Nu_o, was not affected by changes in the ratio of the cylinder diameter to nozzle width, D/w. However for D/w smaller than 15, the off-stagnation Nusselt numbers were affected by the curvature of the cylinder.

By conducting experiments of a slot jet impinging on a moving flat belt, Subba Raju and Schlunder (1977) determined the effect of surface motion on the average heat transfer coefficients. They found that the average heat transfer rates increased significantly with belt speed, attained a

maximum and then remained essentially constant with further increase in belt speed. The average heat transfer rates were about 1.5 to 2.0 times higher than those predicted for impingement on a stationary surface.

The effect of surface motion on the local heat transfer rates for a confined slot jet impinging on a rotating cylinder has been documented by van Heiningen (1982). Figure 2.2.7 shows the effect of surface motion on the Nusselt number distribution from the data of van Heiningen (1982) for a jet Reynolds number of 8200 and a nozzle-to-plate spacing of H/w=6. The surface motion is expressed as a ratio of the surface mass velocity to jet mass velocity, $M_{vs}=\rho_s V_s/\rho_j U_j$.

From Figure 2.2.7, it is evident that the heat transfer increases when the impingement surface motion is in the direction away from the nozzle centreline, while the reverse is the case when the surface motion is in the direction towards the nozzle centreline.

van Heiningen (1982) noted the following general effects of surface motion:

1) An increase in the stagnation heat transfer but no significant displacement.
2) The minimum and secondary maximum are displaced in the direction of the surface motion. The minimum and secondary maximum on the side where the impingement surface is approaching the nozzle disappear into the stagnation heat

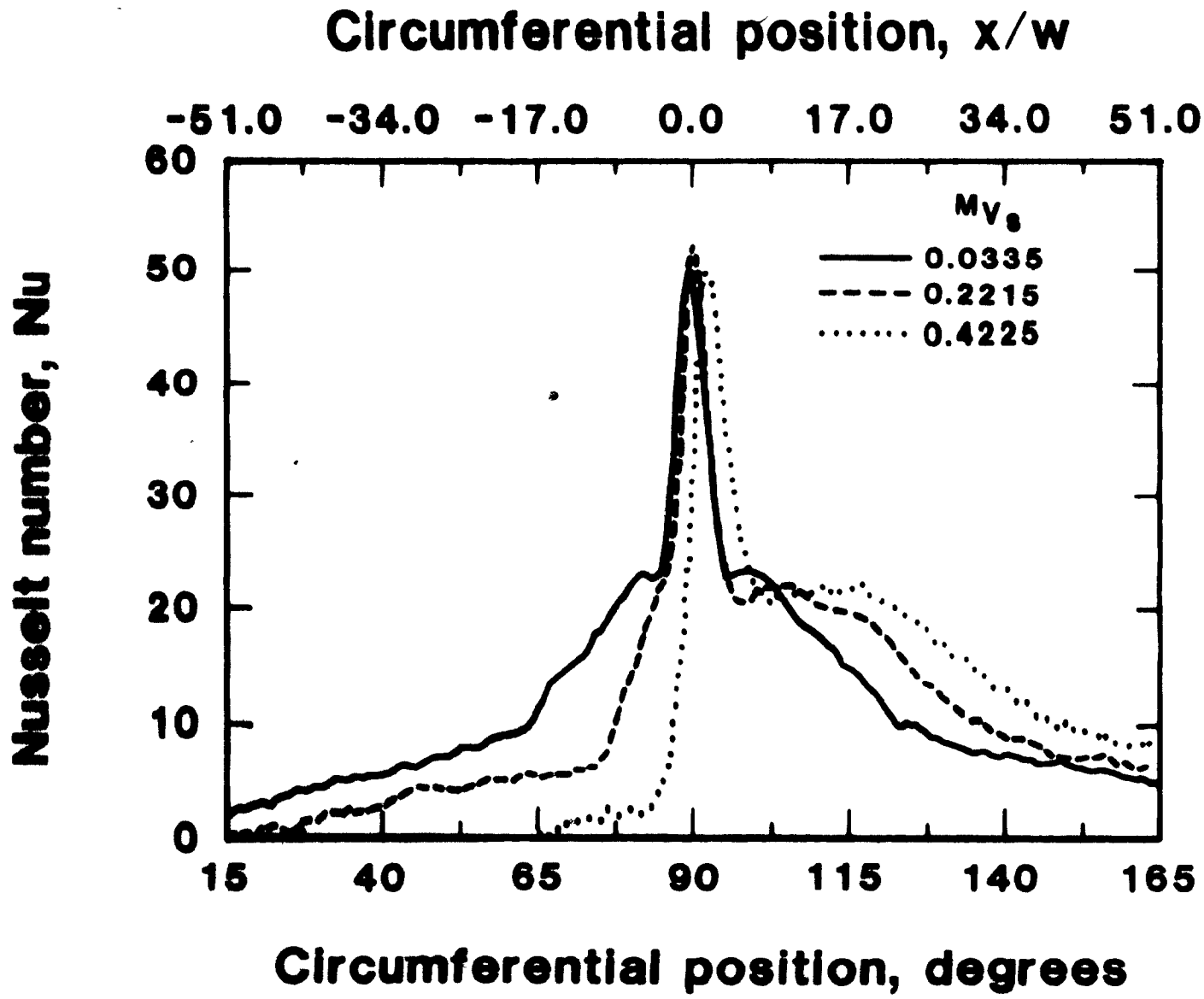

Figure 2.2.7 Effect of M_{Vs} on local Nusselt number distribution at Re = 8200 and H/W = 6.

transfer peak at high values of M_{vs} while the location of the maximum and minimum on the other side is displaced progressively further from the nozzle centreline as M_{vs} is increased.

Average heat transfer coefficients, as measured by van Heiningen (1982) for a confined slot jet decrease with increasing M_{vs}. On the other hand, Fechner (1971) found that increasing the surface motion or M_{vs} produced higher average heat transfer rates for an unconfined slot jet. With Fechner's unconfined jet, more than half the impingement surface was covered by the higher momentum wall jet, which flowed in the same direction as the surface motion. This wall jet region produced higher heat transfer than the one on the opposed side flow.

The local mass transfer coefficients for the impingement of a row of circular jets on a flat stationary surface were determined by Koopman and Sparrow (1976). They investigated two nozzle-to-nozzle spacings of S/d=4 and 6.67, four nozzle-to plate spacings of H/d=2, 4, 7, 10 and four Reynolds numbers ranging from 2500 to 10,000.

The stagnation point transfer coefficients exhibited a maximum at a nozzle-to-plate spacing between 4 and 7 nozzle diameters, for all Reynolds numbers and for both S/d spacings.

The mass transfer coefficient distributions as a function of spanwise distance, x/d, showed a maximum at the location midway between adjacent jets or x/d=S/2. The

presence of this maximum is due to the collision of flows from two impinged adjacent jets. The prominence of this maximum is accentuated at small S/d separations and at larger jet Reynolds numbers.

The distributions of local mass transfer coefficients with y/d showed no off-stagnation peaks except for the low nozzle-to-plate spacing of H/d=2.

The spanwise (x/d) and streamwise (y/d) average transfer coefficients were reported by Koopman and Sparrow (1975) to be higher for the smaller nozzle-to-nozzle spacing of S/d=4 than for the larger spacing of S/d=6.67.

2.3 Conclusion

One important input required for the prediction of the effectiveness of a calender control system is the heat transfer coefficient between the air jets and the calender rolls on which they impinge. The extensive literature on impingement heat transfer has dealt with many of the aspects of this problem. Heat transfer coefficients for single round jets have been studied and information about the effects of nozzle orientation with respect to the surface, surface motion, curved surfaces, and adjacent nozzles have been dealt with to some extent. However, in a calender, all of these elements are combined in one problem. A row of jets impinges on a moving roll, which is confined between two other moving rolls. The question remains as to the extent to which the available information about the

individual effects can be applied when all of these effects are acting simultaneously. The present study was undertaken to answer this question.

3. EQUIPMENT AND PROCEDURE

3.1 Overall Design Concept

An experimental calender stack depicted in Figures 3.1.1 and 3.1.2 and shown schematically in Figure 3.1.3 was built for a study of local and average heat transfer from a row of jets impinging on a calender roll. The equipment, designed to simulate industrial practice as closely as possible, consisted of 3 vertically-stacked rolls, each 457 mm diameter and 810 mm long. This diameter corresponds to roll diameters typical of industrial calenders. Three nozzles, placed on each side of the middle roll, direct cold air onto one side and hot air onto the other side. This arrangement, not typical of industrial practice, was necessary for the measurement technique employed.

The nozzles (Figure 3.1.4) were industrial calender cooling nozzles with an exit diameter of 25 mm. They were provided by Midland Ross of Canada Corp. for this study.

The key parameters of this study are nozzle spacing and nozzle orientation with respect to the middle roll. Orientation of the nozzles about the middle roll was varied by adjusting clamps from which the distribution headers were suspended. The distribution headers were designed in such a way that the spacing between adjacent nozzles could be changed from 100 to 200 mm, i.e. from 4 to 8 nozzle diameters.

Other key parameters, namely rotational speed of the

Figure 3.1.1 Side view of experimental calender stack.

Figure 3.1.2 Front view of experimental calender stack.

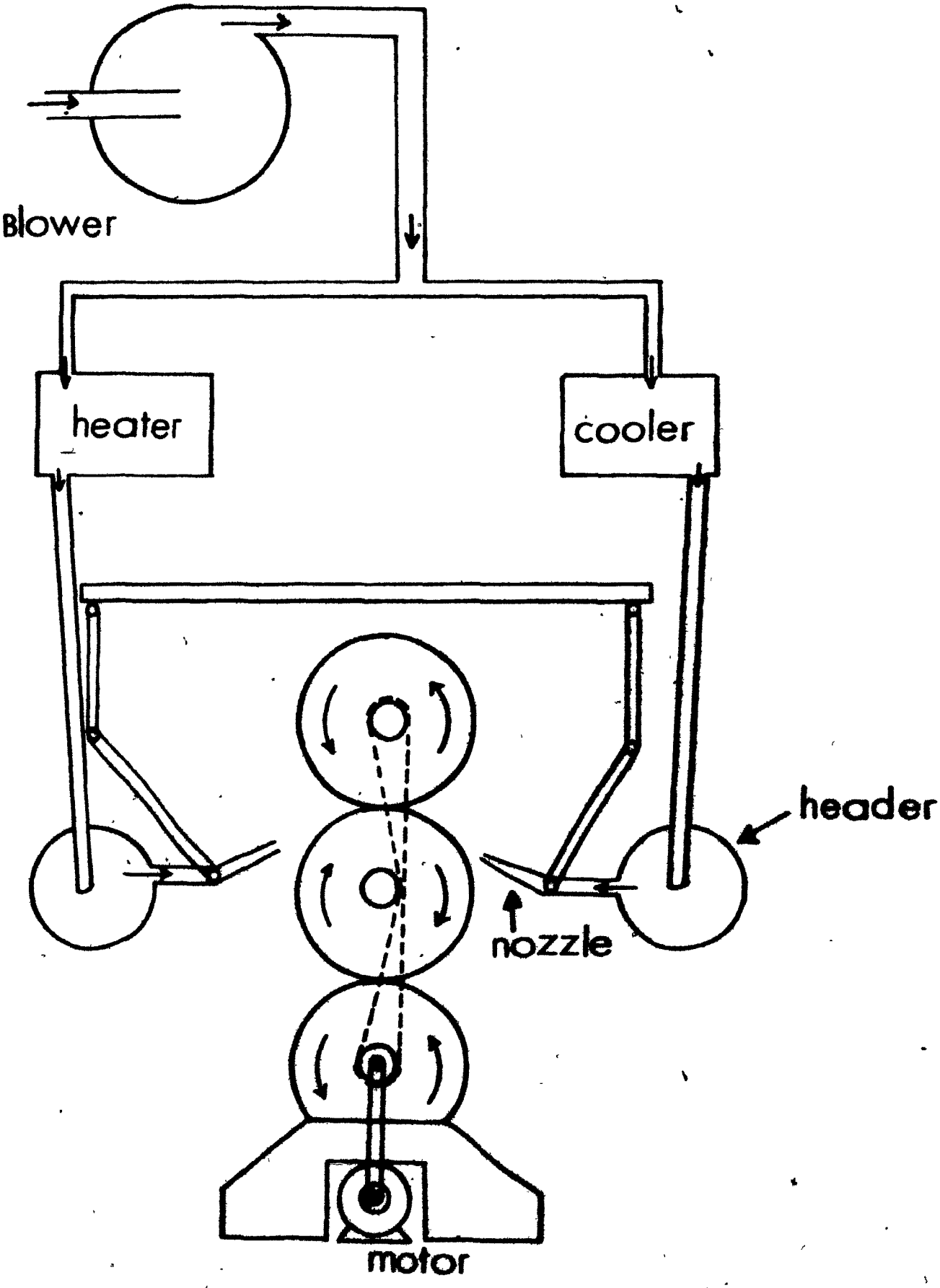

Figure 3.1.3 Schematic of experimental calender stand.

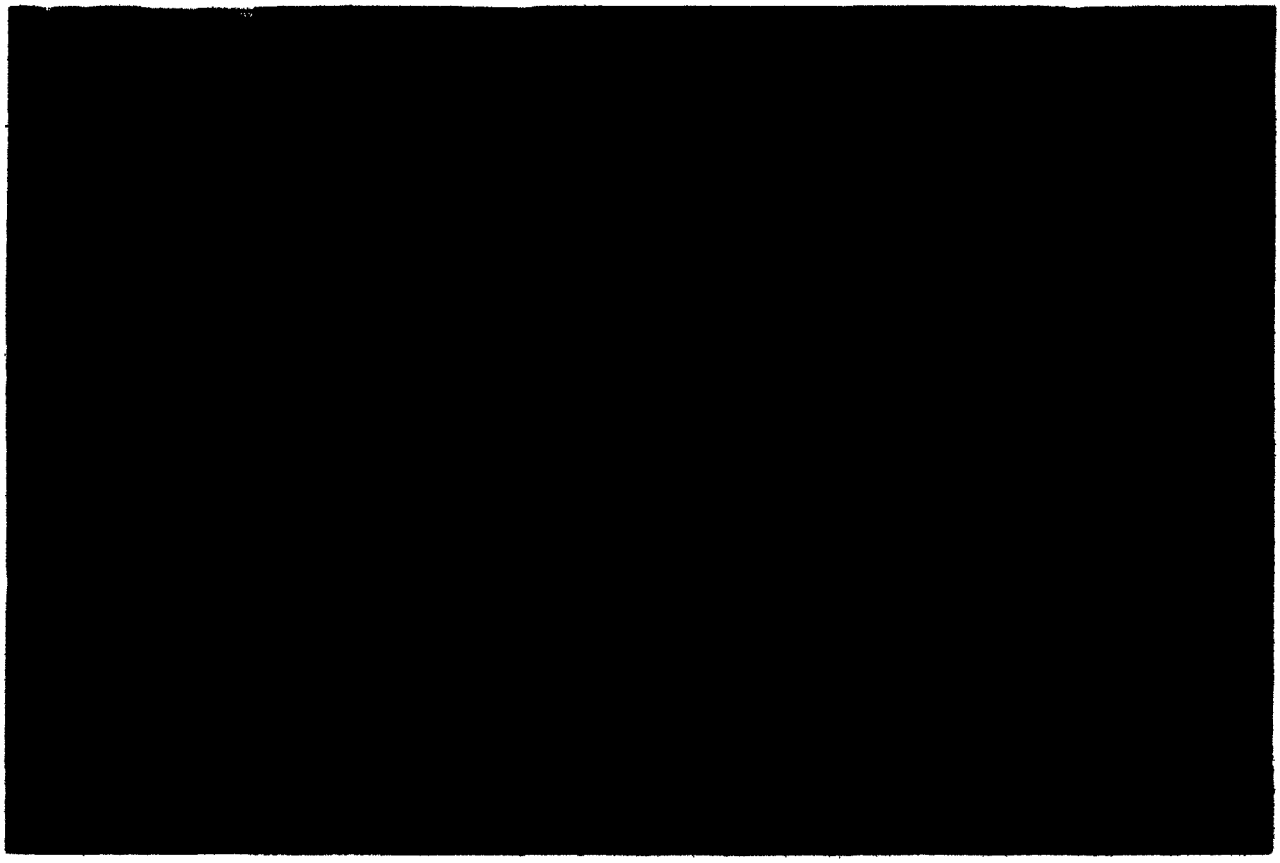

Figure 3.1.4 Side view of nozzle and distribution header.

roll, V_s , and jet velocity, U_j , were maintained constant throughout this study. The roll speed of 700 rpm was chosen to give a peripheral velocity of 1000m/min, corresponding to the the operating speed of an industrial calender on a high-speed newsprint machine. The nozzle air flowrate was maintained at 2.12 m^3/min (70 m/sec), which is 75% of the maximum air flowrate of 2.83 m^3/min recommended for these nozzles.

The method employed for determining the local heat transfer coefficients for air jets impinging on a rotating roll was based on the method developed in this laboratory by van Heiningen (1982). The heat flux sensor consisted of a thin-film resistance thermometer mounted flush on the surface of a rotating roll. As this sensor has a very high sensitivity and a very fast response time (in the order of 10^{-10} seconds), it could measure the essentially instantaneous surface temperature with a high degree of resolution (about 0.001°C at 1670Hz). From the local surface temperature distribution, it was possible to obtain the local Nusselt number distribution by solving the unsteady-state heat conduction equation for the wall of the roll.

A more detailed description of the experimental apparatus follows.

3.2 The Calender

The three calender rolls, identical in shape and size,

were fabricated from PVC pipe, each roll having a diameter of 457 mm, a length of 813 mm and a wall thickness of 12 mm. The diameter of the roll was chosen to correspond to typical diameters of commercial rolls, while the length chosen was sufficient for the study of three nozzles spaced 200 mm apart.

Although calender rolls are normally made of cast iron, PVC was chosen for this model calender to satisfy the special requirements of the heat flux sensor, as will be discussed later. The choice of material in no way affected the impingement heat transfer.

Each roll was mounted between 17 mm thick endplates which were attached to a hollow 38 mm diameter axle. The axles were mounted on the frame with ball bearing pillow blocks.

The bottom roll was driven through a no-slip belt from a 1.2 kW variable speed d.c. motor. The other two rolls were chain-driven from the bottom roll. The top rolls of a calender stack are usually driven by contact with the bottom driven roll. However this was not possible in the experimental apparatus because a gap of approximately 1 mm was required between the rolls to avoid contact of the heat flux sensor with the top or bottom roll.

The heat flux sensor was mounted flush with the surface and equidistantly between the ends of the middle roll. Figure 3.2.1 shows the heat flux sensor in place. Details of the sensor are given in a later section.

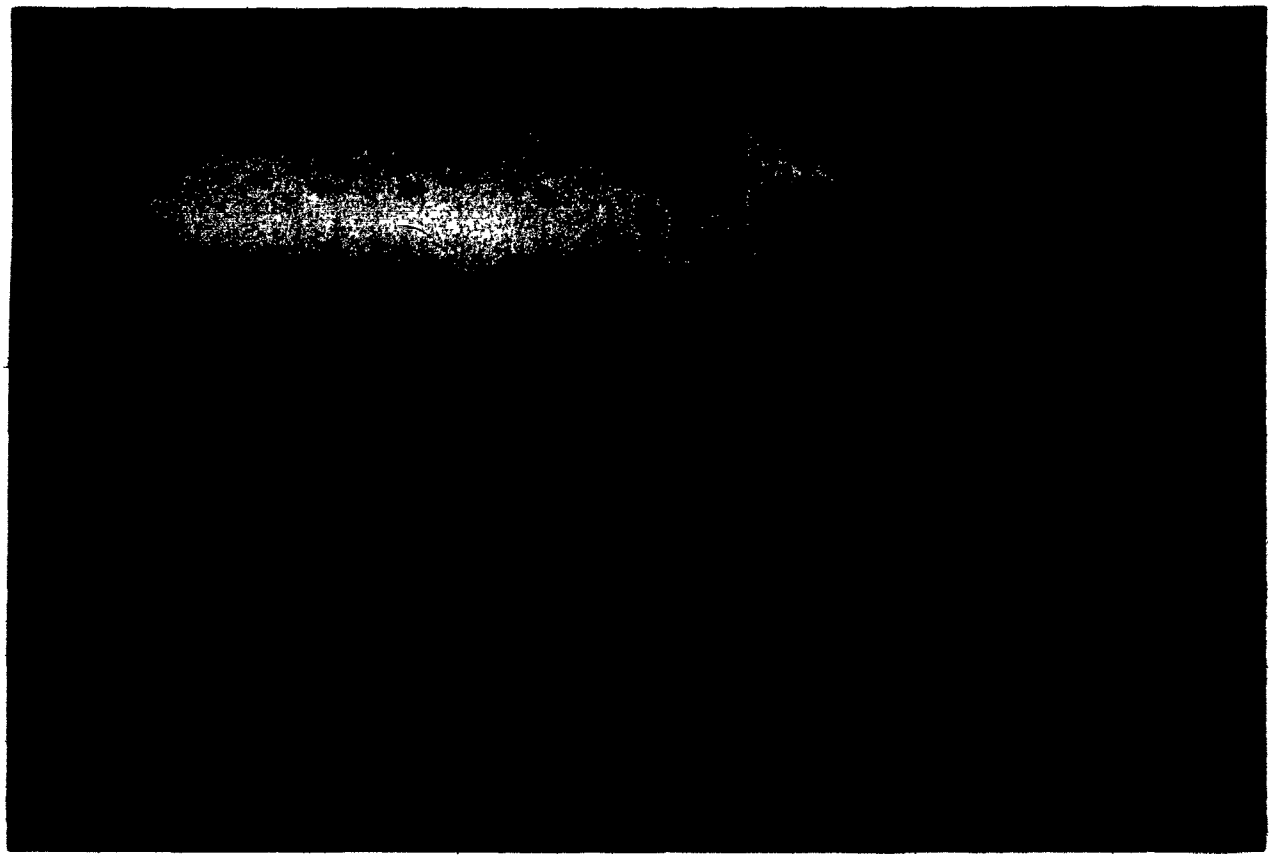

Figure 3.2.1 Heat flux sensor in middle roll.

The leads from the heat flux sensor and thermocouples inside the roll were taken out through a hole in the hollow shaft and were connected to a low-noise 12-channel slip-ring assembly (IEC Corp., Texas, Model IEC-BX-12).

3.3 Air System

The supply air for the nozzles was provided by a 11 kW turboblower (0.9 m^3/sec at 10 kPa) which drew air from the laboratory. A damper divided the air into two streams, one passing through a heater, the other through a cooler. From the heater or the cooler, the air passed through 3.0 m long 200 mm diameter flexible hose to the distribution headers.

The heater had six separate 1 kW, 110 volts heating elements (6 kW total). Each element was controlled separately. Four stages had on-off controls, and one stage was controlled by a potentiometer. For fine adjustment of the nozzle air temperature, the sixth stage was connected to a proportional controller, actuated by a thermistor in the distribution header. The heater was equipped with a thermal cut-off switch set at 170°C.

The cooler consisted of an air conditioner, a Kold Wave 25-C10893, of 7 kW capacity, adapted for this equipment by removing the fan and installing a temperature controller actuated by a thermistor in the exit converging section.

Identical distribution headers were used on the heating and cooling side. They were 210 mm in diameter, 635 m long. Five threaded unions were welded on these

distribution headers, with centre-to-centre spacing of 100 mm (equivalent to 4 nozzle diameters). The three nozzles could thus be mounted on these unions with a choice of two nozzle-to-nozzle spacings. For the narrower (S/d=4) spacing, the first and last unions were capped and the nozzles installed in the three central positions. For the wider (S/d=8) spacing, the nozzles were installed on the first, third and fifth positions, the second and fourth unions were capped.

The shape and dimensions of the nozzles used are shown in Figure 3.3.1. Each nozzle consisted of two straight pipe sections, 41 mm ID (1.5 inch Schedule 40 aluminum pipe) joined by a 135° elbow. The 25 mm ID, 25 mm long nozzle tip was joined to this pipe with a 70 mm long reducing section. The length of the nozzle assembly was 246 mm from the distribution header to the centre of the elbow and 414 mm from there to the nozzle tip.

Each nozzle was fitted with a flow control valve (Figure 3.3.1) These valves consisted of cylindrical plugs with three V-shaped notches. The plugs fitted snugly into the openings of the nozzles from inside the distribution header, and were attached by threaded rods to the opposite wall of the header. By turning the rods, the plugs could be inserted or retracted from the nozzle entrance, thereby varying the open area of the notches available for air flow. When inserted fully, the plugs blocked the air flow completely.

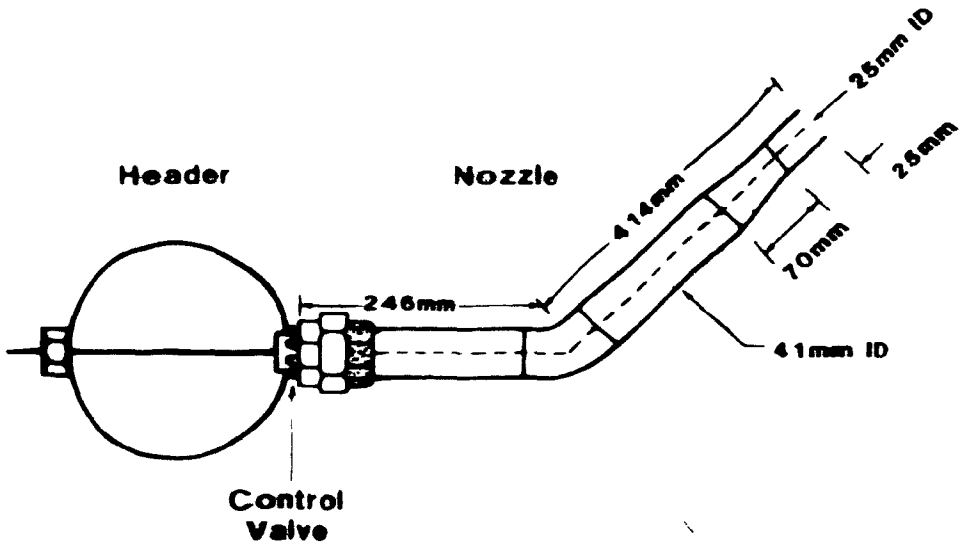

Figure 3.3.1 Schematic of nozzle and distribution header.

Nozzle exit velocity was measured using a static pressure tap located 200 mm upstream from the nozzle exit. A calibration curve, velocity versus static pressure was prepared using velocity measurements made at the nozzle exit with a Pitot tube. The equation obtained was

$$U_J = 6.68\sqrt{\frac{P_{sJ} \times T_J}{P_B}} \qquad 3.1$$

where U_J is the jet velocity in m/s, P_{sj} is the static pressure in mm of H_2O, T_J is the jet temperature in °C, and P_B is the barometric pressure in mm of Hg.

Air temperature in each of the nozzles was measured with chromel/constantan fine wire (0.1 mm) thermocouples located 100 mm upstream from the nozzle exit, and was displayed on a digital thermocouple readout.

The distribution headers were suspended from a common carriage using clamps of hardwood and aluminum pipe with which the position of each nozzle set relative to the roll could be fixed (Figures 3.1.1, 3.1.2 and 3.1.4). The carriage could be moved parallel to the axis of the rolls, thus changing the position of both sets of nozzles relative to the heat flux sensor. Axial heat flux distributions were obtained by making measurements at several axial locations.

3.4 Heat Flux Sensor

3.4.1 Measuring Technique

The method used to determine the local Nusselt numbers for a jet impinging on a rotating surface was developed by van Heiningen (1982). The heat flux sensor measured to a high precision the cyclically varying temperature at one point on the surface of the rotating roll. In the present application, local surface temperature could be measured to about 0.001°C at a sampling frequency of 1670 Hz. This surface temperature was used as a boundary condition for the solution of the one-dimensional unsteady-state heat conduction equation describing the temperature profile within the wall of the cylinder. From this solution, heat flux and Nusselt numbers at the surface of the cylinder were extracted.

The heat flux sensor was a gold thin-film resistance thermometer. The gold film was deposited on the surface of a block of PVC taken from the rolls, and thus identical in thermal response characteristics of the roll. After deposition of the film, the sensor was mounted flush and smooth in the calender roll. The choice of material of construction of the calender rolls was subject to several constraints. For use as the substrate, it had to be electrically insulating and with a surface texture onto which an extremely thin (about 1500 Å) gold film could be deposited. Moreover, the material for the rolls also had to

be isotropic and be available as a roll of this diameter with no seams (i.e. cast or extruded). PVC met these requirements.

3.4.2 Instrumentation for the Heat Flux Measurements

Figure 3.4.2.1 is a schematic diagram of the circuit used with the heat flux sensor. The leads from the heat flux sensor sensor (a resistance thermometer) were attached by means of a slip-ring assembly to a 4-decade Wheatstone bridge, thus producing a voltage proportional to the sensor resistance. The bridge was balanced when the average of the fluctuating voltage from the bridge was zero. Thus the average and the fluctuating voltage were measured.

The fluctuating voltage, V, from the Wheatstone bridge was amplified 2500 times by a low-noise differential amplifier (DANA Model 2860) then filtered with a filter (Rockland Lab. Inc., Model 1022F) to remove high-frequency noise. The signal was then sent to the McGill University Mechanical Engineering Department data acquisition computer facility (DATAC) for digitizing. The signal was amplified by a factor of 2, then digitized by a high-speed analog-to-digital converter (ADC). The input voltage range for the ADC was -5.00 to +5.00 volts. The digitized signal was stored on tape. Data reduction was performed on a computer at the Pulp and Paper Research Institute of Canada, Pointe Claire.

The circumferential position of the sensor was

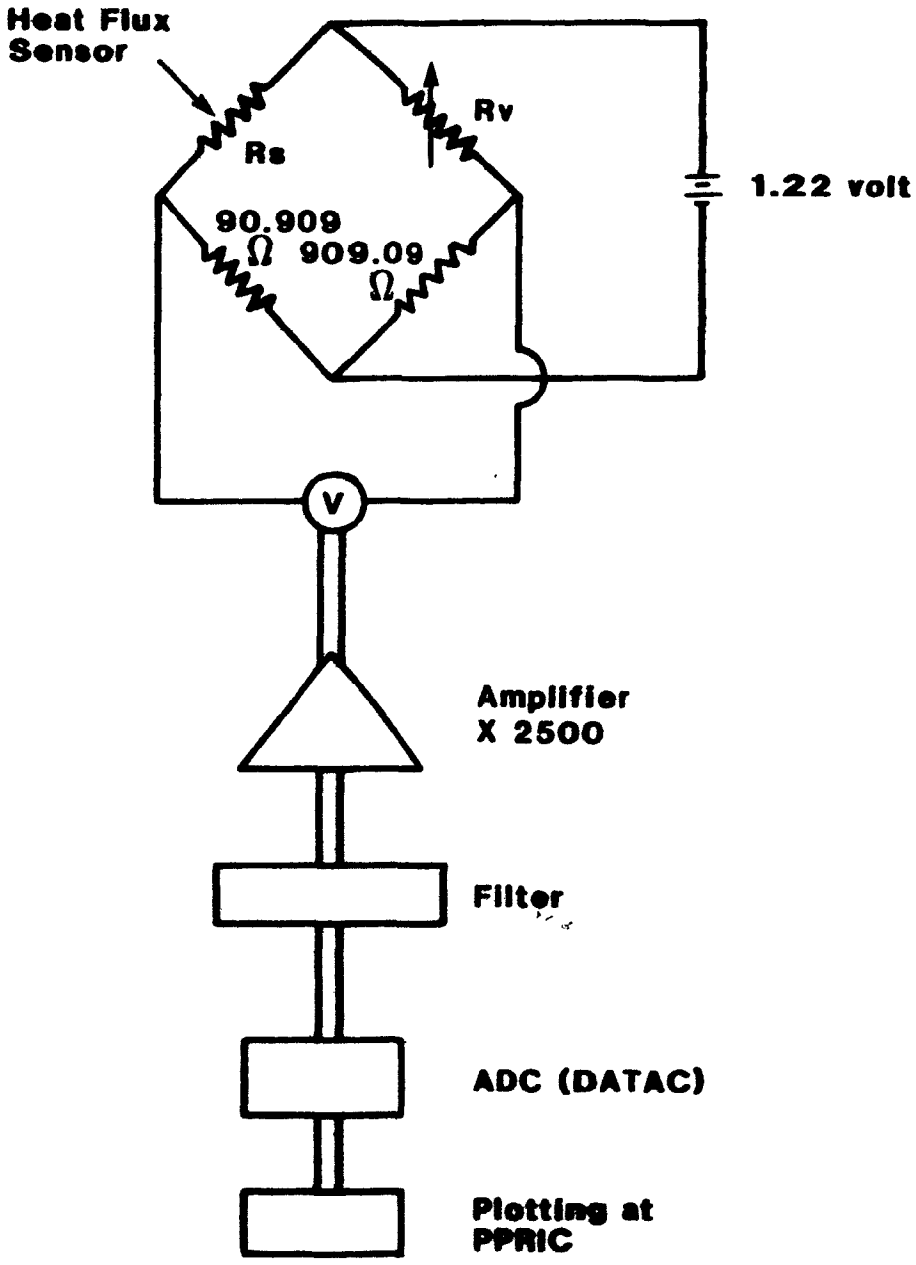

Figure 3.4.2.1 Circuit diagram of heat flux sensor.

identified during rotation by an optical switch. The switch, when closed by a small lever approximately 10 mm wide produced a voltage of 4.0 volts. When open, the switch produced a voltage in the range of 0.4 to 0.8 volt. Thus this arrangement produced a square wave. The signal was sent to the high-speed ADC on a second channel for storage on tape simultaneously with the signal from the sensor.

3.4.3 Manufacture of the Heat Flux Sensor

The thin-film sensor mounted centrally in the surface of the middle roll is shown in Figure 3.2.1. A thin slab of PVC of dimensions 70 x 15 x 10 mm was glued to the back of the substrate to prevent the sensor from slipping out of place during rotation of the rolls.

The outside dimensions of the sensor were 50 x 10 x 10 mm and those of the gold film pattern were 39 x 8 mm. The film pattern dimensions were minimized in order to obtain the best approximate possible point values of Nu in both the axial and circumferential directions.

The sensitivity, A, of a thin film resistance thermometer is proportional to length and inversely proportional to the square root of thickness of the film, as illustrated in the following relationship, which was derived by van Heiningen (1982):

$$A = \alpha_t L(\theta_f q_{mm}/d)^{1/2} \qquad 3.2$$

with α_t = temperature coefficient of resistance

L = length of the film

δ_f = resistivity

q_{sm} = maximum self-heating heat flux

d = film thickness.

Hence decreasing film thickness and increasing film length, increases temperature sensitivity.

The film thickness was kept to the minimum practical value, 1500 Å. A thinner film was too fragile and could not withstand any chemical or physical treatment.

Two constraints limited the maximum film length:

a) the total resistance of the sensor could not exceed 350 Ω, a condition set by the amplifier,

b) the overall size of the sensor had to be kept as small as possible to obtain values of Nu approximating point values in both the axial and circumferential directions.

In order to minimize the overall size of the heat flux sensor, the smallest practical values for width and spacing of the gold film strips were used. The final design of the sensor which met these criteria is shown in Figure 3.4.3.1 It was composed of 14 strips, each 0.25 mm wide and 26.5 mm long, spaced 0.30 mm apart. Overall film length was 371 mm.

The gold film pattern of Figure 3.4.3.1 was produced by a photofabrication technique. The entire surface was

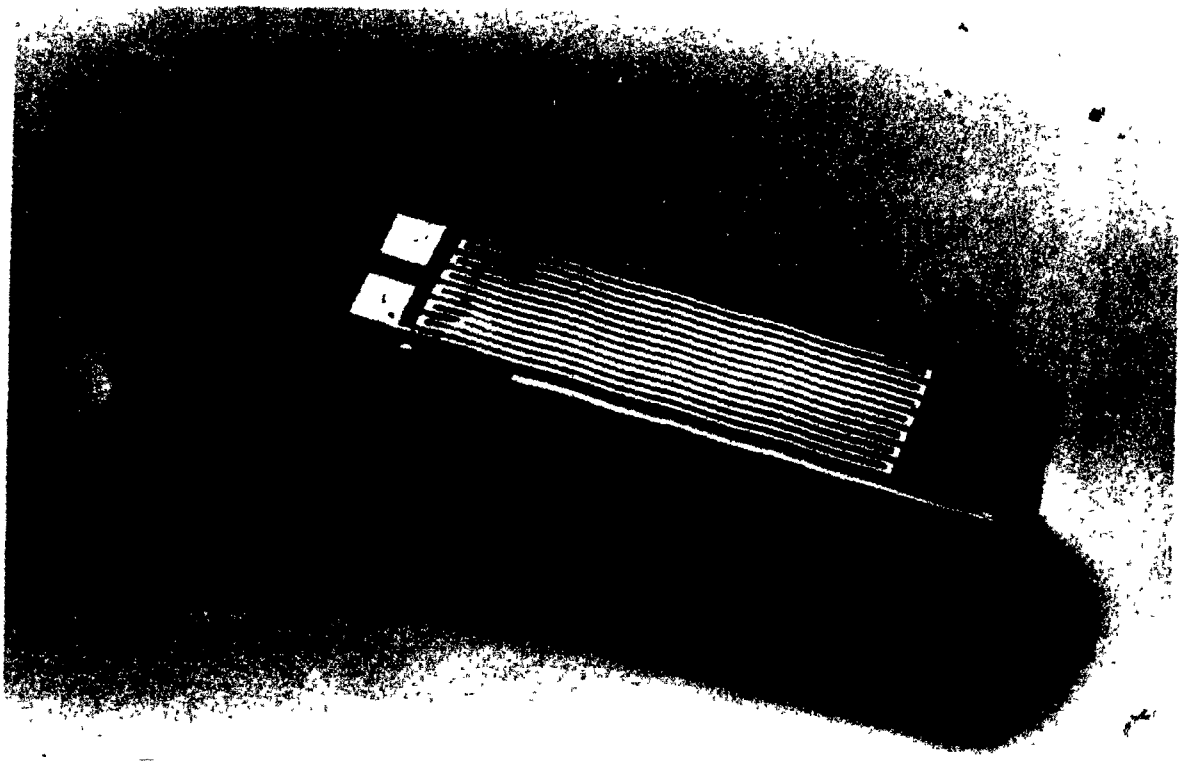

Figure 3.4.3.1 Close-up of heat flux sensor.

first covered with gold. The pattern was produced by removing the unwanted gold using a mask and a gold etching solution, as detailed below:

1. The surface of the PVC was completely covered with 1500 Å of gold by vacuum deposition.
2. The gold surface was coated with positive photoresist (AZ1350J) using a whirl coating machine then baked at 65°C for 30 minutes. This temperature and time had to be monitored very closely. Temperature in excess of 65°C would cause the PVC to distort and fracture the gold film.
3. The mask, which was mimiturized in the Electrical Engineering Dept., McGill University, was pressed onto the photoresist. A quartz lamp, placed 50 mm above the mask, illuminated the masked surface for 30 seconds with UV light.
4. The exposed photoresist was removed with developer. The substrate was again baked at 65°C for 1 hour.
5. The exposed gold was removed using a gold etchant solution consisting of $KI:I_2:H_2O$ diluted in 4 parts H_2O.
6. The photoresist remaining over the gold pattern was then removed with an organic solvent.

7. The surface of the sensor was protected by depositing a film of SiO_2 approximately 1000 Å thick on the surface of the gold.

In preparation for the photofabrication technique, the PVC substrate was rough polished with 600 grit sand paper for 2 hours and then fine polished with a cotton cloth for another 2 hours.

The two connections between the gold pads and the pure silver lead wires were made with a silver paint, Conductive Silver 200, from Degussa.

Two fine wire (0.1 mm diameter) thermocouples, type E, were inserted into holes drilled at the back of the sensor. The thermocouples were located 20 mm apart and 5 mm from the surface of the heat flux sensor. Special thermocouple glue (TRABOND 2151, TRA-CON Inc., Medford, Mass.) was used to fix the thermocouples in place. The temperature at the back of the sensor was measured using a digital thermocouple read-out (Omega).

3.4.4 Calibration of the Heat Flux Sensor

The sensor, placed inside a waterproof bag, was calibrated using a constant temperature bath and a 0.1°C NBS calibrated thermometer graduated to 0.1°C. The resistance of the sensor was measured using a 4-decade Wheatstone bridge, a 1.22 volt power supply and an ammeter.

The calibration obtained is shown in Figure 3.4.4.1.

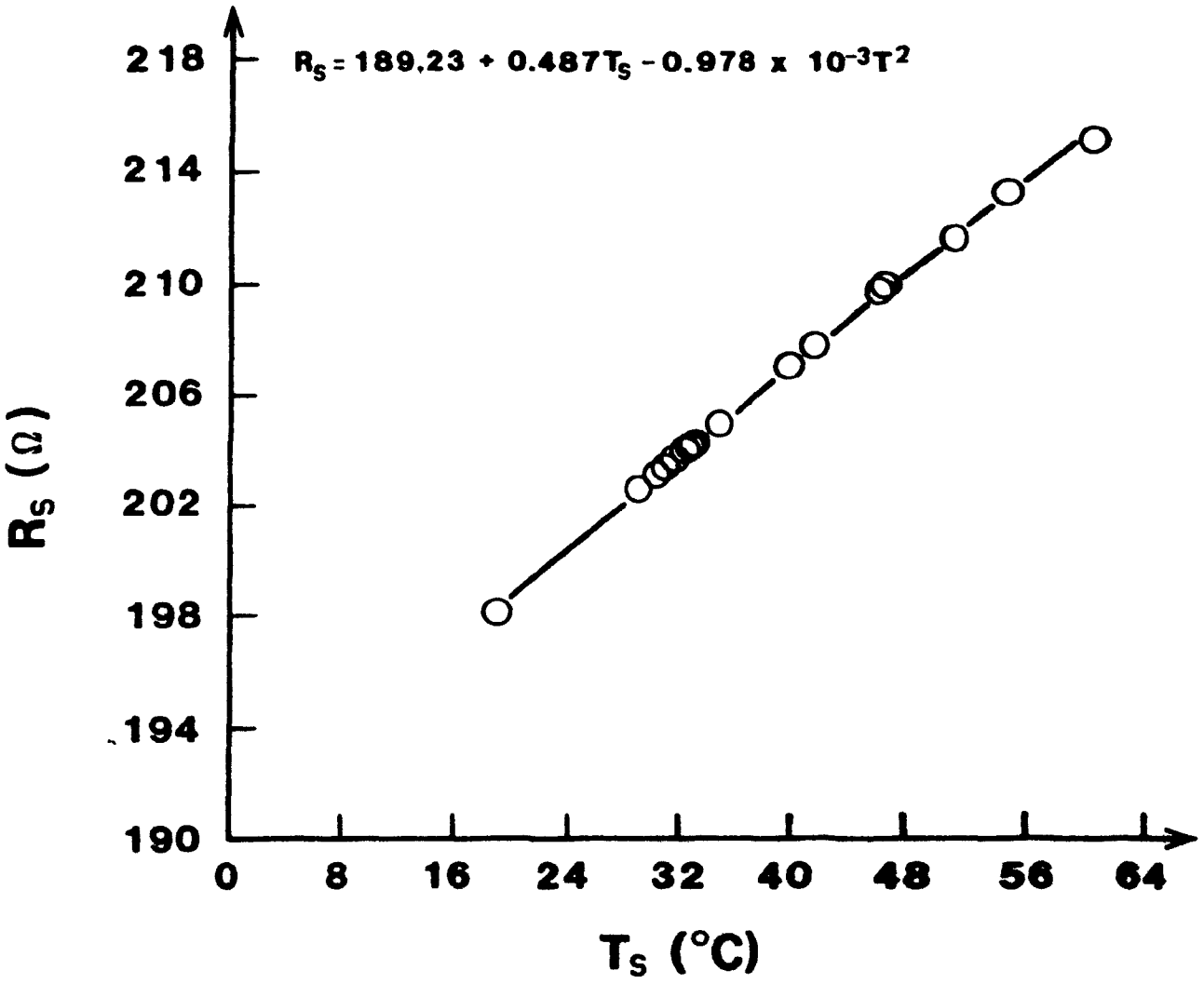

Figure 3.4.4.1 Calibration of heat flux sensor.

The following equation was fitted to the calibration measurements.

$$R_s = 189.23 + 0.489T_s - 0.98 \times 10^{-3} T_s^2 \qquad 3.3$$

with T in °C and R in ohms.

Successive calibrations of the sensor indicated that the sensor resistance decreased with time to an extent unacceptable for the accuracy desired. This change in the calibration was a consequence of the restriction of the temperature to 65°C to avoid distortion of the PVC substrate. This temperature was too low to fully stabilize the microstructure of the very thin gold film. No other satisfactory annealing methods were found to solve this problem. Consequently, it was necessary to recalibrate repeatedly throughout the experimental program.

3.4.5 Sensitivity of the Heat Flux Sensor

The fluctuating bridge voltage, V, is related to the sensor and variable resistances by

$$V = \frac{1.22(R_s - R_v/10.0)}{(R_s + 90.909)(1 + R_v/909.09)} \qquad 3.4$$

The resistance of the sensor Rs can be described as

$$R_s = R_o + \alpha T_s + \beta T_s^2 \qquad 3.5$$

so

$$V = \frac{1.22\ (R_o + \alpha T_s + \beta T_s^2 - R_v/10.0)}{(R_o + \alpha T_s + \beta T_s^2 + 90.909)(1 + R_v/909.09)} \qquad 3.6$$

Differentiating equation 3.6, gives

$$\frac{\Delta V}{\Delta T_s} = \frac{1.22\ (\alpha + 2\beta T_s)}{(R_o + \alpha T_s + \beta T_s^2 + 90.909)(1 + R_v/90.909)} \qquad 3.7$$

For a typical experiment, Ts is 30 ^{o}C and using the first calibration of

$$R_s = 189.23 + 0.489T_s - 0.98 \times 10^{-3}\ T_s^2 \qquad 3.3$$

to obtain Ro, α and β, a value of 203.02 ohms is obtained for Rs. Therefore Rv must be set at 2030.2 ohms. Insertion of these values into equation 3.7 gives

$$\frac{\Delta V}{\Delta T_s} = 552\ \mu V/^{o}C \qquad 3.8$$

This sensitivity is at least one order of magnitude larger than a thermocouple.

3.4.6 Response Time of the Heat Flux Sensor

The response time of the heat flux sensor was critical. For a typical experiment, the sampling rate was 1670 Hz, which meant that the time between successive sample points was 0.0006 sec (0.6msec). For the sensor to measure

the correct temperature, its response time must be at least one order of magnitude smaller than 0.0006 sec.

To estimate the response time of the heat flux sensor, it was considered to be a gold film supported by a perfect insulator. This assumption is valid for very short contact times and because the thermal diffusivity of gold is 2650 times larger than that of PVC.

The response time for the heat flux sensor was found by calculating the time required for the sensor to respond to a step change in temperature. Since the heat flux sensor can be treated as a semi-infinite solid, the transient conduction equation is

$$\frac{\delta T}{\delta T}(x,t) = \alpha \frac{\delta^2 T}{\delta x^2}(x,t) \qquad 3.9$$

The sensor is initially at temperature To. At time t>0, the surface at x = 0 is suddenly raised to temperature T1 and maintained at that temperature for t>0.

The following initial and boundary conditions are;

$$\text{at } t = 0,\ T(x,0) = To$$

$$\text{at } x = \infty,\ T(\infty,t) = To \text{ for all } t$$

$$\text{at } x = 0,\ T(0,t) = T1 \text{ for } t>0$$

The solution to equation 3.9 subject to the two boundary

conditions and the initial condition is

$$\frac{T - T_1}{T_0 - T_1} = \qquad\qquad (3.10)$$

Since the Fourier number is defined as

$$\frac{\alpha t}{x^2} \qquad\qquad (3.11)$$

the term $x \sqrt{t}$ can be replaced by the inverse of the square root of Fo

Therefore

$$\frac{T - T_1}{T_0 - T_1} = \text{erf} \left(\frac{1}{\sqrt{Fo}} \right) \qquad\qquad (3.12)$$

This equation is integrated to obtain the average temperature which results in

$$\frac{\bar{T} - T_1}{T_0 - T_1} = \qquad\qquad (3.13)$$

for a Fourier number of Fo = 0.446.

By inserting the values of thermal diffusivity of gold (α = 6.62E-05 m ^{2}/sec) and thickness of gold film (x = 1500 Å) into equation 3.11, the response time t was found to be in the order of 10^{-10} seconds. Obviously, the response time of the sensor was fast enough to allow a sampling rate of 1670 Hz.

3.4.7 Self-Heating of the Heat Flux Sensor

When current is passed through a resistor heat is generated. The amount of heat generated is related to the voltage drop across the resistor and to its resistance. In order to utilize a resistor as a thermometer the heat generated denoted the self-heating heat flux must be reduced.

The effect of the sensor self-heating on the local Nusselt numbers can be calculated for the present case as follows:

The self-heating heat flux q_{sh} is described by

$$q_{sh} = v^2/(LWR_s) \qquad 3.14$$

where v = the voltage drop over the sensor in the Wheatstone bridge

L = overall length of gold film

W = width of gold film

R_s = sensor resistance.

For a voltage reference of 1.22 volts applied across the Wheatstone bridge, the voltage drop over the sensor, v was 0.84 volt. For a sensor having a film length L of 371 mm, a film width W of 0.25 mm, and an average resistance in the order of 200 Ω, the resulting self- heating heat flux is 38 W/m^2.

The stagnation heat flux is normally in the order of 6600 W/m^2. Thus the self-heating heat flux constitutes less

than 0.5% error at the stagnation point, and the voltage drop across the sensor is sufficiently low that the error from self-heating is not significant.

3.4 Resolution of Heat Flux Sensor

Equation 3.15 gives the relationship between the fluctuating bridge output voltage V and the Wheatstone bridge resistances as

$$V = \frac{1.22(R_s - R_v/10.0)}{(R_s + 90.909)(1 + R_v/909.09)} \qquad 3.15$$

The sensor resistance Rs is described by the equation

$$R_s = R_o + \alpha T_s + \beta T_s^2 \qquad 3.16$$

so

$$V = \frac{1.22(R_o + \alpha T_s + \beta T_s^2 - R_v/10.0)}{(R_o + \alpha T_s + \beta T_s^2 + 90.909)(1 + R_v/909.09)} \qquad 3.17$$

Differentiating equation 3.17 for Ts gives

$$\Delta T_s = \frac{\Delta V(R_o + \alpha T_s + \beta T_s^2 + 90.909)(1 + R_v/909.09)}{1.22(\alpha + 2\beta T_s)}$$

Since the output voltage from the Wheatstone bridge V is amplified 2500 times by the differential amplifier and again 2 times by the DATAC amplifier, the change in surface temperature ΔT_s can be expressed as a function of the digitized voltage change ΔV_d .

$$\Delta T_s = \frac{\Delta V_d (R_o + \alpha T_s + \beta T_s^2 + 90.909(1 + R_v/409.0)}{.22 \times 2500 \times 2 \times (\alpha + 2\beta T_s}$$ 3.18

For run #8, the following input was used,

Ro = 186.59

α = 0.50409

β = -0.01211

Rv = 199.4

Ts = 26.33

From this, it follows that the change in surface temperature is

$$\Delta T_s = .13162\ \Delta V_d$$

With the resolution of 0.01 volt for ΔV_d, the smallest ΔT_s becomes 0.001316°C. Obviously, the heat flux sensor is sufficiently sensitive to permit resolution of surface temperature down to at least 1/1000°C.

3.5 Computation of Nusselt Number

3.5.1 Computation of Instantaneous Local Heat Flux

The heat flux sensor measures the instantaneous surface temperature. In order to determine the instantaneous heat flux, the one-dimensional unsteady state heat conduction equation is solved numerically. The sensor substrate is considered as a semi-infinite slab.

The sensor substrate can be divided into n layers of thickness Δx, as illustrated in the Figure 3.5.1.1. The sensor surface is referred to by the subscript 0; the back

of the sensor has the subscript n.

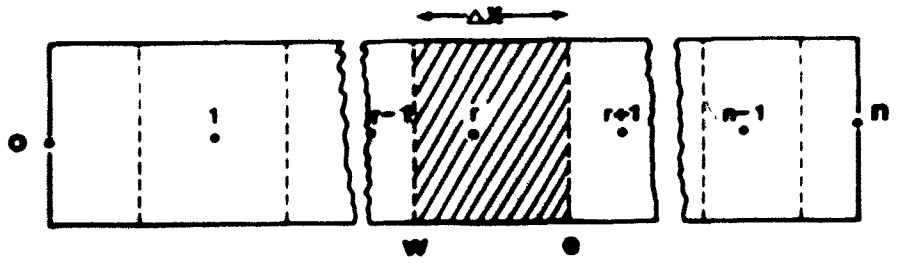

In order to calculate the instantaneous local heat flux, the temperature distribution must first be calculated. The equation for transient conduction in one-direction is

$$\frac{\delta T}{\delta t} = \alpha \frac{\delta^2 T}{\delta x^2} \qquad 3.9$$

This equation is solved by considering the control volume, r, shaded in Figure 3.5.1.1, and integrating equation 3.9 from w to e and from t - Δt to t.

$$\int_w^e \int_{t-\Delta t}^{t} \frac{\delta T}{\delta t}\, dt\, dx \rightarrow \int_{t-\Delta t}^{t} \int_w^e \alpha \frac{\delta^2 T}{\delta x^2}\, dx\, dt$$

For a fully explicit scheme, the solution is

$$T_{r,t} = \frac{1}{2}\left(T_{r+1,t-1} + T_{r-1,t-1}\right) \qquad 3.19$$

for r=1,2,3,...,n-1 and t=1,2,3,...,N.

The restriction on this expression for the temperature is that the Fourier number,

$$Fo = \frac{\alpha \Delta t}{\Delta x^2}$$

with Δt being the time step or the sampling time. For this condition the layer thickness becomes a function of the sampling time,

$$\Delta x = \sqrt{2 \alpha \Delta t} \qquad 3.20$$

In order to determine the instantaneous heat flux at the surface, a heat balance must be performed on the first control volume, as indicated in Figure 3.5.1.2.

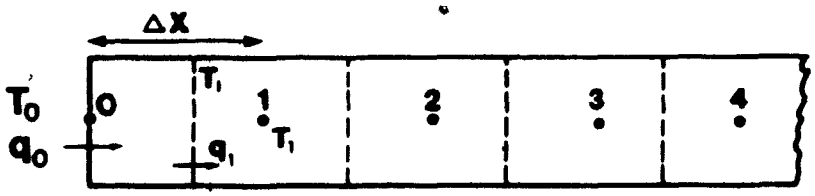

Input - Output = Accumulation

$$q_o - q_1 = \Delta x \rho Cp \left(\frac{T_{i,t} - T_{i,t-1}}{\Delta t} \right) \qquad 3.21$$

Since

$$q_1 = -k \left(\frac{\delta T}{\delta x} \right)_i \qquad 3.22$$

the heat flux at the surface, q_o, is

$$q_o = \Delta x \rho Cp \left(\frac{T_{1,t} - T_{1,t-1}}{\Delta x} \right) - k \left(\frac{T}{dx} \right)_1 \qquad 3.23$$

To evaluate

$$\left(\frac{\delta T}{\delta x} \right)_1 \qquad 3.24$$

which is

$$\left(\frac{\delta T}{\delta x} \right)_1 = \left(\frac{T_o - T_1}{\Delta x} \right) \qquad 3.25$$

some expression for To and T1 as function of time must be found. For short contact times, an average of the old and the new can be used. Therefore

$$T_1 = \frac{1}{2} \left(T_{1,t} + T_{1,t-1} \right)$$

$$T_o = \frac{1}{2} \left(T_{o,t} + T_{o,t-1} \right) \qquad 3.26$$

So equation 3.25 becomes

$$q_o = \Delta x \rho Cp \left(\frac{T_{1,t} - T_{1,t-1}}{\Delta t} \right) - \frac{k}{2\Delta x} \left(T_{o,t} + T_{o,t-1} - T_{1,t} - T_{1,t-1} \right) \qquad 3.27$$

The temperature at the control volume boundary, Ti can be calculated by averaging the two neighbouring points, namely To and T1,

$$T_i = \frac{T_o + T_1}{2}$$

Equation 3.23 now becomes

$$q_o = \frac{\Delta x \rho Cp}{2}\left(T_{1,t} + T_{o,t} - T_{1,t-1} + T_{o,t-1}\right) - \frac{k}{2\Delta x}\left(T_{o,t} + T_{o,t-1} - T_{1,t} - T_{1,t-1}\right) \qquad 3.28$$

Using the restriction on the Fourier number that

$$Fo = \frac{\alpha \Delta t}{(\Delta x)^2} = \frac{1}{2}$$

the heat flux at the surface is now

$$q_o = \frac{k}{\Delta x}\left(T_{1,t} - T_{o,t-1}\right) \qquad 3.29$$

which holds true for t=1,2,3,...,N

The boundary conditions in this case are that the surface temperature $T_{o,t-1}$ is measured for all times and that the heat flux at the back of the sensor, q_n is 0. This last boundary condition is identical to stating that $T_{n,t} = T_{n-1,t}$ which arises from considering the sensor substrate as a semi-infinite solid. It also implies that the net heat flux to the roll is equal to zero or that the total heat transferred to the roll by the heating jets is equal to the total heat removed by the jets on the cooling side.

The penetration depth, Z, is calculated by

$$Z = 1.6\sqrt{\pi \alpha \tau_o} \qquad 3.30$$

This penetration depth Z is defined as the location where the amplitude of a sinusoidal surface temperature variation of frequency τ_o^{-1} is reduced to 1%.

The number of finite difference layers, n, of

thickness Δx is calculated by

$$n = \frac{Z}{\Delta x} = 2.0\sqrt{\frac{\tau_o}{\Delta t}}$$

where τ_o is the time for one complete rotation. For a sampling of about 145 measurements per rotation, the value of n is approximately 40.

3.5.2 Calculation of Local Nusselt Numbers

At a sampling rate of 1670 Hz, and a cylinder speed of 700 rpm, the number of measurements per rotation was approximately 145. Thus the local heat flux was determined at 145 points along the circumference of the cylinder. The location of each measurement was identified by examining the signal from the optical switch, which was digitized simultaneously with the heat flux sensor signal.

In order to obtain the mean value of local heat flux at each circumferential position, local heat flux was averaged over 100 rotations.

Local values of Nusselt number were calculated from the following definitions

$$Nu = \frac{hd}{k}$$

and

$$h = q_o (T_j - T_{o,t})$$

where Tj is the jet air temperature and $T_{o,t}$ is the local temperature at the surface of the cylinder. The

characteristic length, used in the relation above, is the nozzle diameter, d.

Depending on the location of the heat flux sensor around the circumference, Tj was taken to be the temperature of the hot or the cold jet.

The computer printout included a listing of the conditions of the experiment as well as the local and average values of Nusselt numbers for the heating and the cooling jets

3.5.3 Display of Nusselt Number Profiles

The analysis of the data was followed by a computer plotting of the local Nusselt numbers. The Nusselt number profiles for the heating and cooling jets was incorporated into a single plot. The pertinent experimental conditions were also included on each plot. Plotted on the horizontal axis is the circumference position of the heat flux sensor as it rotated. The circumferential position ranging from 0° to 180° indicates the impingement surface for the heating jets while the impingement surface for the cooling jets ranges from 180° to 360°.

The distributions of the local Nusselt numbers due to the cooling jets have been inverted to indicated that the heat flux is in the opposite direction from that of the heating jets.

4. RESULTS AND DISCUSSION

4.1 Introduction

The position and orientation of an air nozzle in the plane perpendicular to the calender roll axis can be described uniquely with three parameters. These parameters, which are illustrated in Figure 4.1.1, are

θ - the roll circumferential angle

φ - the deflection angle

H - the nozzle-to-roll spacing

The roll circumferential angle, θ , describes the angular position on the roll circumference of the point of intersection between the centreline of the nozzle and the roll surface. Circumferential position can also be described in terms of y/d, the dimensionless circumferential distance from the stagnation point. The distance, y/d, is defined as positive in the direction of rotation of the roll.

The bottom nip (the six o'clock position) on the centre roll was defined as $\theta = 0°$, the top nip thus corresponds to $\theta = 180°$. For consistency in representation of results of the present study, the roll is considered to rotate clockwise from 0° to 180° through the zone affected by the heating jets, and from 180° to 360° (0°) through the zone affected by the cooling jets.

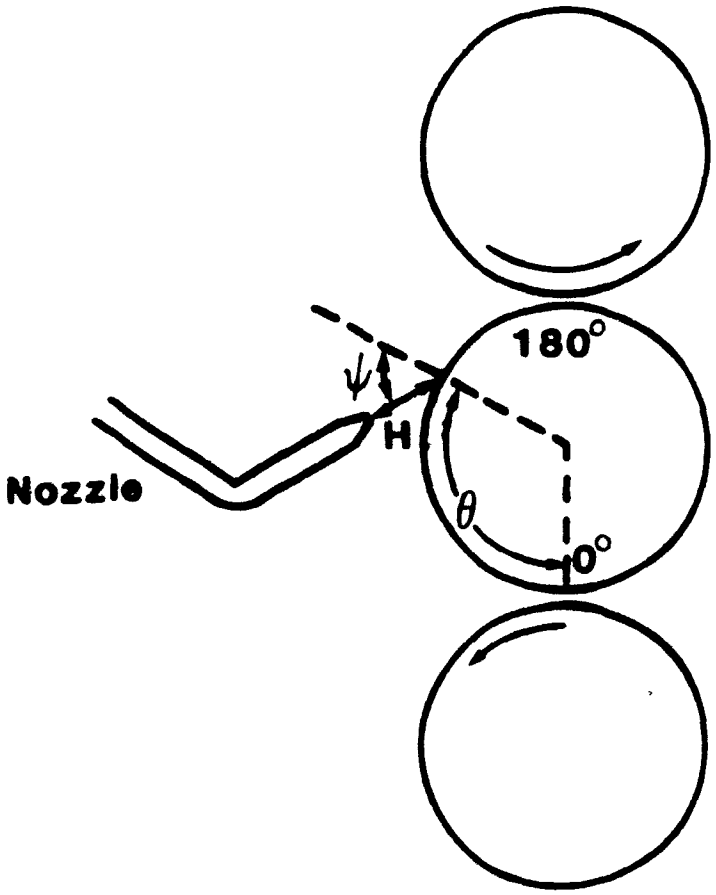

H - nozzle-to-roll spacing

θ - circumferential angle

ψ - deflection angle

Figure 4.1.1 Position of a nozzle relative to a calender roll.

The deflection angle, ϕ , describes the angle by which the nozzle centreline is inclined with respect to the normal to the roll surface at the circumferential position defined by θ. Thus when the nozzle is orientated perpendicularly to the roll surface, $\phi = 0°$. The angle was defined as positive when the deflection angle directs the jets in the same direction as the rotation of the roll (clockwise in Figure 4.1.1).

The nozzle-to-roll spacing, H, was defined as the distance along the nozzle centreline from the nozzle exit to the roll surface.

The position of the nozzle relative to the adjacent nozzles was described by the centreline to centreline spacing, expressed nondimensionally as S/d. The parameter, x/d, describes axial position with respect to the centre nozzle. Thus the position of the centre nozzle is x/d = 0, while the adjacent nozzles are at x/d = $\pm$S/d.

The effects of each of the five position parameter, θ , ϕ , H/d, S/d, and x/d, were determined independently by variation individually from a neutral position. The same values of H and S, and corresponding values of γ and ψ were always selected for the two sets of jets, i.e. for the heating and cooling jets. The neutral position and the experimental conditions used in this study are shown in Table 1.

The results for all the experiments reported in this study, are summarized in Table 2. The table includes the

Table 1 - Position parameters of the nozzles

Parameter	Neutral Position	Experimental Conditions
θ_H	heating jets 90°	120°, 90°, 60°
θ_C	cooling jets 270°	300°, 270°, 240°
ϕ	0°	-45°, -30°, 0°, 30°, 45°
H/d	4	1, 2, 4, 6, 8
S/d	8	8, 4
x/d	0	-2, -1, 0, 1, 2 (for S/d=4)
		-4, -3, -2, -1, 0, 1, 2, 3, 4 (for S/d=8)

Table 2. Experimental Results.

Expt	s/d	H/d	x/d	θ_H	θ_C	ψ_H	ψ_C	T_{JH}	T_{JC}	T_S	ΔT_H	ΔT_C	T_A	Nu_{oH}	Nu_{oC}	$\overline{Nu}_H$	$\overline{Nu}_C$
1	8	4	0	90	270	0	0	60	24	38	22	14	32	273	309	51	92
2	8	4	4	90	270	0	0	60	25	37	23	12	32	64	110	22	45
3	8	4	3	90	270	0	0	59	23	36	23	13	31	79	125	22	49
4	8	4	2	90	270	0	0	58	23	36	22	13	31	158	205	34	70
5	8	4	1	90	270	0	0	61	24	38	23	14	32	229	260	46	84
6	8	4	-1	90	270	0	0	60	23	38	22	15	32	222	280	48	86
7	8	4	-2	90	270	0	0	60	24	38	22	14	32	163	205	36	73
8	8	4	-3	90	270	0	0	57	23	35	22	12	31	89	150	26	56
9	4	4	-4	90	270	0	0	59	23	35	24	12	31	58	108	20	44
10	4	4	2	90	270	0	0	59	23	37	22	14	32	185	235	41	76
11	4	4	1	90	270	0	0	60	24	39	21	15	33	227	260	47	82
12	4	4	0	90	270	0	0	58	22	37	21	15	32	280	290	51	89
13	4	4	-1	90	270	0	0	59	24	38	21	14	32	236	280	46	84
14	4	4	-2	90	270	0	0	53	17	30	23	13	28	188	215	36	72
15	8	1	0	90	270	0	0	56	22	34	22	12	30	305	400	51	103
16	8	2	0	90	270	0	0	58	23	35	23	12	31	297	390	51	112
17	8	6	0	90	270	0	0	58	21	34	24	13	30	212	295	42	89
18	8	8	0	90	270	0	0	61	25	37	24	12	32	161	230	34	77
19	8	4	0	60	300	0	0	55	20	32	23	12	29	262	310	43	97
20	8	4	0	120	240	0	0	55	21	34	21	13	30	275	326	49	101
21	8	4	0	90	270	-30	30	58	22	34	24	12	30	296	300	44	97
22	8	4	0	90	270	-45	45	58	24	34	24	10	30	278	279	38	100
23	8	4	0	90	270	30	-30	57	24	34	23	10	30	215	345	39	110
24	8	4	0	90	270	45	-45	53	17	28	25	11	27	189	310	35	97
25	8	4	0	90	270	0	0	60	24	38	22	14	32	282	290	51	91

operating temperatures, nozzle position and orientation and resulting stagnation and average Nusselt number for both the cooling and heating jets. Expt. 25 is a duplicate run of Expt. 1, which was perfomed with the nozzles at the neutral position.

4.2 Local Nusselt Numbers

The profile of local Nusselt number around the circumference of the middle roll is shown in Figure 4.2.1 for the case of the nozzles in the neutral position (Exp 1). The profiles of local Nusselt number for the heatingjets (θ = 0° to 180°) are presented in the left quadrants, those for the cooling jets (θ = 180° to 360°) in the right quadrants. Also recorded on the plot are the stagnation point Nusselt numbers, Nu_o, and the circumferentially averaged Nusselt numbers, $\overline{Nu}$, for the heating and cooling sides of the roll. The five position parameters noted earlier, i.e. θ, ϕ, H/d, S/d, and z/d, are recorded in the upper left quadrant.

In the lower left quadrant, a summary of the temperatures for the experiment is shown. The heating and cooling jet temperatures, T_{jH} and T_{jC}, were measured at the nozzle exits. The ambient air temperature T_A was measured near the calender. T_s represents the average surface temperature of the middle roll, and ΔT_H and ΔT_C, the average differences between the nozzle exit temperatures and T_s. The average surface temperature and the average temperature

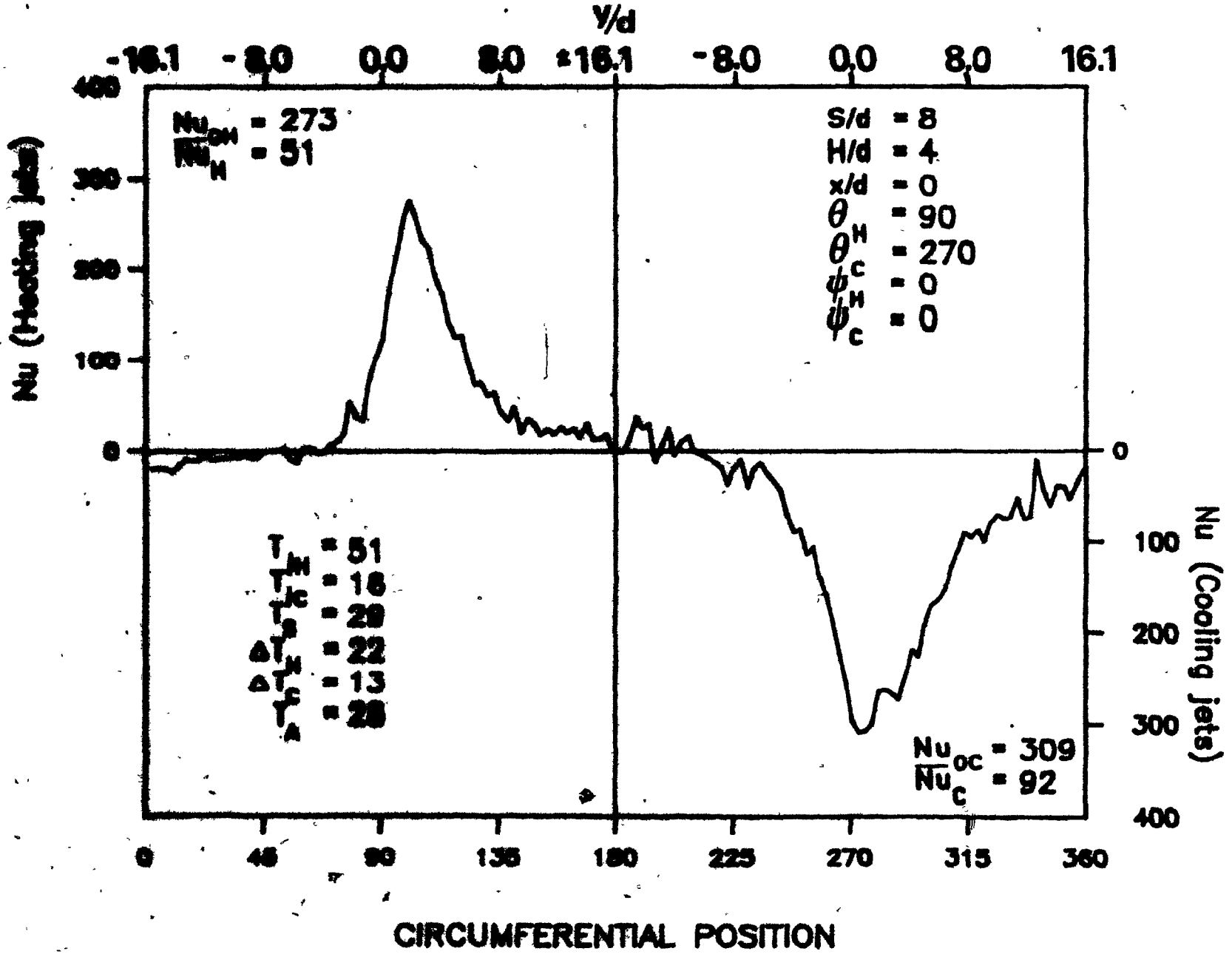

Figure 4.2.1 Nusselt number distributions for nozzles placed at neutral position (Expt. 1).

differences were not used for any calculations. The actual local surface temperatures, which varied less than 2°C, and the temperature differences based on the local surface temperatures were used for the calculation of local heat transfer coefficients. The circumferentially averaged Nusselt numbers were calculated as the average of the local Nusselt numbers.

Figure 4.2.1 contains many features, which are typical for all of the results obtained in the present study. Following the local Nusselt number distribution from the diverging nips (at $\theta = 0°$ on the heating side or $= 180°$ on the cooling side) in the direction of rotation of the roll to the converging nips, the same features are apparent in both heating and cooling curves. From the diverging nips, where the Nusselt number is small but in the opposite direction from the main part of the corresponding profile, the Nusselt number increases, first gradually and then steeply to a maximum at the stagnation points. Past the stagnation point, Nusselt number decreases less rapidly than on the approach side, showing a secondary peak in the cooling curve at $y/d = 2.4$. A secondary peak is not always apparent in the heating curve. Approaching the converging nips, there is no reversal of heat flux as occurs at the diverging nips.

The negative Nusselt number near the diverging nips is attributed to air passing through the nips. A gap of approximately 1 mm had to be left between the rolls to

prevent the sensor from touching the top or bottom roll. The air passing through these nips would bring cool air to the heating side and hot air to the cooling side, thus causing a small negative heat flux in the affected areas. This negative heat flux would not occur in a real calender stack, where air cannot pass through the nips.

The skewed shape of the curves is clearly attributable to the motion of the surface. For the case of a single slot jet impinging on a rotating cylinder, van Heiningen (1982) found non-symmetry in the Nusselt number profiles for mass velocity ratios ($M_{VS} = \rho_S V_S / \rho_j U_j$) as low as 0.06. In the present study M_{VS} was maintained constant at 0.23. At this level of surface motion, van Heiningen (1982) obtained significantly skewed Nusselt number profiles, which displayed many of the features found as well in the profiles presented here.

Surface motion affects heat flux by changing the flow characteristics and temperature profiles in the region adjacent to the impingement surface. For the region where the surface motion is directed towards the nozzle, there are several factors which affect the heat transfer coefficient, not all of which act in the same direction. Surface motion in the direction opposite to the wall jet tends to increase the velocity gradient at the surface, hence increases the heat transfer coefficient. However, opposed motion of the surface and the wall jet also has the effect of reducing the velocity of the wall jet more quickly than for a stationary

impingement surface, which has just the opposite effect, i.e. of tending to reduce gradients at the wall and hence the heat transfer rates. Moreover, surface motion results in an unequal distribution of the nozzle exit flow, with the wall jet on the opposed motion side containing less than half of the nozzle exit flow. Furthermore, surface motion conveys air from the direction of the wall jet region towards the stagnation region, i.e. drags boundary layer fluid from the region where its temperature is closer to the surface temperature. This thermal effect reduces the local effective temperature driving force between the wall jet and the surface, hence reduces the heat transfer rate and Nu. Of these several effects, the data indicate, as did those of van Heiningen (1982), that the effects tending to decrease Nu in the region of surface motion approaching the nozzle axis predominate over the contrary effects.

On the other side of the stagnation point, where the surface motion is in the same direction as the wall jet, all of these effects are reversed, as is the net effect on the Nu profile.

It is interesting to note that there was no substantial displacement of the stagnation points caused by the roll surface motion. Even for a value of the surface velocity mass ratio, M_{VS} as high as 0.6, van Heiningen (1982) reported a shift of the stagnation point in the direction of motion of the cylinder, by only about 0.5 the width of his slot jet. For the much smaller value of M_{VS}

for the the present study the shift in the stagnation point position was too small to be measured and is not important in any case.

The cooling Nusselt number distribution exhibits a secondary maximum at y/d = 2.4 on the side where the surface recedes from the stagnation point. No off-stagnation peaks are evident on the other side, where the surface approaches the stagnation point. For the heating Nusselt number distribution, no secondary peak was found on either side of the stagnation point. The position y/d = 2.4 on the heating side corresponds approximately with the position of the optical switch. The peak may have been lost in the process of numerically matching the temperature profile for successive rotations

For a round jet impinging on a stationary flat plate, Obot (1980) found an off-stagnation maximum located at y/d = 2.0 for jet Reynolds numbers in the range of 15,000 to 60,000. Thus it appears that the off-stagnation peak at y/d = 2.4 in Figure 4.2.1 was displaced away from the stagnation point as a result of the surface motion. Displacement of off-stagnation maxima in the direction of cylinder surface motion was also found by van Heiningen (1982), but for a slot jet. It is well documented that the secondary maximum reflects the completion of the boundary layer transition from laminar to turbulent. In the region between stagnation and the off-stagnation maximum, the principal effect of surface motion is to increase the

velocity gradient at the surface on the side with motion approaching the nozzle centreline, and to decrease it on the leaving side. This change in velocity gradient at the surface advances boundary layer transition on the approach side and retards it on the leaving side. As a consequence, the surface transition occurs so quickly on the approach side that the secondary maximum disappears into the central peak, while on the leaving side the secondary maximum becomes more prominent because it is moved farther out.

The stagnation point Nusselt numbers in Figure 4.2.1 are 273 for the heating jets and 309 for the cooling jets. For the same Reynolds number and H/d = 4, den Ouden and Hoogendorn (1974) reported Nu_o = 270 for impingement of a single round jet on a stationary flat surface. Extrapolation to a Reynolds number of 110,000 of Obot's (1980) results for a single cooling jet on a stationary flat surface would yield Nu_o= 175.

The effects of roll surface motion on stagnation Nusselt number cannot be extracted from the results of the present study, because neither jet velocity nor roll surface velocity varied (i.e. constant M_{VS}). An indirect assessment by comparision with published data for stationary surfaces would not be very effective because of the large number of other factors like nozzle geometry, flow conditions and impingement surface geometry which affect Nu_o, as is evident from the difference in the results reported by den Ouden and Hoogendorn (1974) and Obot (1980). Based on the findings of

van Heiningen (1982), a value of surface velocity mass ratio, M_{VS}, of 0.23, as applies in the present study, increased Nu_o by about 2% and 4% for impingement surface spacings of 2.6 and 6 nozzle widths. Thus for the spacing of H/d=4 in the present study, it is safe to conclude that these values of Nu_o were increased by <5% by the effect of motion of the roll surface.

The most striking features of the results shown in Figure 4.2.1 are the fact that the rotating roll assumed a steady-state temperature, T_S, which is significantly closer to T_{JC} than to T_{JH}, and that the average Nusselt numbers are much larger for the cooling jets than for the heating jets. If Re_H and Re_C were identical and the heat exchange from the ends of the roll to the environment were negligible, it might be expected that the average Nusselt numbers on the heating and the cooling sides of the roll would be equal and that the rotating roll would assume a temperature, T , equidistant between T_{JH} and T_{JC}.

The condition of insignificant heat transfer from the ends of the roll is an acceptable approximation. The heat transfer area from the ends of the roll (0.33 m²) is only 28% of that of the circumference (1.17 m²). The ΔT for the impingement heat transfer at the circumference is in the range 22° to 25°C on the heating side and 10° to 15°C on the cooling side. The ΔT for convective heat transfer from the ends, i.e. $T_S - T_A$, is by comparison in the range from 1° to 5°C. Thus the combination of the much smaller area, much

smaller ΔT and much smaller heat transfer coefficients leads to heat losses at the roll ends which are negligibly small compared to the impingement heat transfer around the circumference of the roll.

Another of the conditions noted above, i.e. $Re_H = Re_C$, does not apply fully in this study. The nozzle exit velocities U_{jH} and U_{jC} were both adjusted to be equal to 70 m/s. With the difference in kinematic viscosity of the air caused by the difference in temperatures, the jet Reynolds numbers were approximately 100,000 on the heating side and 120,000 on the cooling side. At the stagnation point, where the Nusselt number varies approximately as $\sqrt{Re}$, the 20% difference in Reynolds number would account for a 10% difference in Nu_o. The differences were found to be consistently larger than 10%, particularly for large H/d and positive deflection angles. Hence the ambient temperature appears to have had a significant effect on the Nu_o.

For a dependence of mean Nusselt number to the 0.7 power of Reynolds number (Martin (1977)), the 20% Reynolds number difference corresponds to a Nusselt number ratio $\overline{Nu}_C/\overline{Nu}_H$ of 1.4 rather than 2, as found in this study. Hence a very strong effect other than that attributable to the Reynolds number differences must have contributed to the difference between the average Nusselt numbers for the cooling and the heating sides of the roll. This is the effect of the ambient air temperature.

An unconfined jet will exchange heat both with the

impingement surface and the ambient air by the entrainment of the air. In both cases, the heat transfer rates are governed by the temperature differences between the air in the jet and the surface ($T_j - T_S$) on the one hand, and between the air in the jet and the ambient air ($T_j - T_A$) on the other hand. If the ambient temperature is such that it accelerates the decrease in temperature difference between the surface and the jet, then the heat transfer coefficient, which is defined with reference to the temperature difference between the impingement surface and the air at the nozzle exit ($T_{jH} - T_S$ or $T_S - T_{jC}$), will be lower.

The effect of ambient temperature is illustrated using the experimental conditions corresponding to the data shown in Figure 4.2.1. The pertinent temperatures are shown in Figure 4.2.2. The temperature difference between the hot jet and the surface ($T_{jH} - T_S$) was 22°C, and between the hot jet and the ambient air ($T_{jH} - T_A$) 23°C. For the cooling jet, the corresponding temperature differences were 13°C ($T_S - T_{jC}$) and 8°C ($T_A - T_{jC}$). On both sides, the effect of the ambient air was to reduce the difference between the effective local temperature of the jet and the surface, thus decreasing the heat transfer rates and the Nusselt numbers compared with those which might be achieved for confined flow under similar conditions.

For the conditions used in this study, the entrainment of ambient air always caused the effective temperature difference between the air in the wall jet T_e and the roll

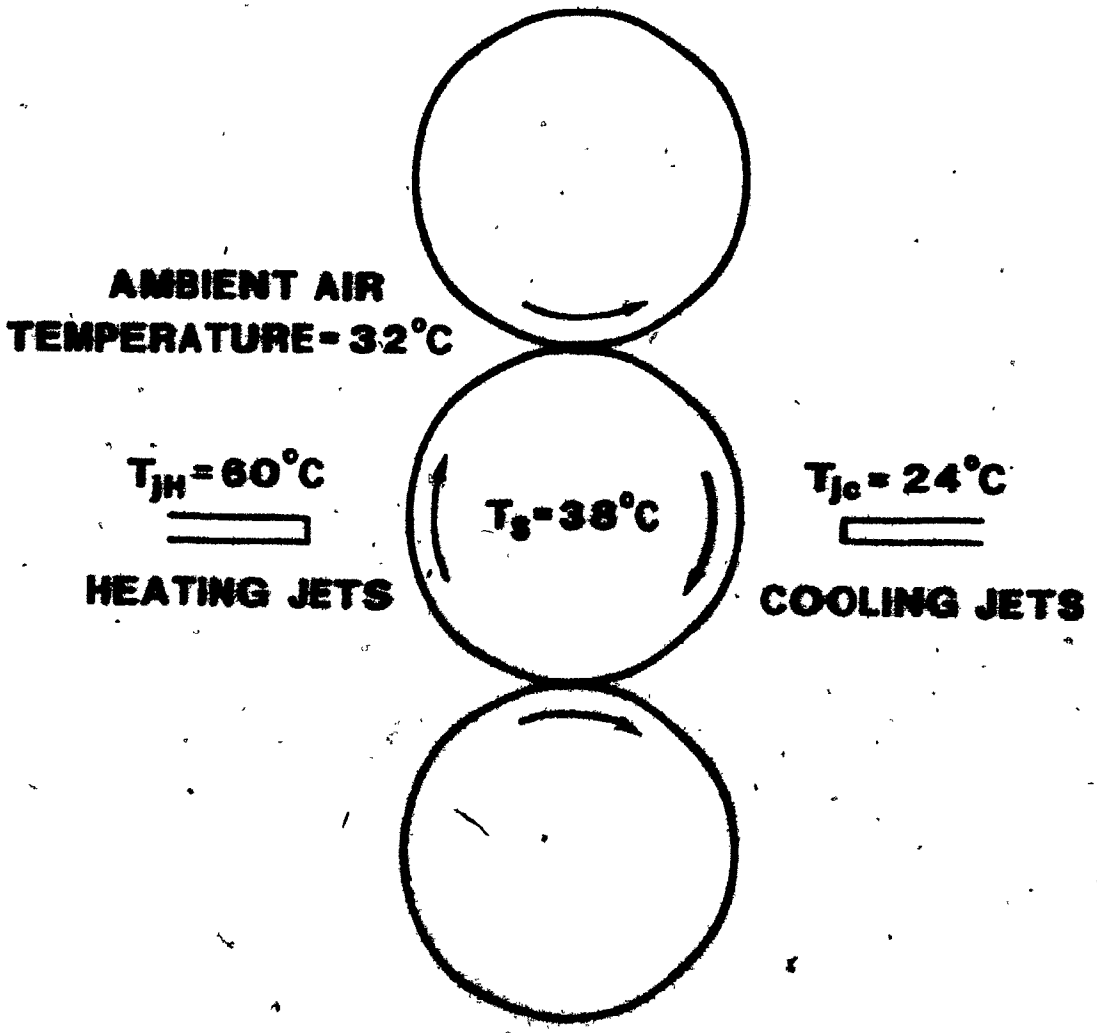

Figure 2.2 Effect of ambient air.

surface T_s to decrease more rapidly than would have been the case without entrainment (i.e. with a confined jet). This caused a reduction in the heat transfer coefficient defined in terms of the temperature difference between the air at the nozzle exit and the roll surface. However, when there is a large temperature difference between the roll surface and the ambient air, the entrainment of ambient air might also cause the heat transfer coefficient to increase. For example, if the temperatures of the jet and the ambient air were approximately equal, then the entrainment of ambient air in the jet would help to maintain the effective temperature difference between the jet and the impingement surface, and thus increase the heat transfer coefficient based on the fixed temperature difference between the nozzle exit and the surface.

It is clear that some account must be taken of the effect of the ambient temperature when dealing with unconfined jets. This might be achieved by including an appropriate temperature ratio in a regression equation for the average Nusselt number, or by redefining the temperature driving force to include some contribution by the ambient air. It might also be appropriate to define the heat transfer coefficients in terms of the actual local temperature differences between the surface and the air in the jet, as proposed by Saad (1981) and Das (1983) for confined jets. However, whereas the local jet temperature can be calculated readily from a heat balance for confined

jets, additional information about the rate of entrainment of ambient air would be required for unconfined jets. An additional difficulty in applying these aproaches in practice is the choice of a suitable ambient temperature. In the case of a calender, the temperature of the air which is carried along by the motion of the roll surface may be quite different from the air surrounding the nozzles. The ambient temperatures reported in the present work were approximate values of the laboratory air near the calender. Unfortunately, these values are not well enough defined to justify using them in a detailed analysis of the data.

4.3 Effect of Nozzle-to-Nozzle Spacing on Axial Nusselt Number Distribution

The jets impinging on the calender roll produce two-dimensional heat flux distributions on the surface of the roll (in the circumferential and in the axial directions) as illustrated in Figure 4.3.1. The experimental technique used in this study produced detailed measurements of the circumferential heat flux distribution. To obtain axial heat flux distributions, measurements of the circumferential heat flux profiles were made with the nozzles at several axial locations relative to the heat flux sensor. In the neutral position (Table 1), the centre nozzle was placed directly over the heat flux sensor, and the sensor would pass through the stagnation point. When the nozzles were displaced axially from the sensor position, and

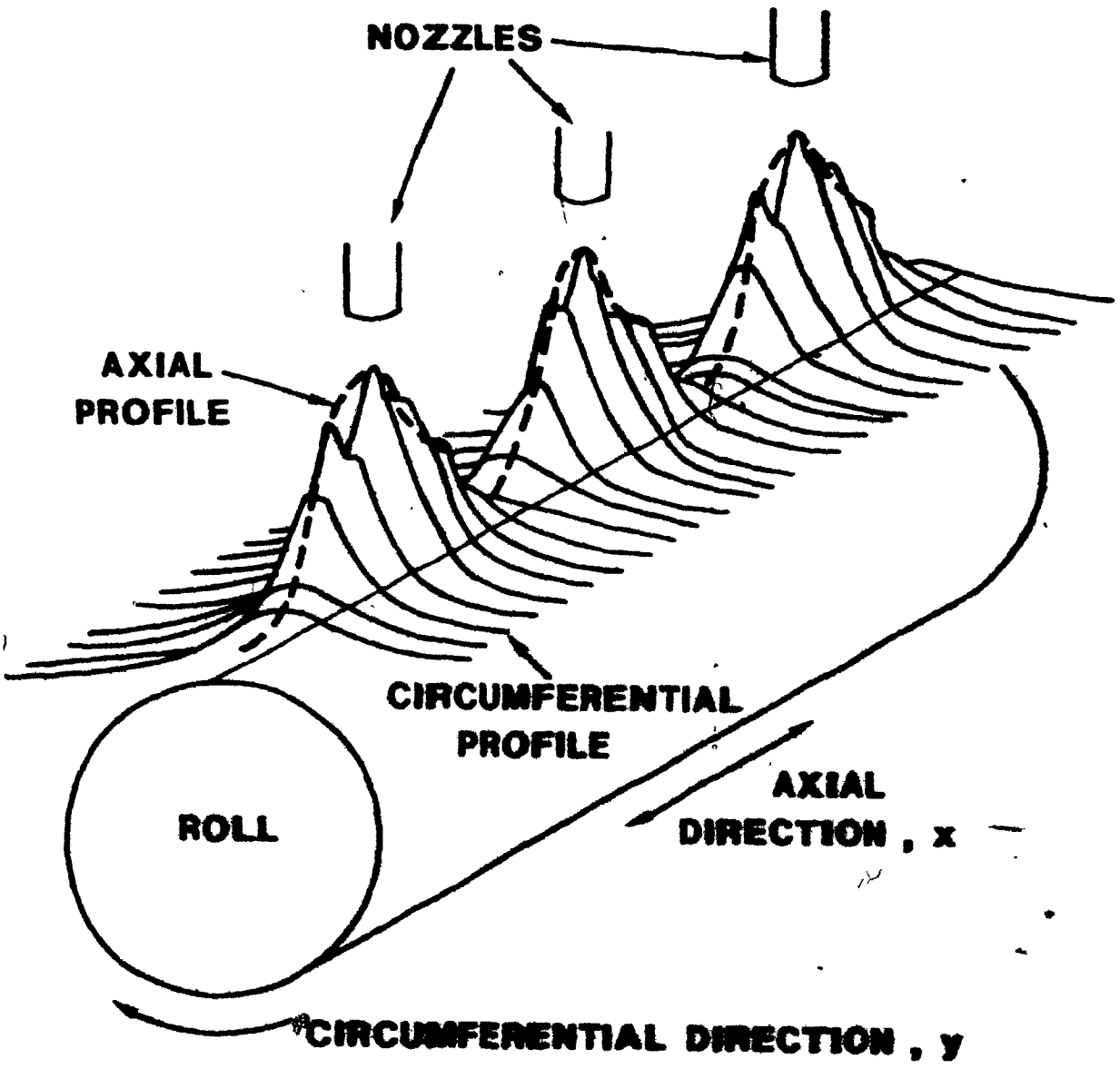

Figure 4.3.1 Two-dimensional heat flux distribution.

the sensor traced the circumferential heat flux distribution at positions x/d≠0, the maxima in the circumferential heat flux profiles, now represented as Nu_{MAX} rather than Nu_o, no longer represented the stagnation point, but approximately the line joining the stagnation points of adjacent nozzles. A plot of the maxima in the circumferential distributions as a function of the axial position, x/d, is then the axial equivalent of the circumferential distribution measured at the neutral position.

Axial distributions were measured, with two nozzle-to-nozzle spacings, S/d = 4 and S/d = 8, which represent the minimum and maximum spacings normally used in commercial application of these nozzles. For both nozzle-to-nozzle spacings, measurements of the circumferential heat flux profiles were made at intervals of one nozzle diameter in axial position. The entire range of positions covered on both sides of the stagnation point correspond to the position midway between the centre and adjacent nozzles, as outlined in Table 1.

The circumferential Nusselt number distributions for nozzle-to-nozzle spacing S/d = 8 are shown in Figures 4.3.2 to 4.3.10 for the axial positions, x/d of 0, ±1, ±2, ±3 and ±4 respectively. Figures 4.3.11 to 4.3.15 illustrate the local Nusselt number distributions for S/d = 4 at x/d of 0, ±1, and ±2 respectively. As expected, the heat flux distribution was found to be symmetrical about x/d = 0. This is illustrated in Table 2 by the small differences in

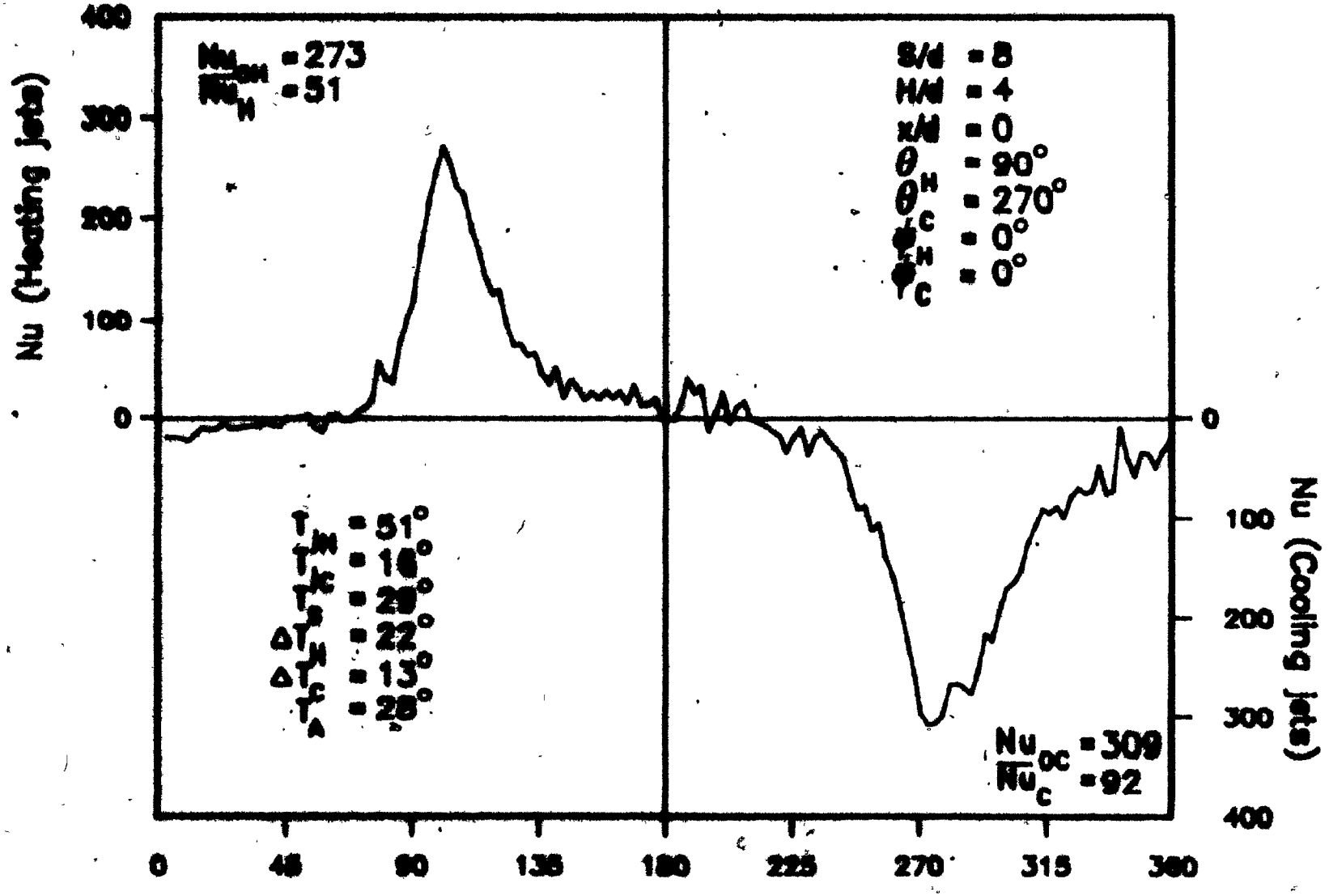

Figure 4.3.2 Circumferential Nusselt number distributions for S/d = 8 and x/d = 0 (Expt. 1).

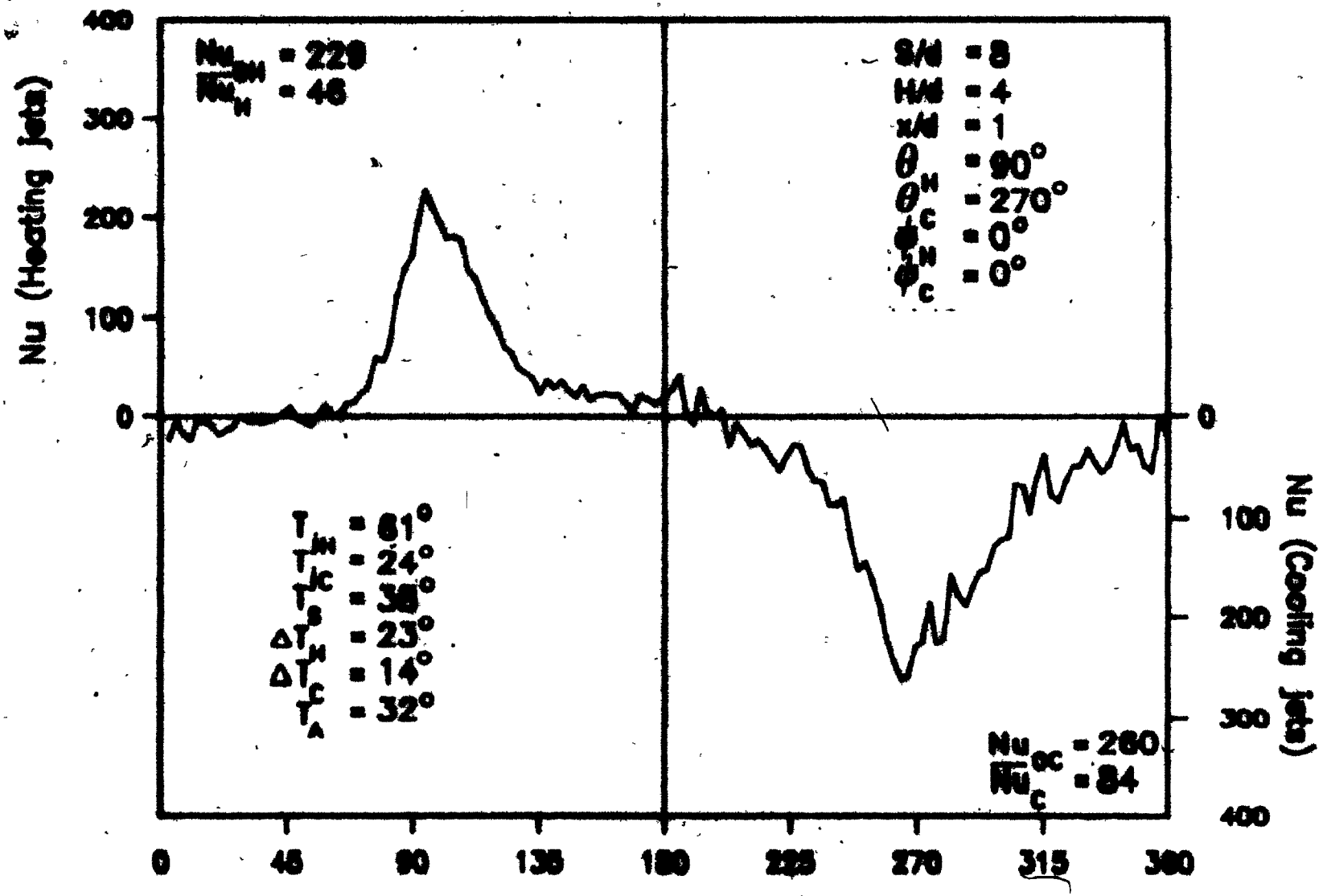

Figure 4.3.3 Circumferential Nusselt number distributions for S/d = 8 and x/d = 1 (Expt. 5).

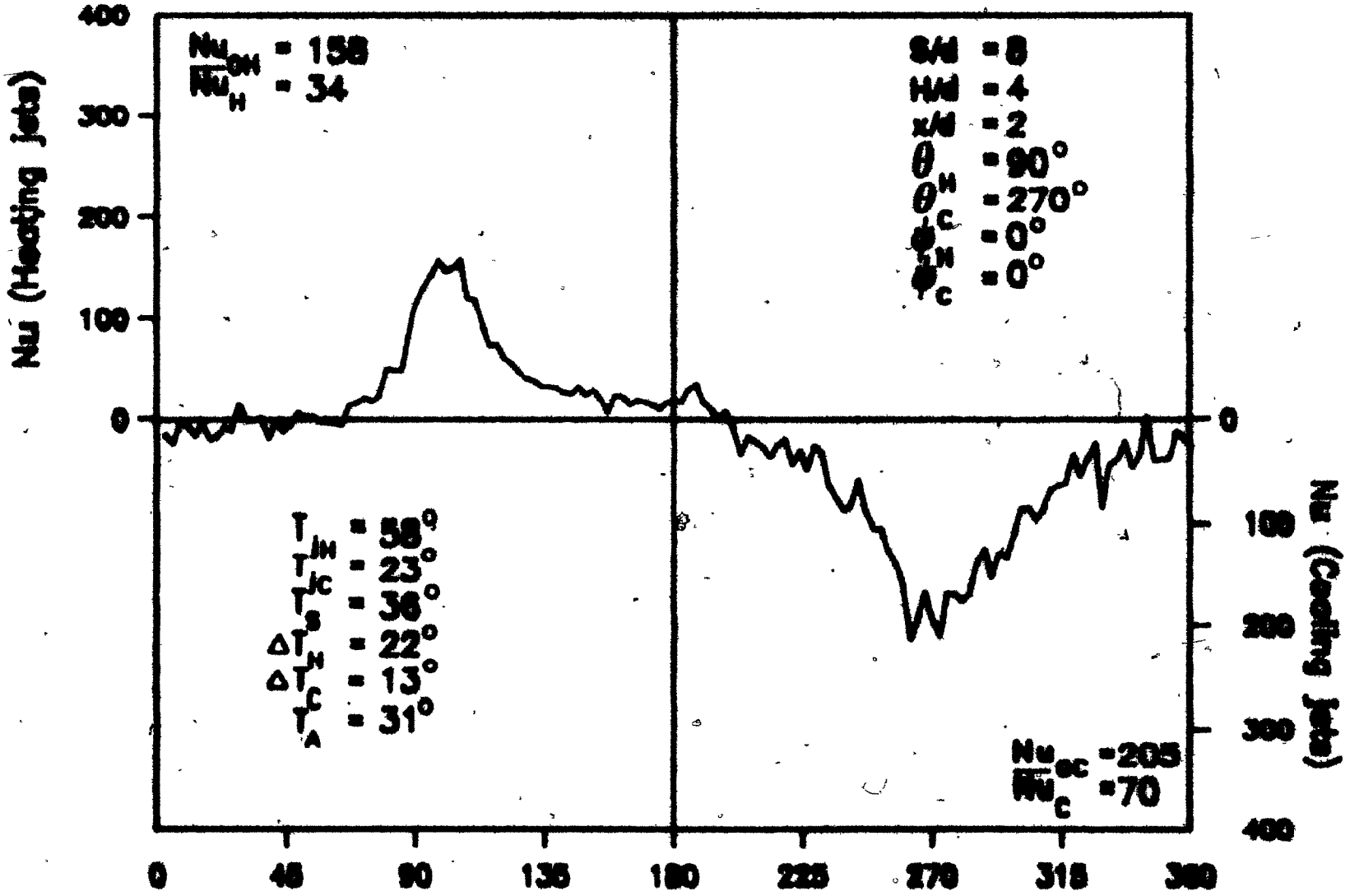

Figure 4.3.4 Circumferential Nusselt number distributions for S/d = 8 and x/d = 2 (Expt. 4).

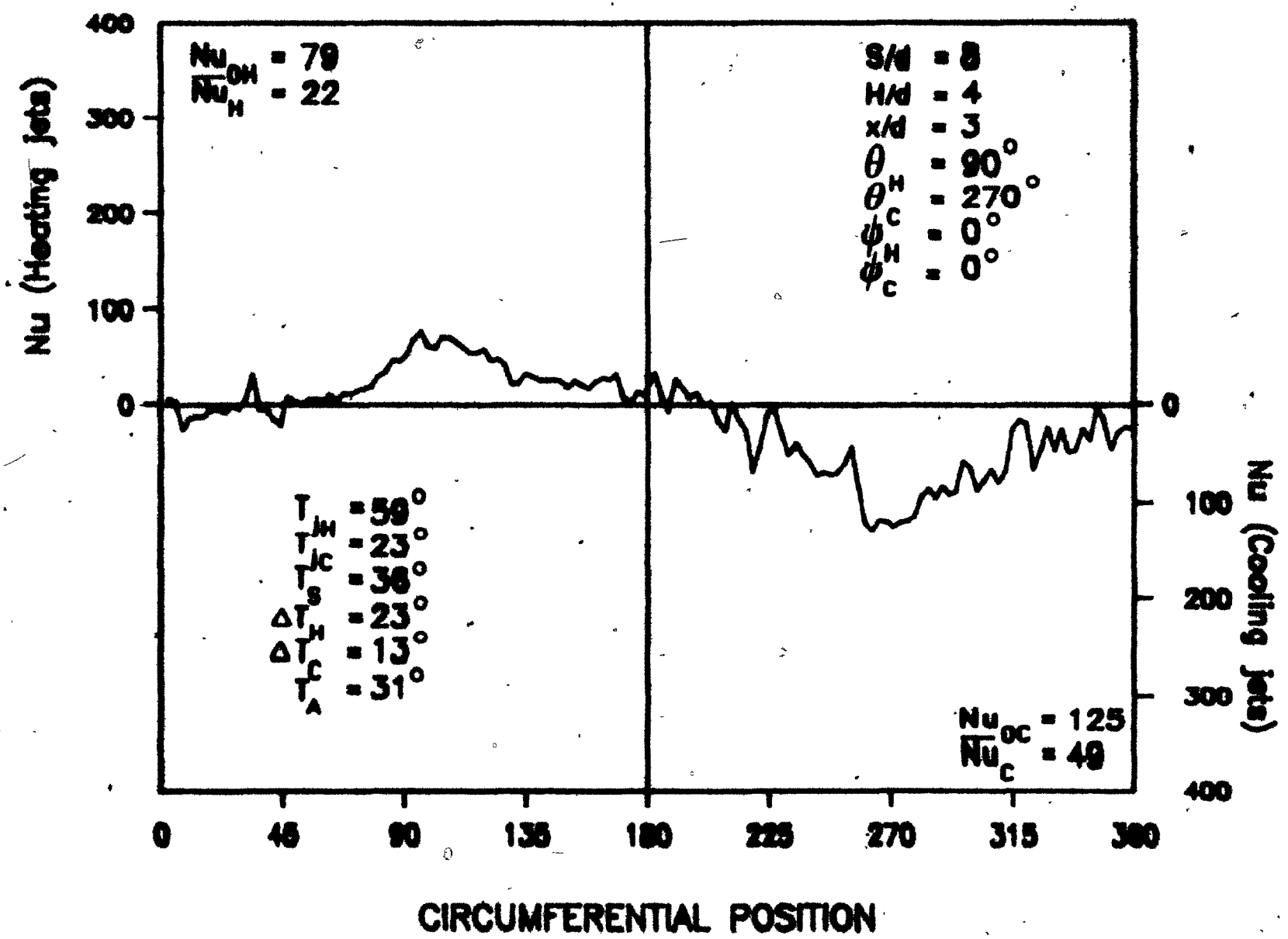

Figure 4.3.5 Circumferential Nusselt number distributions for S/d = 8 and x/d = 3 (Expt. 3).

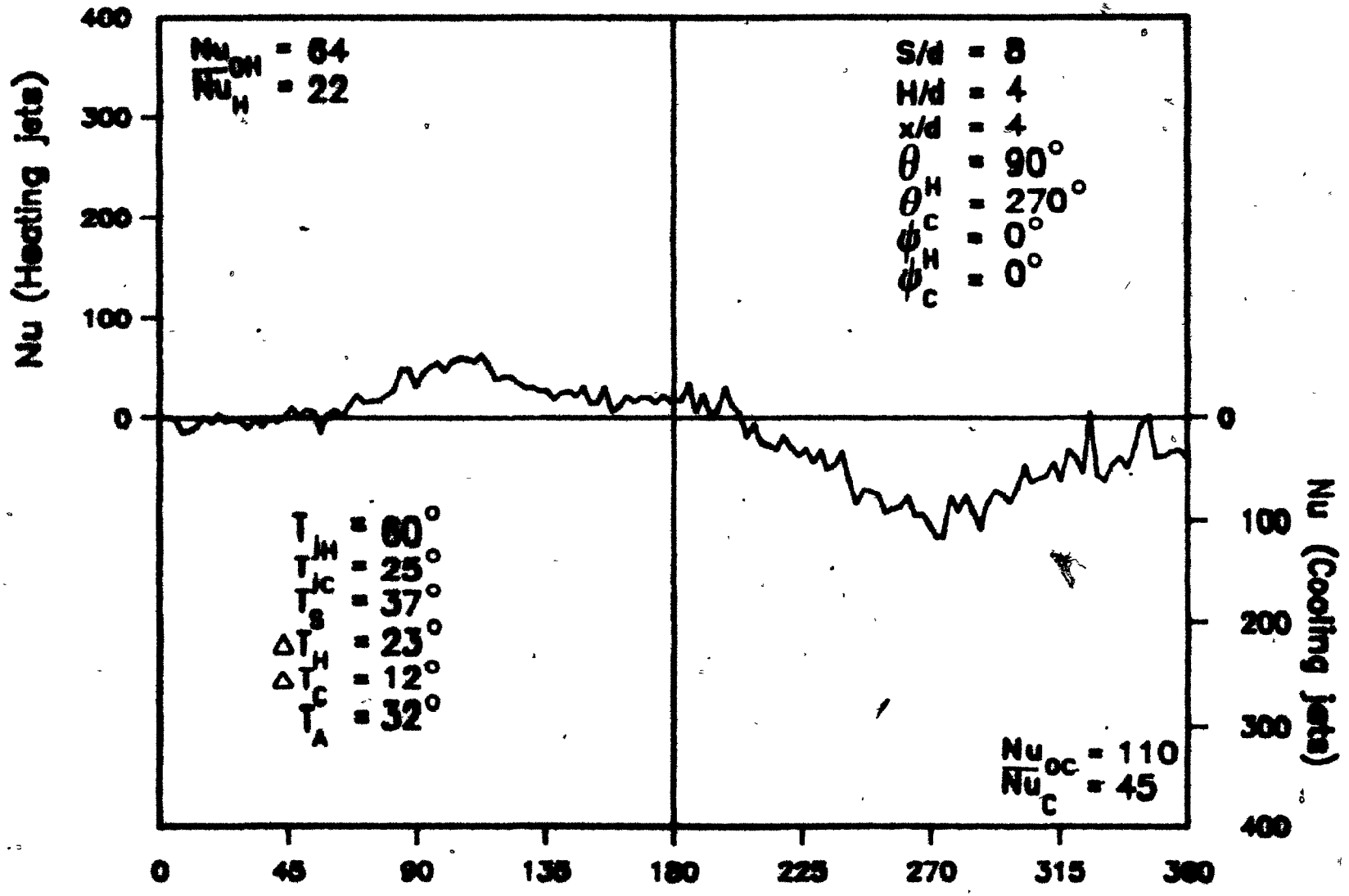

Figure 4.3.6 Circumferential Nusselt number distributions for S/d = 8 and x/d = 4 (Expt. 2).

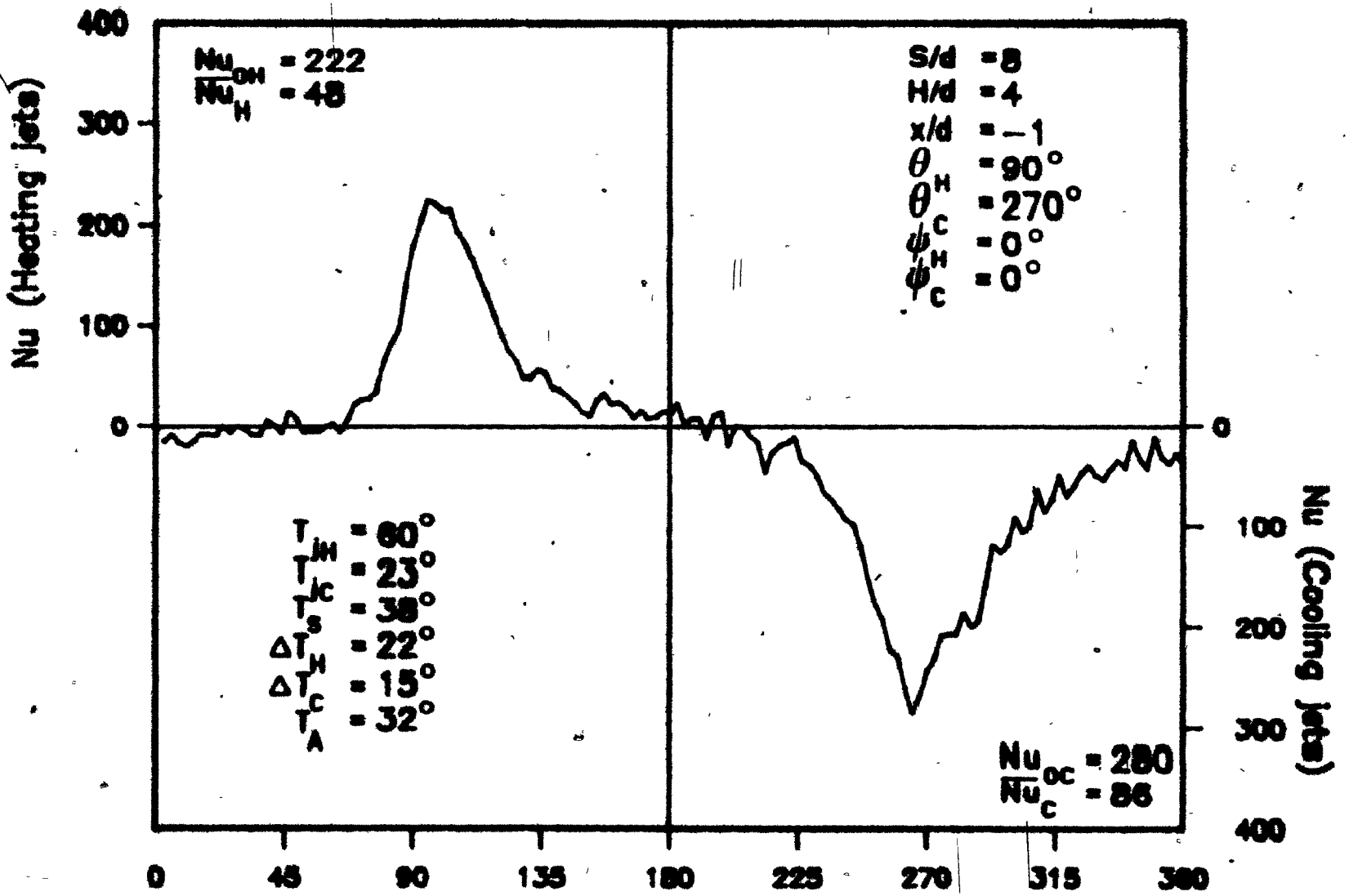

Figure 4.3.7 Circumferential Nusselt number distributions for S/d = 8 and x/d = -1 (Expt. 6).

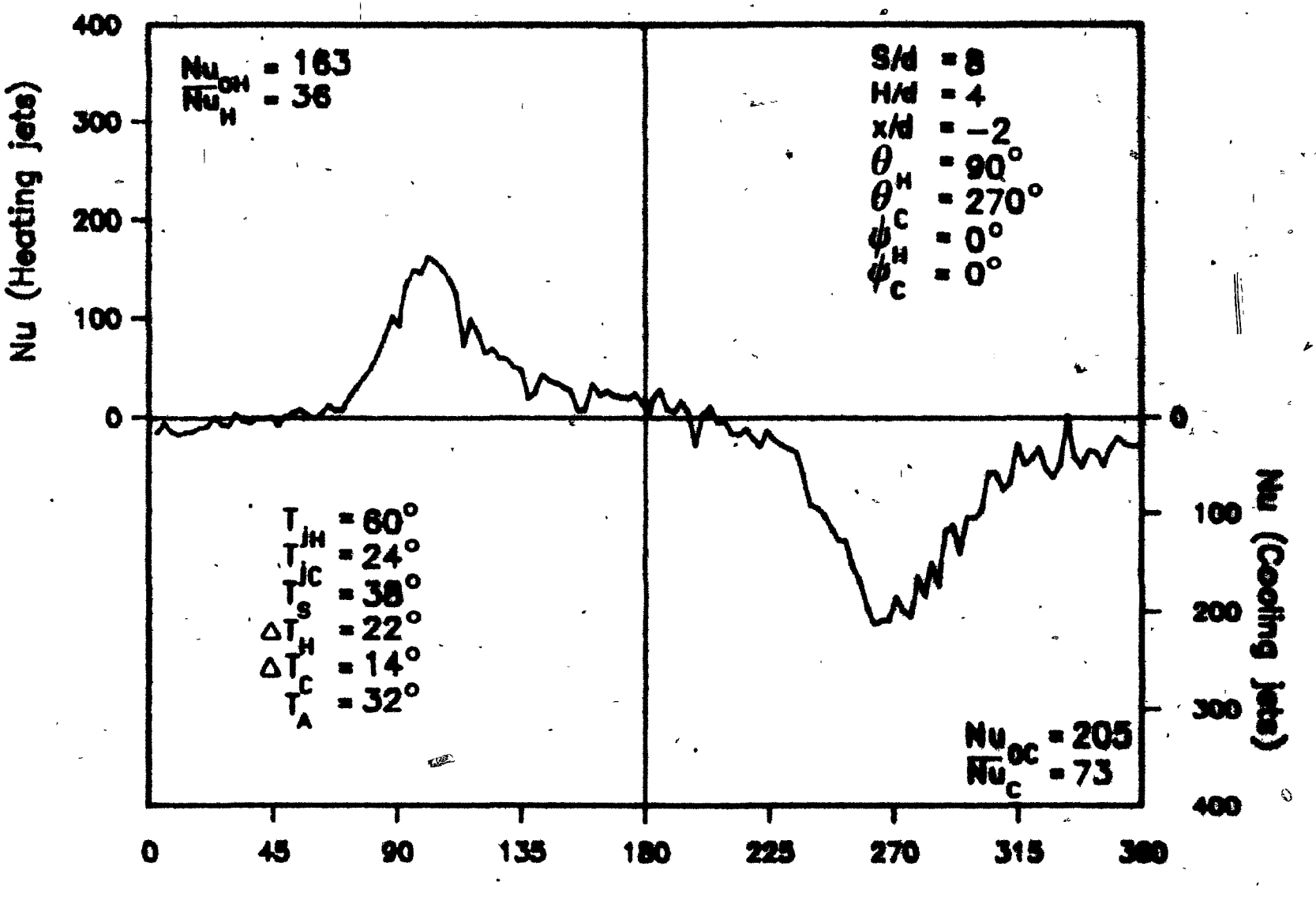

Figure 4.3.8 Circumferential Nusselt number distributions for S/d = 8 and x/d = −2 (Expt. 7).

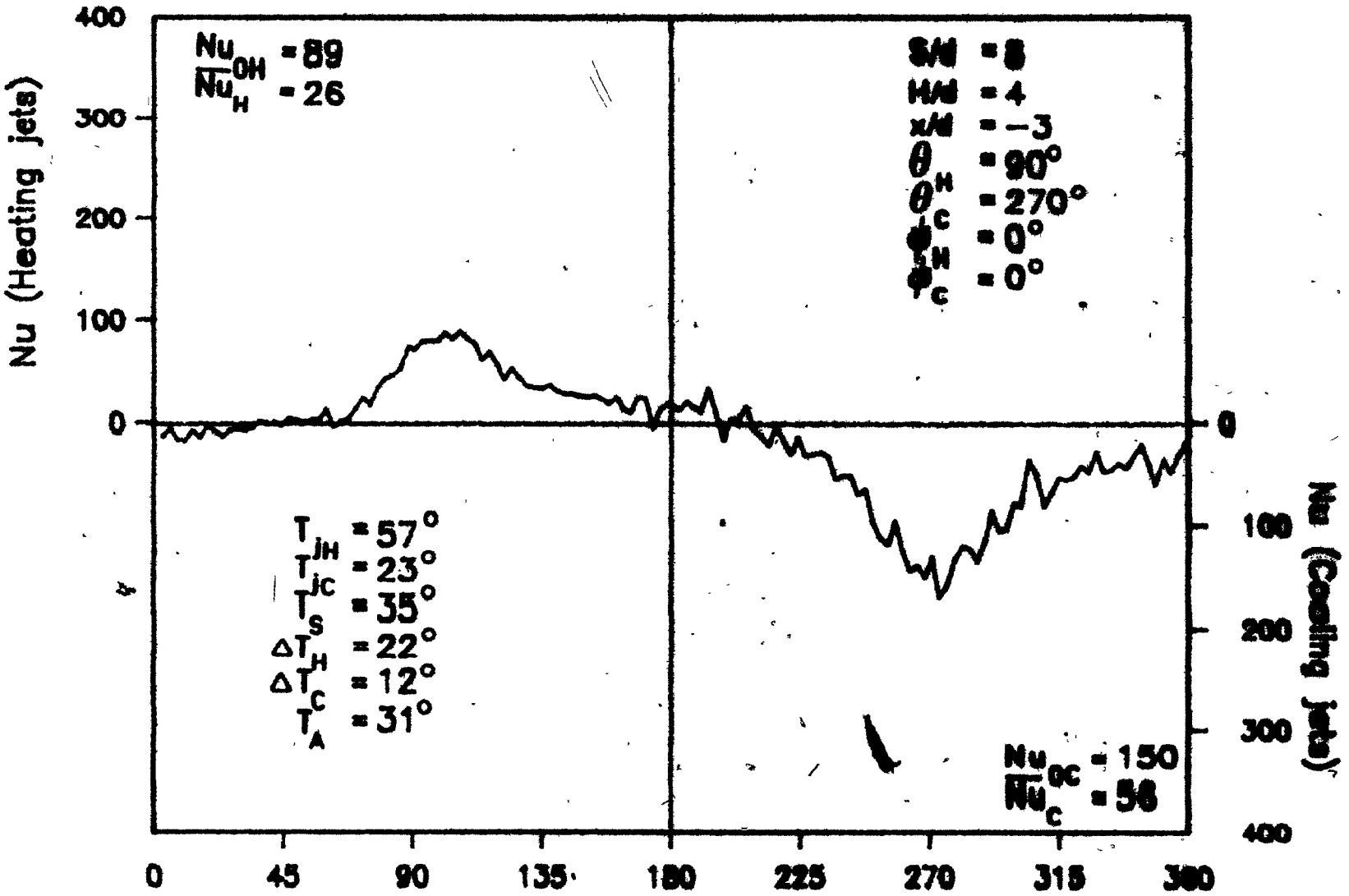

Figure 4.3.9 Circumferential Nusselt number distributions for S/d = 8 and x/d = −3 (Expt. 8).

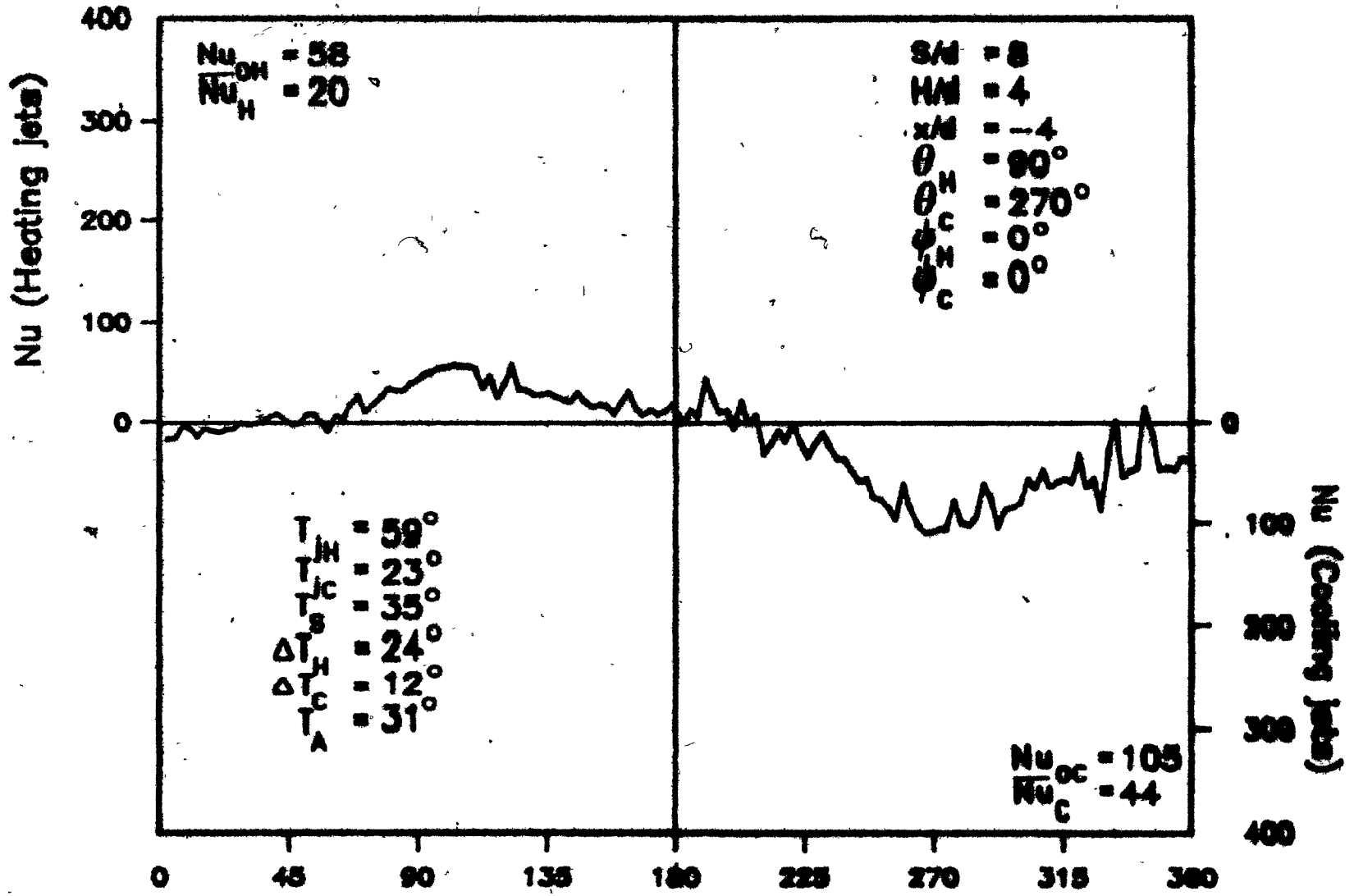

Figure 4.3.10 Circumferential Nusselt number distributions for S/d = 8 and x/d = −4 (Expt. 9).

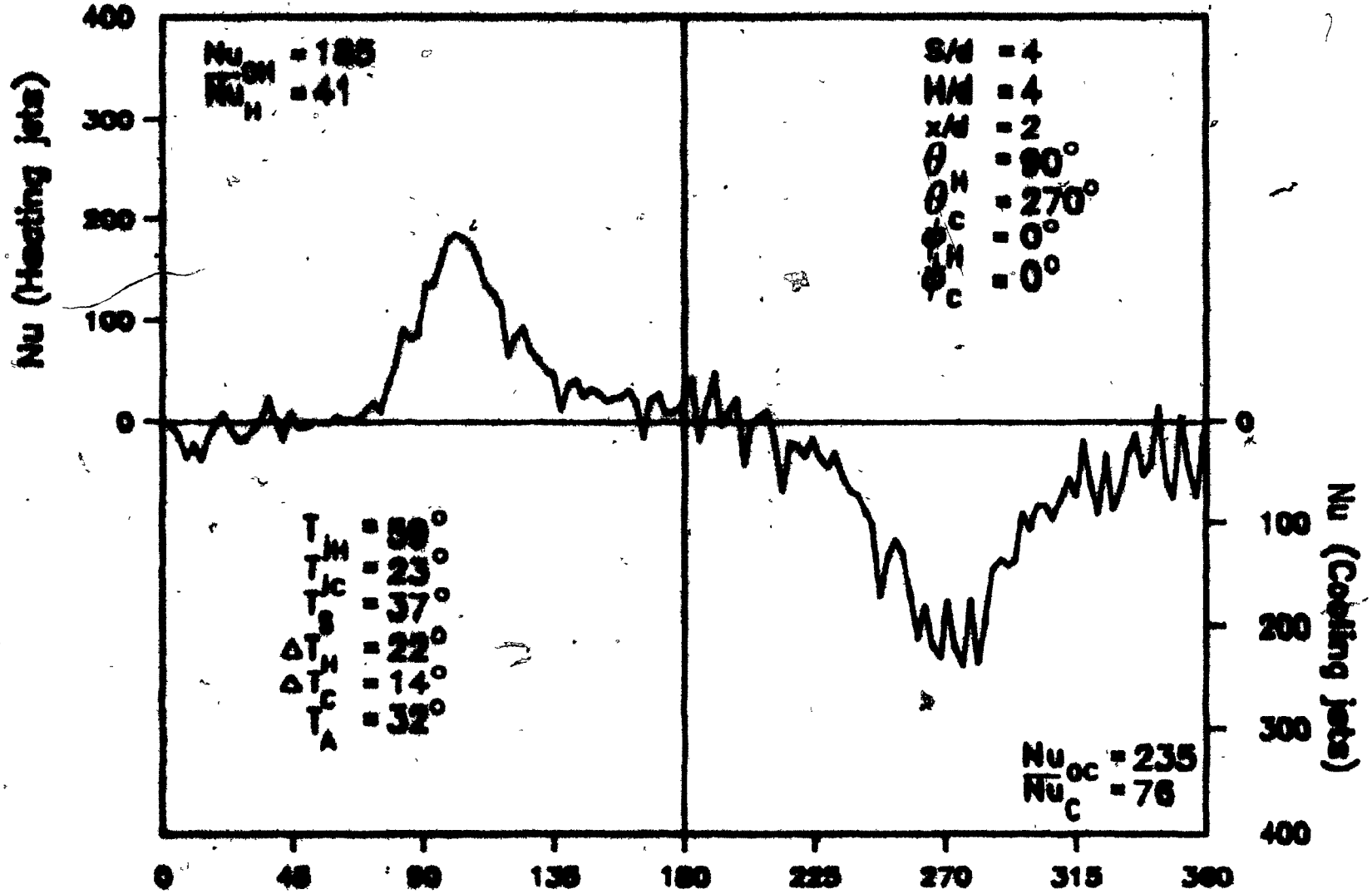

Figure 4.3.11 Circumferential Nusselt number distributions for S/d = 4 and x/d = 2 (Expt. 10).

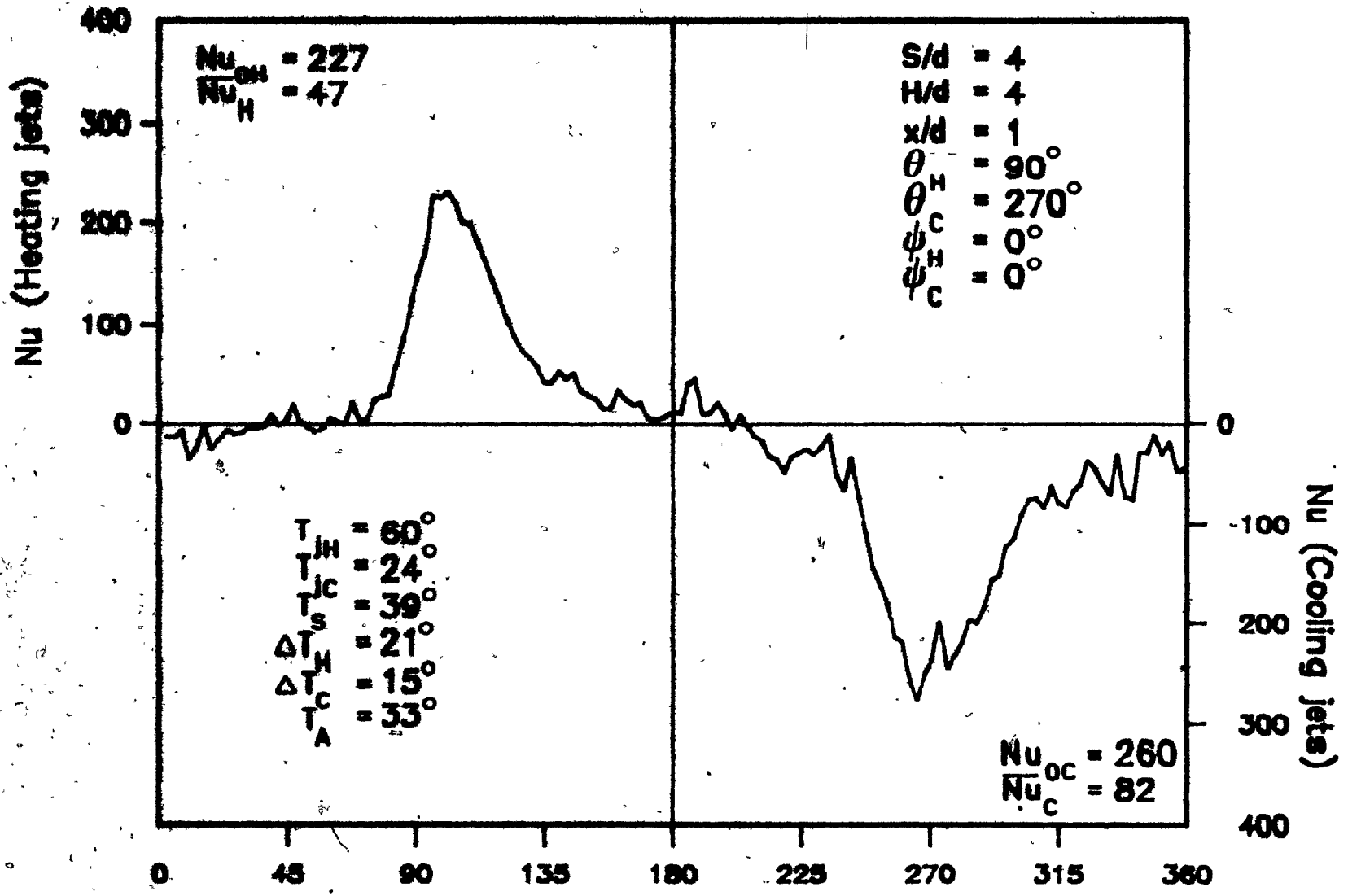

Figure 4.3.12 Circumferential Nusselt number distributions for S/d = 4 and x/d = 1 (Expt. 11).

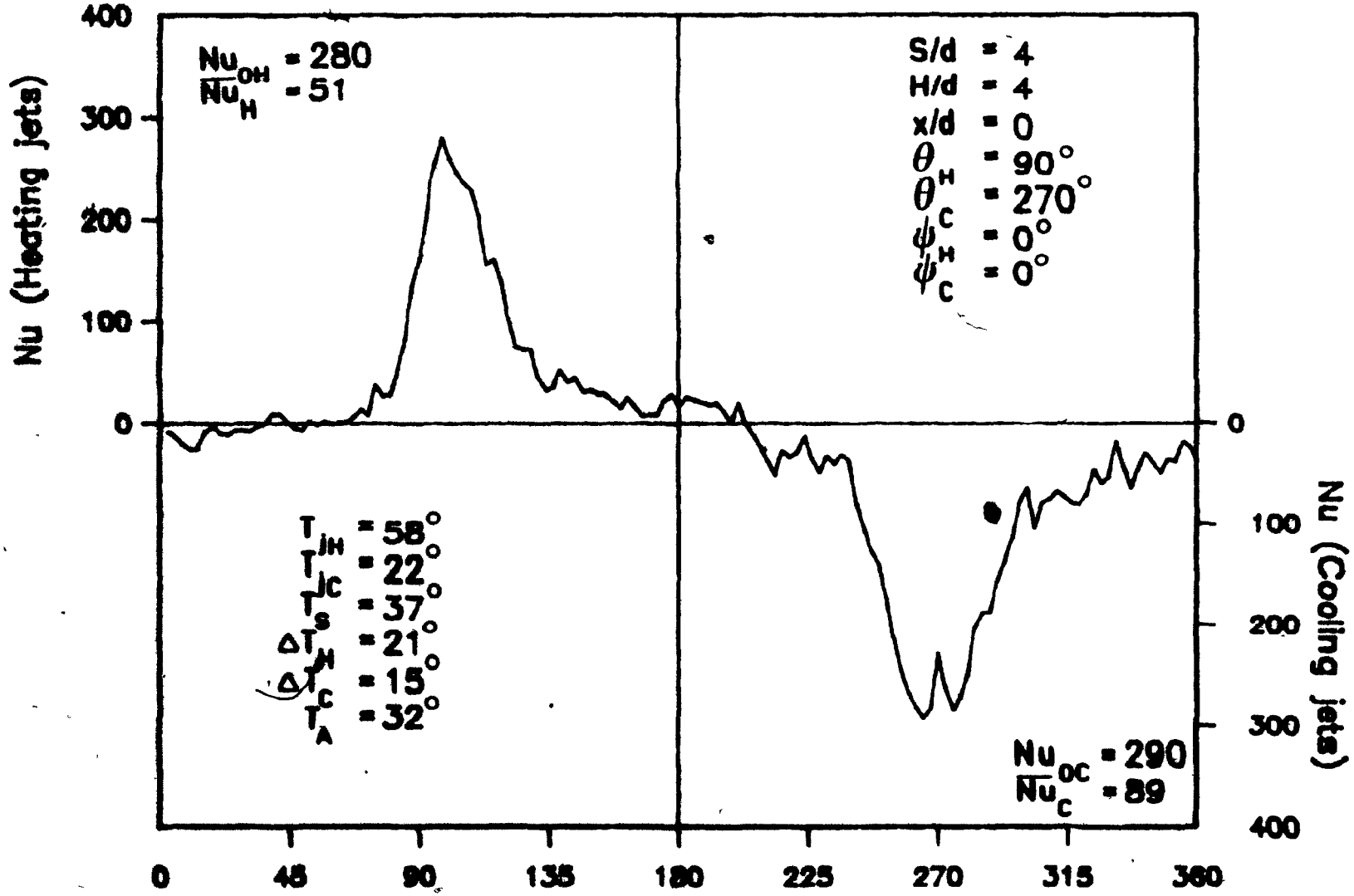

Figure 4.3.13 Circumferential Nusselt number distributions for S/d = 4 and x/d = 0 (Expt. 12).

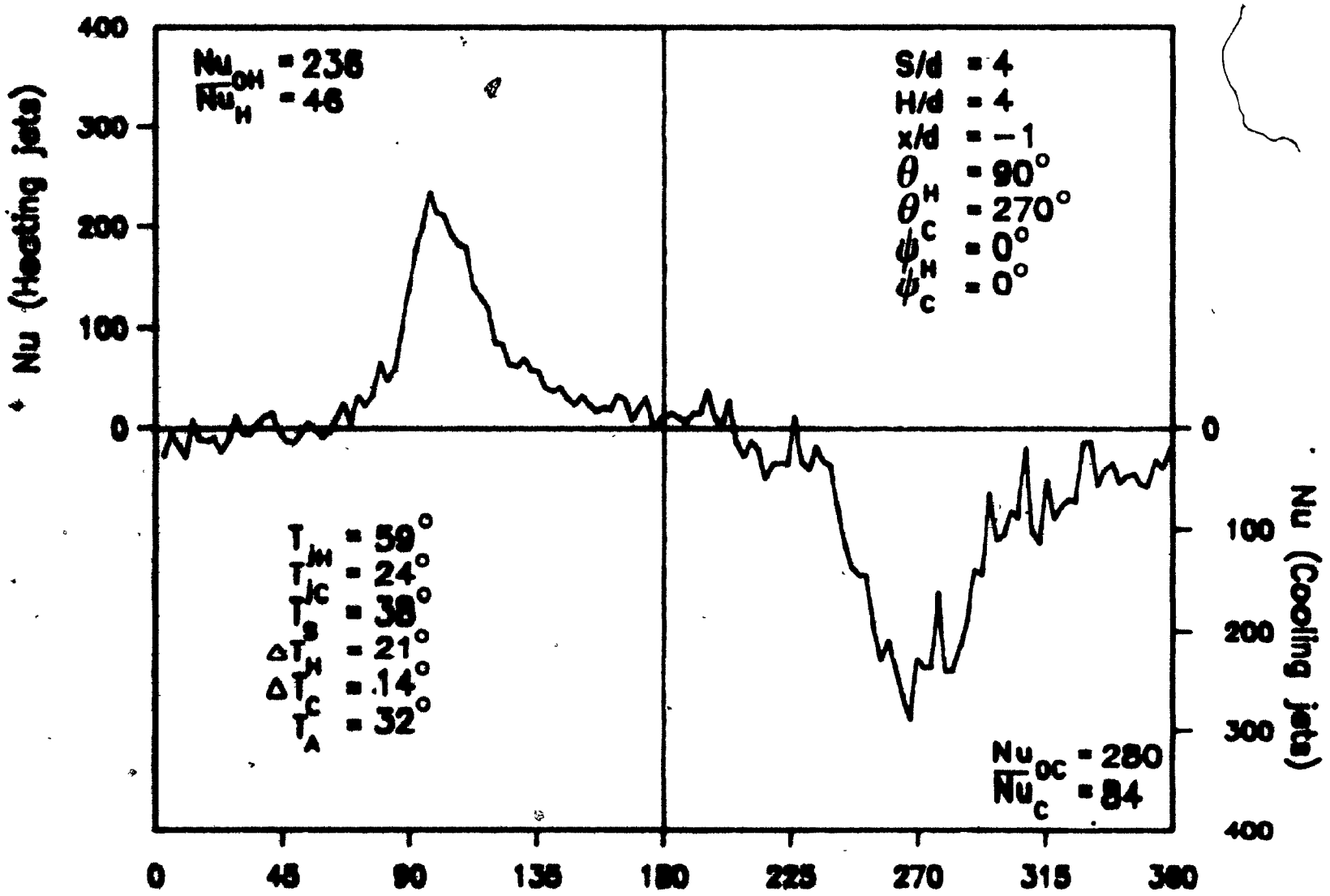

Figure 4.3.14 Circumferential Nusselt number distributions for S/d = 4 and x/d = −1 (Expt. 13).

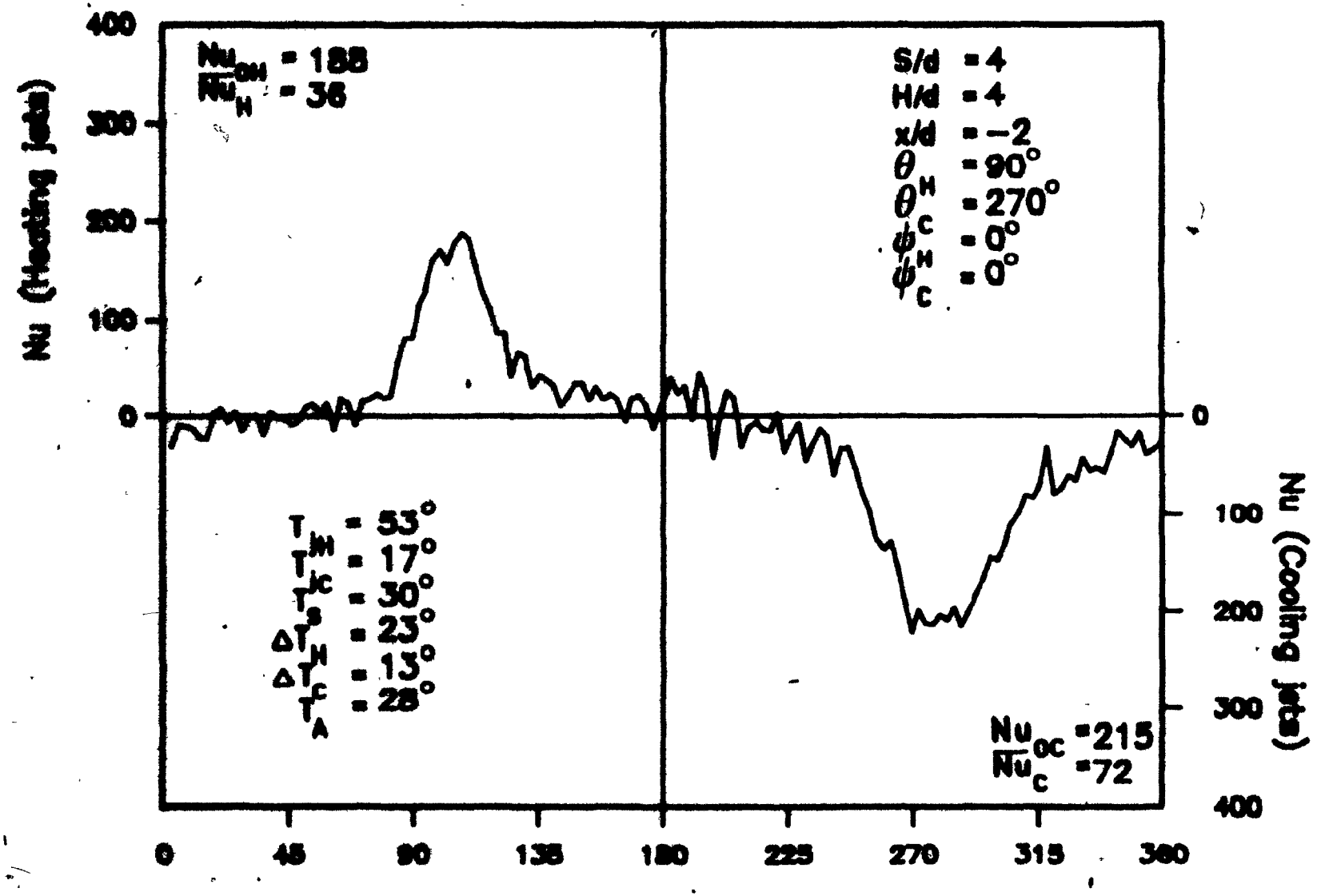

Figure 4.3.15 Circumferential Nusselt number distributions for S/d = 4 and x/d = -2 (Expt. 14).

Nu_{MAX} and $\overline{Nu}$ for corresponding x/d positions. This axial symmetry in the heat flux provides further confirmation of the reliability of the experimental technique.

The Nusselt number distribution at x/d = 0 for S/d = 8 in Figure 4.3.2 is identical to the one already discussed in the previous section (Figure 4.2.1, Section 4.2). The features which were found in this distribution, including the lack of symmetry in local Nusselt numbers about the stagnation point and the occurance of a secondary maximum where the roll surface motion is away from the jets, are also evident in the Nusselt number distribution for x/d≠0. With increasing axial distance, |x/d|, from the stagnation point, Nusselt number decreases, and some of the characteristic features of the circumferential profiles disappear.

The maximum Nusselt numbers, Nu_{MAX}, from each of the circumferential distributions for S/d = 4 and S/d = 8 are shown as a function of x/d in Figure 4.3.16. At x/d = 0, the Nu_{MAX} is in fact the stagnation Nusselt number, Nu_o. From x/d = 0, the Nu_{MAX} decrease to a minimum at the midpoint between adjacent nozzles (x/d = ±2 for S/d = 4, x/d = ±4 for S/d = 8). At the stagnation point, x/d = 0 and in the region from x/d = -1 to x/d = 1, the Nu_{MAX} are essentially unaffected by nozzle-to-nozzle spacing, S/d. The fact that, as S/d is decreased from 8 to 4, Nu_{MAX} for the cooling jets decreased by 11% while Nu_{MAX} for the heating jets increases by 6% is interpreted as experimental scatter, i.e.

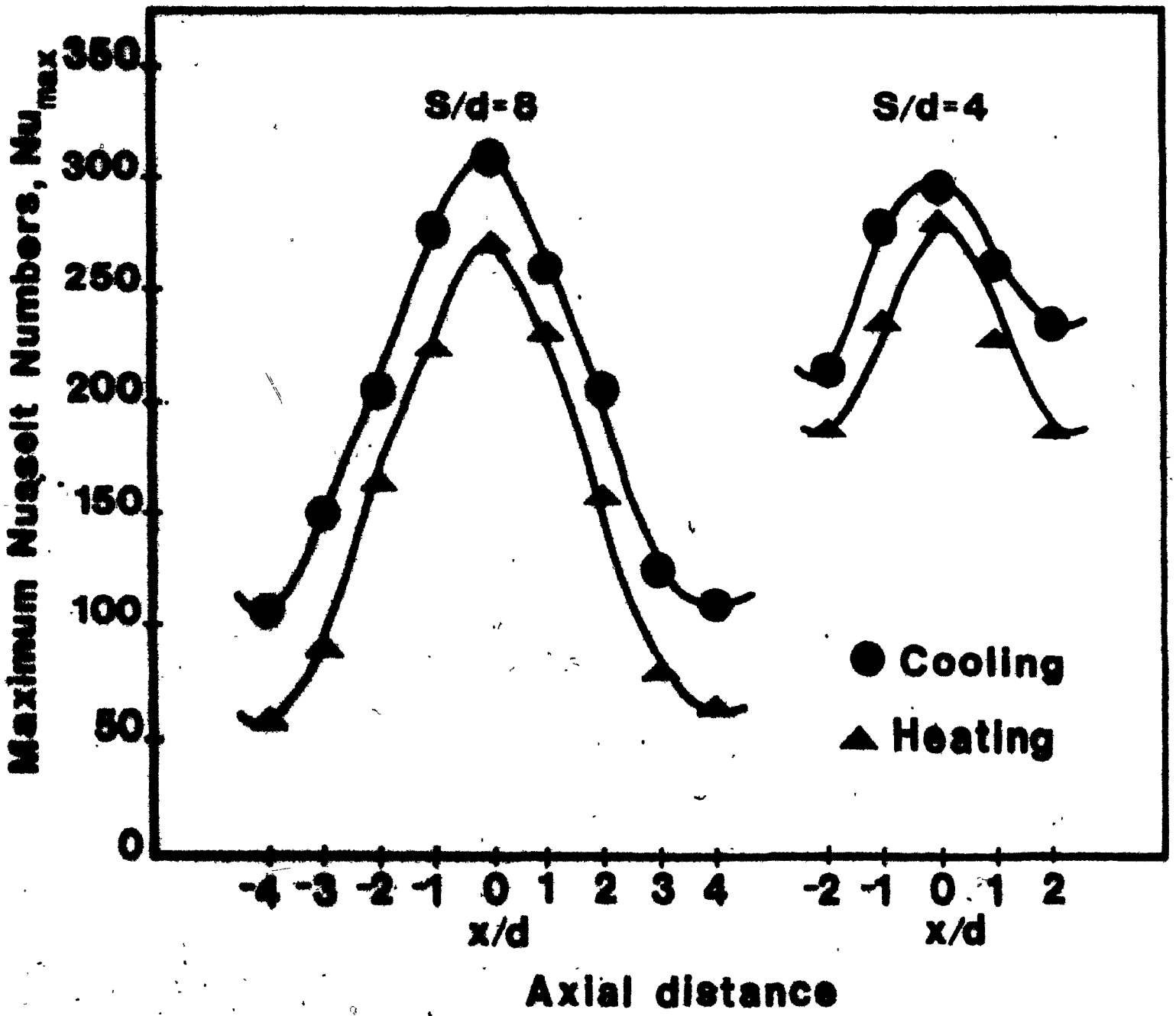

Figure 4.3.16 Effect of axial distance on maximum Nusselt numbers for S/d = 8 and S/d = 4.

that Nu_{max} is not significantly affected by S/d over this range. At x/d = ±2, the results for the spacing S/d = 4 come to a minimum, which is somewhat higher than the x/d=±2 value for a spacing of S/d = 8.

Two types of interactions are possible between adjacent jets in a row of jets impinging on a rotating roll; the interaction of jets prior to impingement on the roll and the collision of wall flows between two adjacent impinged jets. The interaction before impact is enhanced when the jets are closely spaced (low S/d) and the nozzle-to-roll distance is large (high H/d). The collision of wall flows becomes more important when the jets are closely spaced (low S/d), the nozzle-to-roll distance is small (low H/d) and the jet velocity is high.

Based on these interactions, Saad (1981) defined three regimes for confined multiple slot jets. These are defined in terms of a critical dimensionless variable, S/H. The three regimes are:

(1) S/H > 3.0, where the jets are an array of non-interacting jets,

(2) 1.4 ≤ S/H ≤3.0, where the collisions of wall flows increases the Nu at the midpoint between adjacent jets but the interaction of jets prior to impingement is negligible such that Nu_o is unaffected,

(3) S/H < 1.4, where both types of interactions are present which causes a decrease in the

Nu_o but increases the Nu at the midpoint of adjacent jets.

In the present study, for both nozzle-to-nozzle spacings, the heat transfer rates were determined at a nozzle-to-roll spacing of H/d=4, thus the S/d=8 and S/d=4 nozzle-to-nozzle spacings correspond to S/H values of 2 and 1 respectively. The interactions found for S/H = 2 (or S/d = 8) are equivalent to those reported by Saad (1981) for S/H ranging from 1.4 to 3.0. However, at S/H = 1 (or S/d = 4), the interactions found are not those predicted by Saad (1981) for S/H < 1.4, since no significant decrease of Nu was found. Thus it may be concluded that a row of unconfined round jets interacts less than an array of confined slot jets.

The Nu_{MAX} distributions in Figure 4.3.16 are the axial equivalents of the circumferential Nusselt number distributions at x/d = 0. However, the circumferential distributions show much more detail because of the dimensions of the sensor and the spacing of measurements in each direction. In the axial direction, the width of the sensor was 39 mm (1.5d) and measurements were made at 25 mm (1d) spacing. In the circumferential direction, the width of the sensor was 8 mm (0.3d) and measurements were made at every 8 mm or 2.5° (0.4d).

The similarity between the circumferential and the axial profiles is illustrated in Figure 4.3.17. In this figure, the axial Nu_{MAX} vs x/d distributions and the

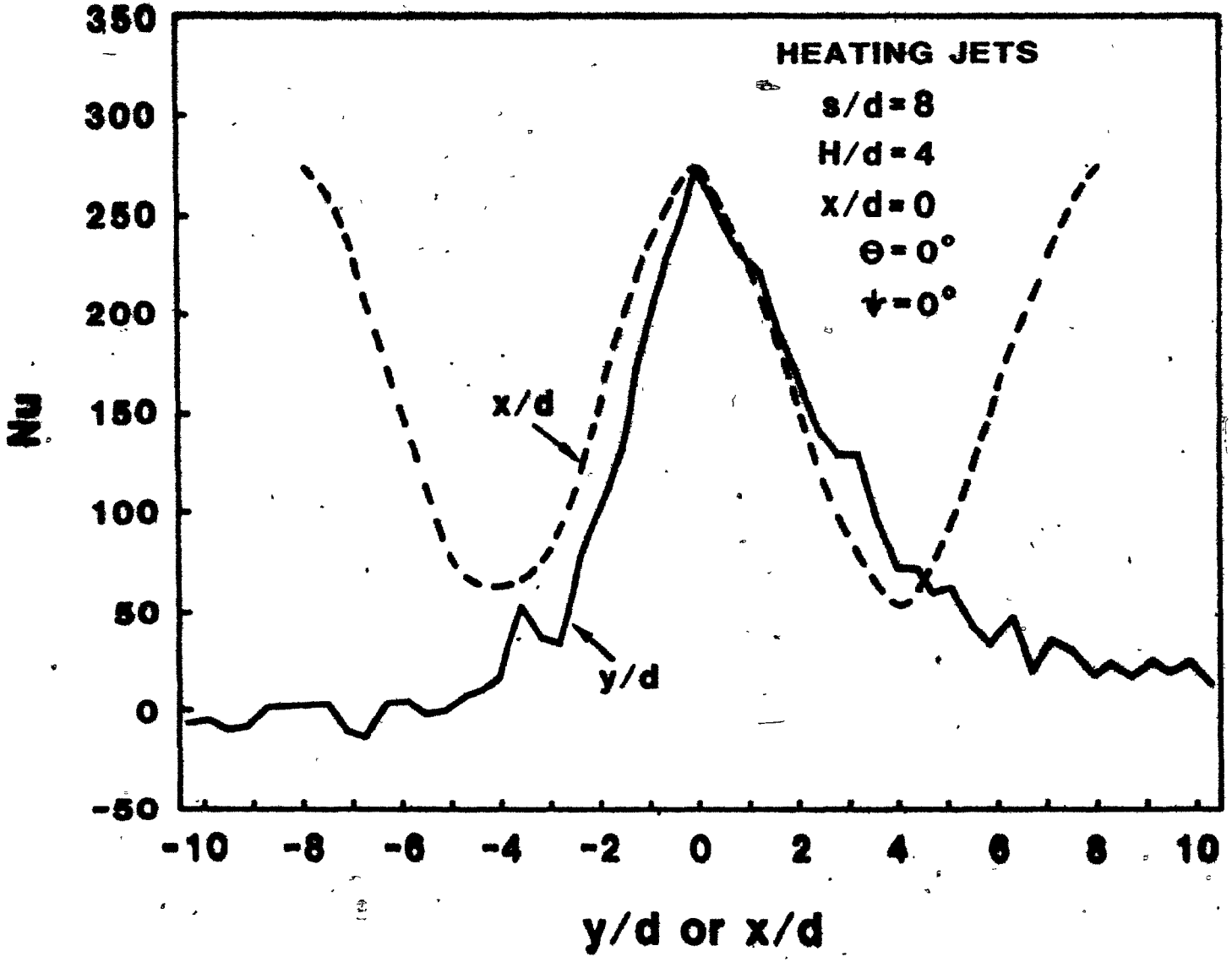

Figure 4.3.17 Circumferential (y/d) and axial (x/d) heat flux distribution.

circumferential Nu vs y/d at x/d = 0 are shown superimposed. Apart from the circumferential profile being skewed in the direction of motion of the roll surface, the shapes of the profiles are amazingly similar as far from the stagnation point as y/d = ±4 and x/d = ±4. Beyond that, the Nusselt numbers in the axial profiles increase again, as they are under the influence of the adjacent nozzles, while the circumferential Nusselt number profiles continue to decrease with distance from the stagnation point. Figure 4.3.17 seems to suggest that with the exception of the slight skewness and the areas of jet interactions near x/d = ±4, the jets behave much like a row of non-interacting jets impinging on a flat plate.

The purpose of using air nozzles on a calender is to adjust the diameter of the roll selectively along its length by cooling or heating the roll. The local diameter change will be proportional to the total amount of heat added or removed at that axial position. Hence it is the circumferentially averaged heat flux at any axial location that is the important factor for cross-machine calender control. Figure 4.3.18 shows the circumferentially averaged Nusselt numbers, $\overline{Nu}$, as a function of x/d for the two nozzle-to-nozzle spacings. These profiles in the axial direction of Nu_{MAX} and $\overline{Nu}$ are very similar in appearance.

The $\overline{Nu}$ vs x/d profiles for S/d = 4 and 8 are very similar from x/d = -1 to x/d = 1. The small apparent changes because of S/d in $\overline{Nu}$ at x/d = 0, which are less than

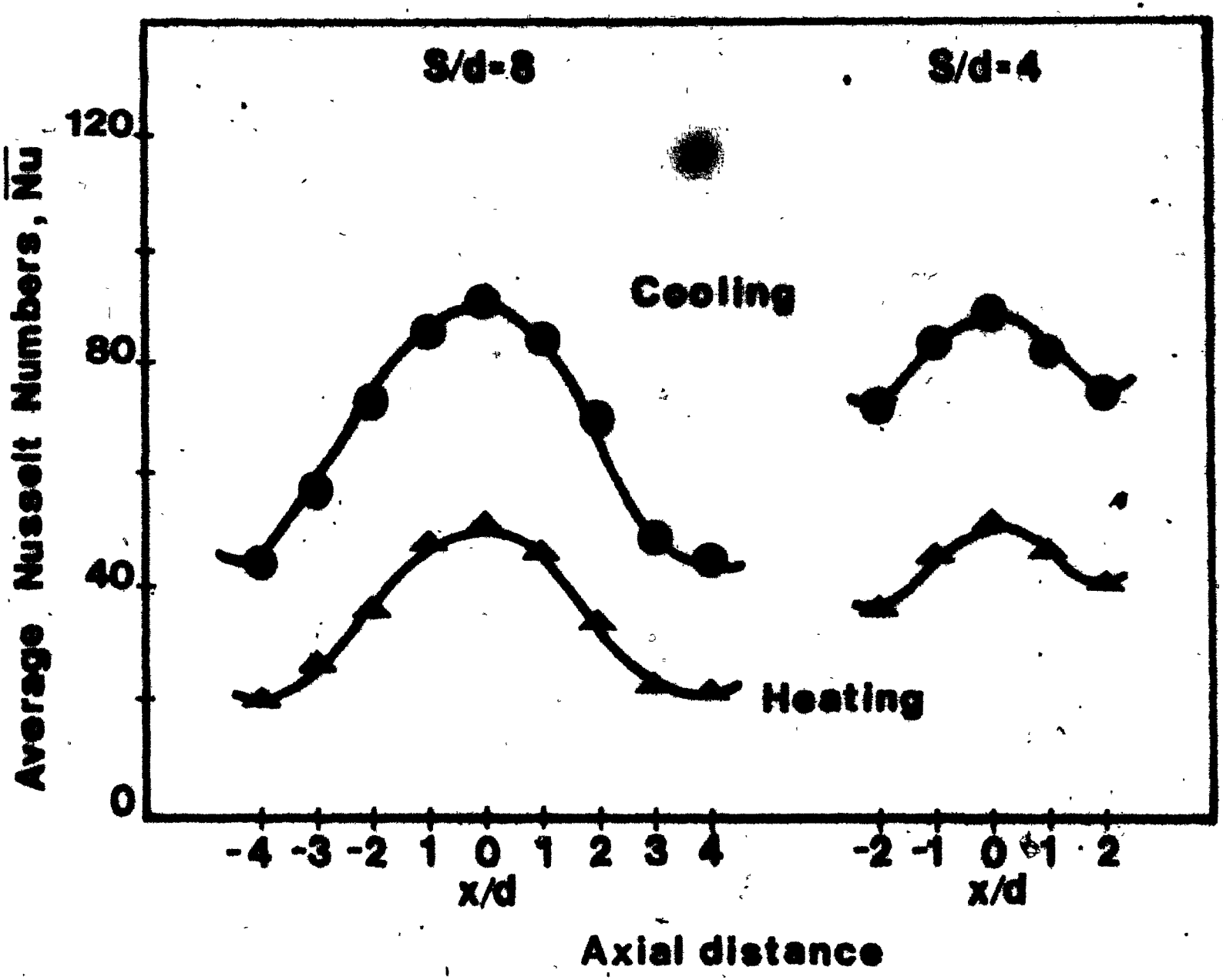

Figure 4.3.18 Effect of axial distance on average Nusselt numbers for S/d = 8 and S/d = 4.

5% for both the heating and cooling jet cases, may be considered to be fluctuations within the limits of experimental error. The small differences in the values of $\overline{Nu}$ are due to the different ambient temperature. At x/d=±2, the S/d = 4 curves have reached a minimum, whereas the S/d = 8 curves continue to descend toward a minimum at x/d = ±4. Apparently, there is no interaction between adjacent nozzles for $|x/d| \leq 1$, but there is for $|x/d| > 1$.

Two important differences between the S/d = 4 and S/d=8 $\overline{Nu}$ vs x/d profiles are the smaller variations in heat flux along the length of the roll and the higher total heat transfer for the S/d=4 spacing. For S/d=4, $\overline{Nu}_{MAX}/\overline{Nu}_{MIN}$ = 1.3, while for S/d = 8 this ratio is 2.0. In cast iron calender rolls, the axial fluctuations will be reduced by conduction in the roll, nonetheless, large fluctuations are undesirable and should be minimized. The axial average Nusselt number, which is indicative of the total heat transferred is 20% higher for the S/d = 4 arrangement. However, it must be realised, that this is a consequence of using twice the number of nozzles and thus twice the amount of air. Per nozzle, the S/d = 8 arrangement actually transfers 50% more heat than the S/d = 4 arrangement.

Clearly it would be desirable to space the nozzles 8 diameters apart to derive more benefit per nozzle, yet by spacing the nozzles 4 diameters apart, a higher and more uniform total heat transfer could be achieved. Both advantages could perhaps be realised by using two rows of

nozzles with an nozzle-to-nozzle spacing of 8 diameters. These would be staggered, so that axially there would be one nozzle every 4 nozzle diameters, and the rows would be separated far enough, that the spacing between the nozzles of the two rows would be at least 8 diameters. In the experimental calender, rows spaced 8d apart would correspond to an angular displacement of 51° between the rows.

In Figure 4.3.19, a comparison is made of the circumferentially averaged Nusselt number as a function of x/d for three cases:

1. One row of nozzles with S/d = 4 (experimental data)
2. One row of nozzles with S/d = 8 (experimental data)
3. Two rows of nozzles, each with S/d = 8 but staggered along the axis by x/d = 4 and positioned 51° apart on the circumference, (approximated as the sum of two rows of the case 1 arrangement).

It was assumed that displacement of the nozzles by $\theta = \pm 25.5°$ from the neutral position will not affect the Nusselt numbers significantly.

It is clear from Figure 4.3.19 that the two separate rows of nozzles spaced at S/d = 8 would be substantially more effective than the single row of nozzles spaced at S/d=4, both in terms of total heat transfer and in terms of the heat transfer uniformity.

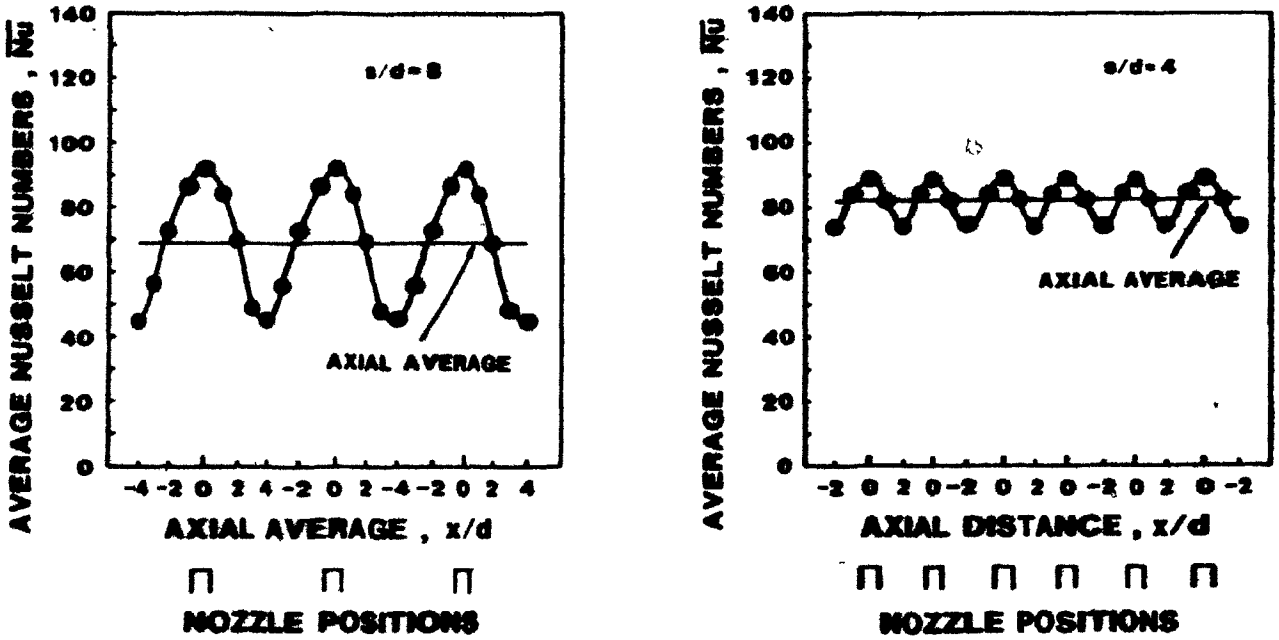

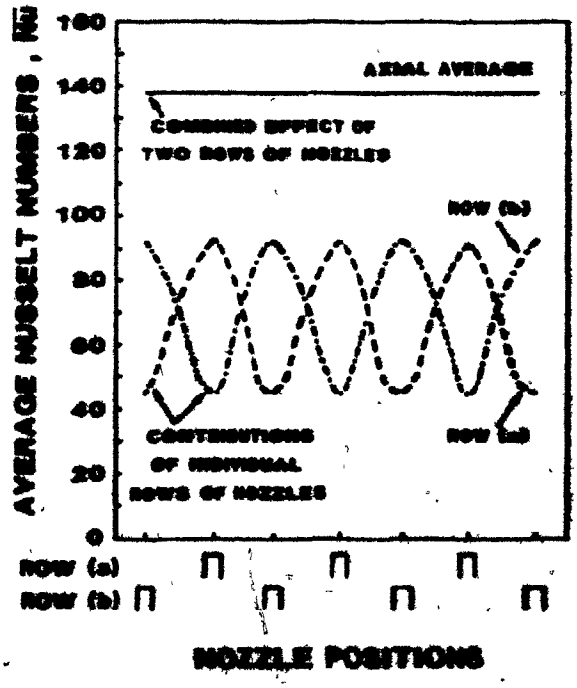

Figure 4.3.19 Comparison of axial heat flux for
(a) 1 row of nozzles with S/d = 8,
(b) 1 row of nozzles with S/d = 4, and
(c) 2 rows of nozzles.

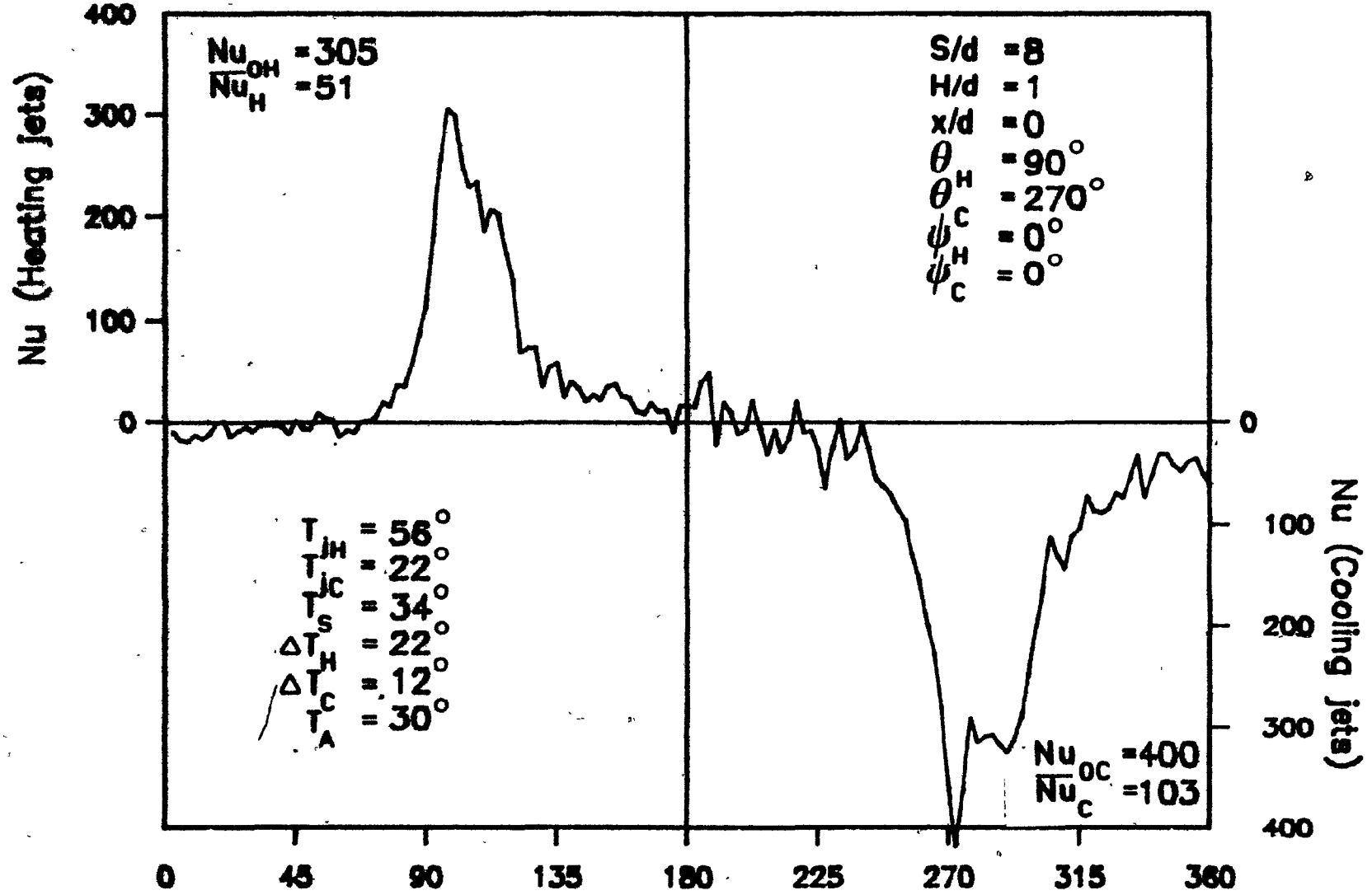

Figure 4.4.1 Circumferential Nusselt number distributions for H/d = 1 (Expt. 15).

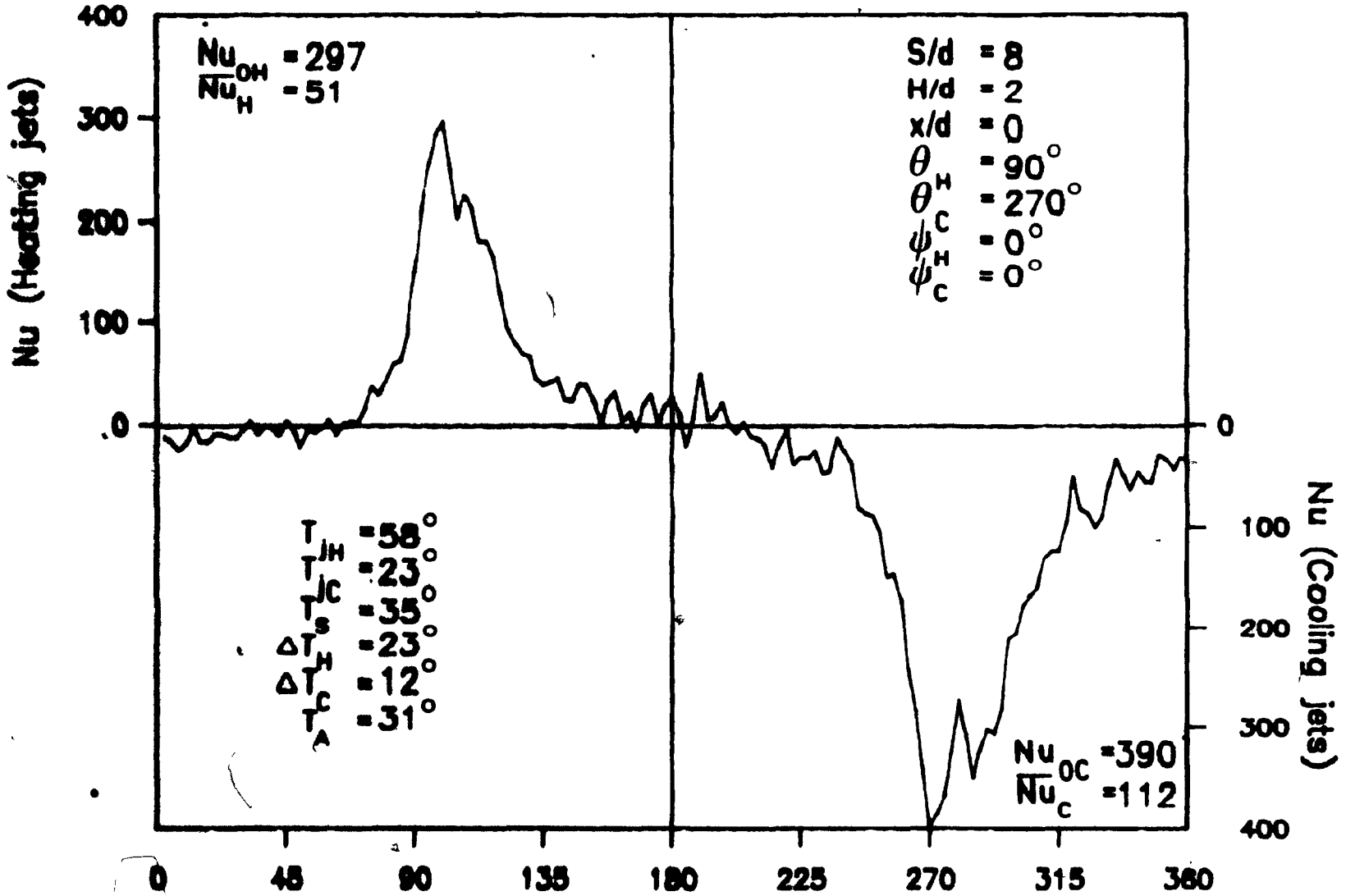

Figure 4.4.2 Circumferential Nusselt number distributions for H/d = 2 (Expt. 16).

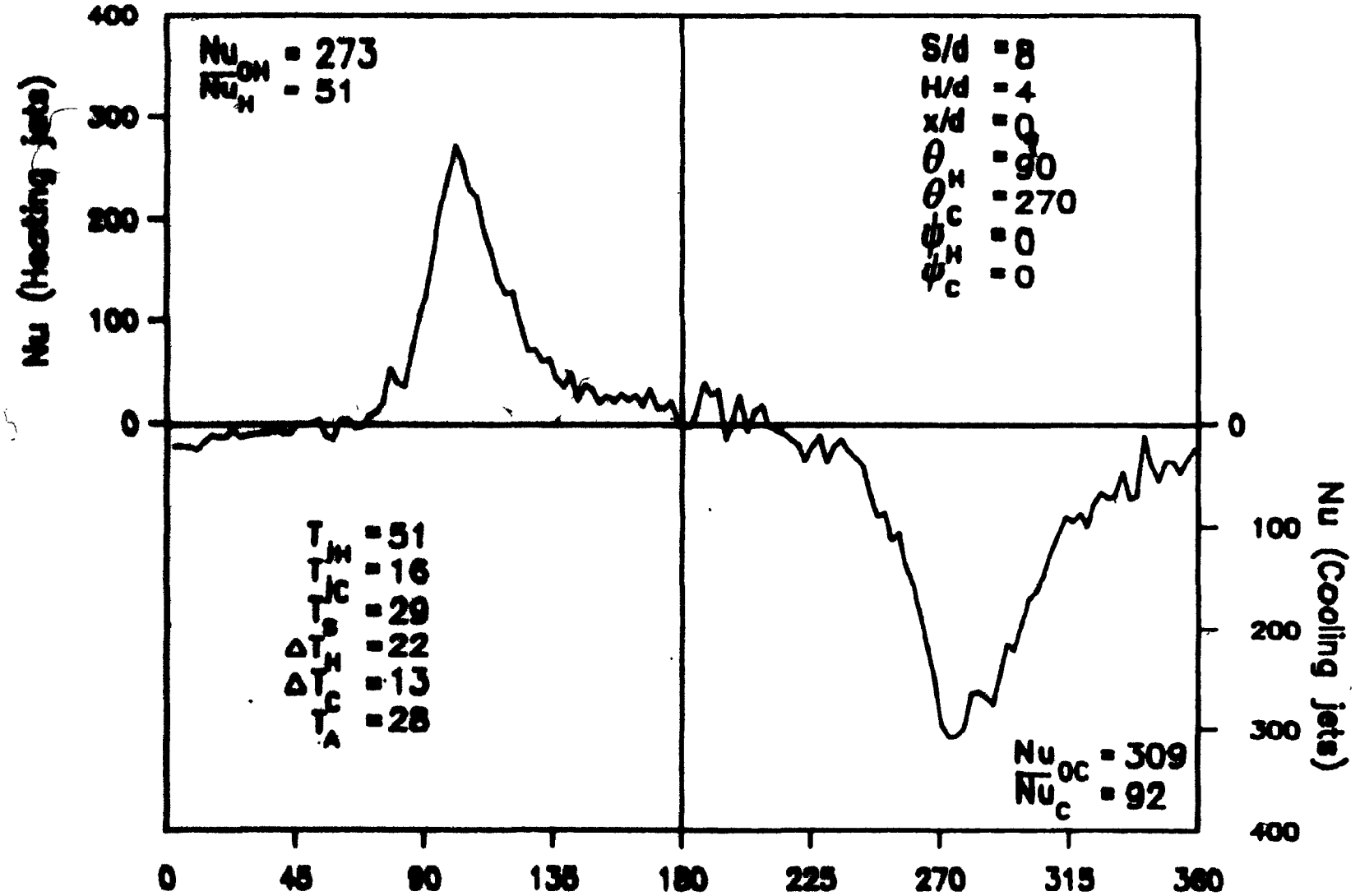

Figure 4.4.3 Circumferential Nusselt number distributions for H/d = 4 (Expt. 1).

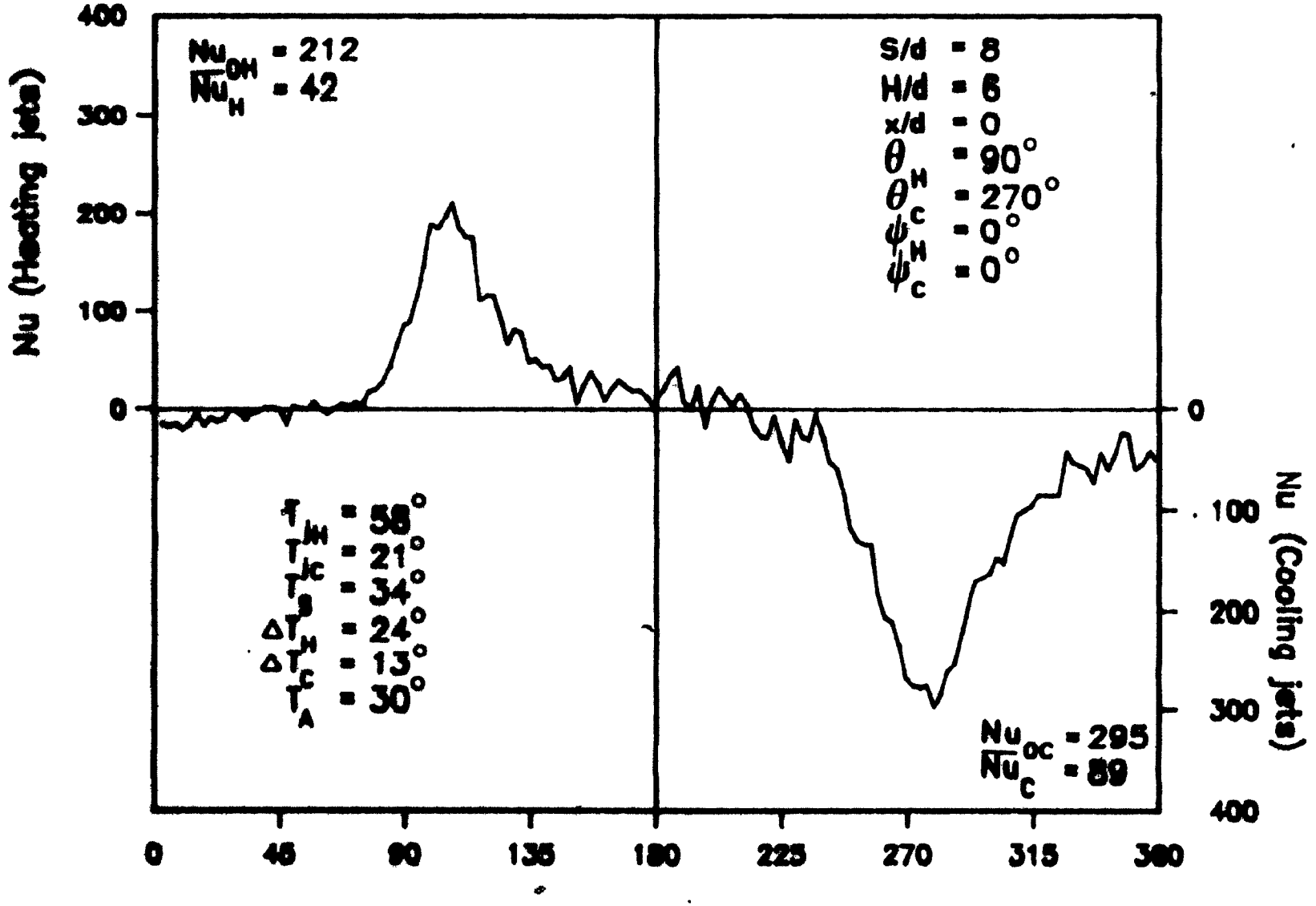

Figure 4.4.4 Circumferential Nusselt number distributions for H/d = 6 (Expt. 17).

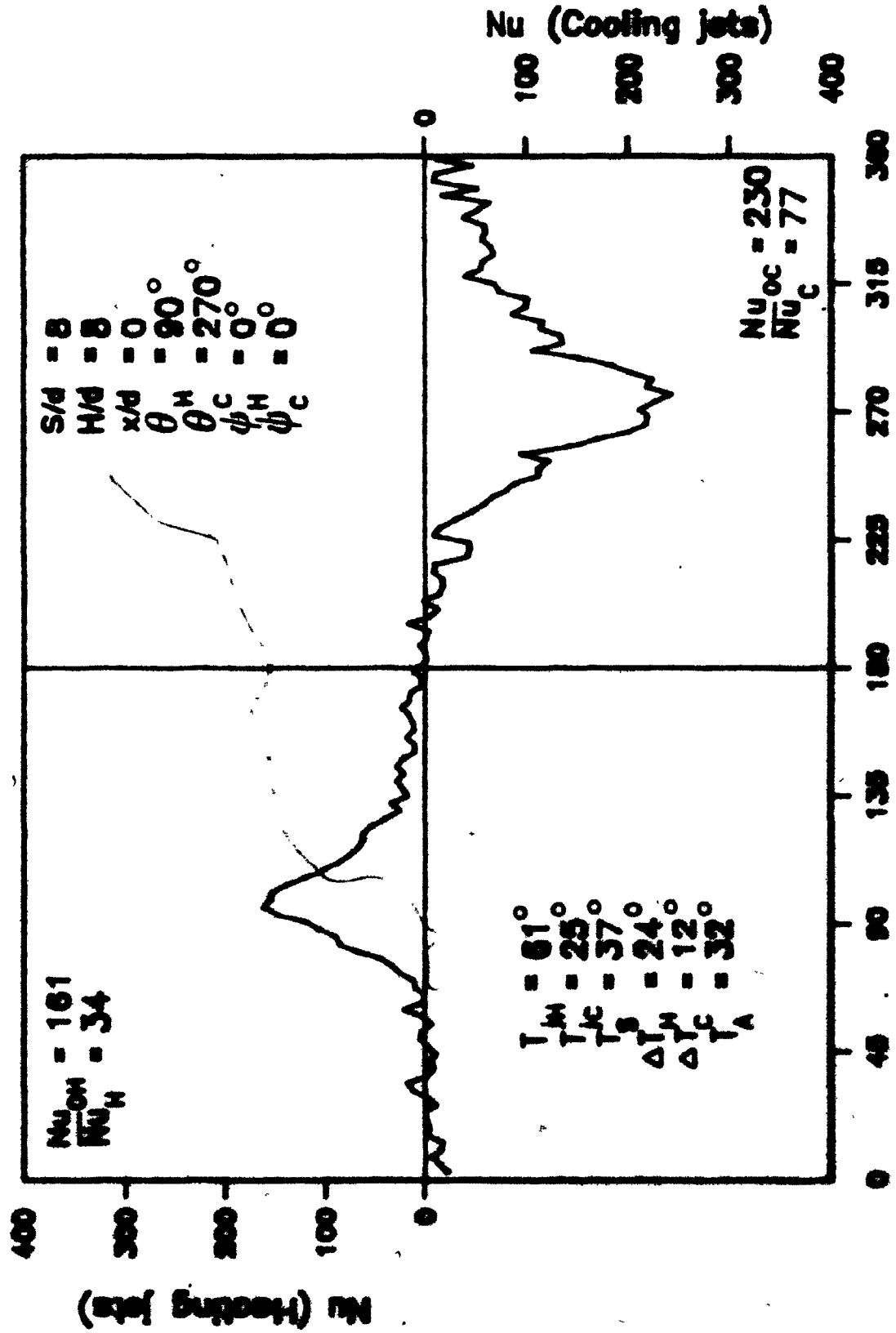

Figure 4.4.5 Circumferential Nusselt number distributions for H/d = 8 (Expt. 18).

H/d = 4 spacing.

The effects of surface motion on the Nusselt number distributions are very pronounced at H/d = 1 but hardly noticeable at H/d = 8. The Nusselt number distribution for H/d = 1 are strongly skewed in the direction of the motion of the roll, while those for H/d = 8 appear almost symmetrical.

The effects of surface motion on the local Nusselt number distributions appear to be proportional to the momentum of the jet near the surface of the roll. The momentum of the jet near the surface of the roll is higher for the jet with the low H/d spacing than for the jet with a high H/d spacing. Thus the motion of the roll surface will have greater influence on the jet with the low H/d spacing.

The secondary peak, found at y/d = 2.4, diminished with increasing H/d spacing, following the trend of the stagnation point Nusselt numbers, Nu_o . The position of the secondary peak did not shift with H/d spacing but became less noticeable until H/d = 8 when the peak disappeared.

The stagnation point Nusselt numbers, Nu_o, for the heating jets and the cooling jets are presented in Figure 4.4.6 as a function of H/d spacing. For the entire range of H/d spacing from 1 to 8, Nu_o decreased with increasing H/d spacing.

The heating and cooling jets exhibit the same trends in Nu_o as a function of H/d spacing. The Nu_o for the cooling jets are higher than the heating jets. The

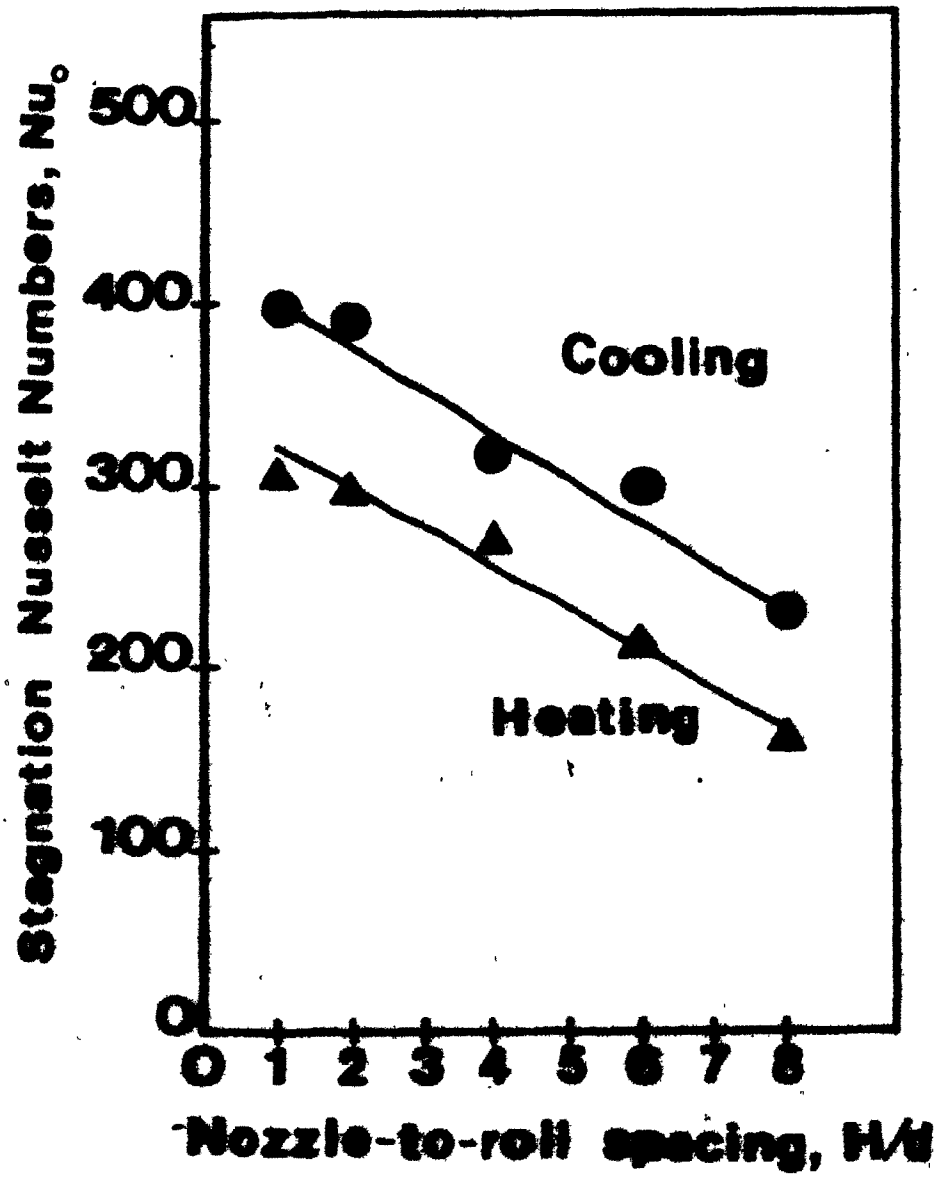

Figure 4.4.6 Effect of nozzle-to-roll spacing on stagnation Nusselt numbers.

following linear relationships were fitted to results and are included in Figure 4,4.6 for $1 \leq H/d \leq 8$

Heating: $Nu_o = 338.0 - 21.1\ H/d$ for Re = 100,000

Cooling: $Nu_o = 426.6 - 24.2\ H/d$ for Re = 120,000

Obot (1980) reported that a maximum in Nu_o existed for short (l/d=1) sharp-edged inlet nozzles at H/d = 4 and at H/d = 8 for contoured inlet nozzles. Kataoka and Mizushina (1974) and Gardon and Akfirat (1965) have also reported a maximum in Nu_o at a H/d spacing close to 8. Koopman and Sparrow (1976) who used short sharp-edged inlet nozzles reported an apparent maximum in stagnation point mass transfer coeffecient at H/d = 4. No evidence of a maximum in Nu_o at H/d spacing of 4 or 8 was found in this study.

The trend in Nu_o with H/d spacing is quite similar to that noted by Gardon and Akfirat (1965) for a jet with a high level of artificially induced turbulence. Gardon and Akfirat (1965) concluded that the linear variation of Nu_o with H/d was the result of the high level of turbulence in the jet at the nozzle exit. Thus it appears that the trend in Nu_o shown in Figure 4.4.6 is the result of a high turbulence level in the jet. However no turbulence measurements were made, which might verify this hypothesis.

The regression equation proposed by Martin (1977) the impingement heat transfer for a single round nozzle has been included in Figure 4.4.6. This equation was fitted to data from various sources. The scatter of the data around his equation was aproximately ±15%. Our data fits within this

scatter, but indicate a stronger variation with H/d than does Martin's correlation.

Figure 4.4.7 illustrated the circumferentially averaged Nusselt numbers, $\overline{Nu}$, as a function of H/d spacing for the heating and the cooling jets, for the single axial position, x/d = 0, of this series of runs. The $\overline{Nu}$ decrease more slowly with increasing H/d than Nu_o. No clear maximum exists, but $\overline{Nu}$ tends to level off for H/d spacing between 1 and 4.

A similar trend in $\overline{Nu}$ was seen by Wedel (1980) for an array of rounded-entrance round jets. He reported that for a fractional area, defined as the ratio of the nozzle area to the impingement area, of f =0.0138, the nozzle-to-plate spacing had no effect on $\overline{Nu}$ for H/d spacing between 1 and 4.

Obot (1980) noted that the maximum found in the curve of $\overline{Nu}$ vs H/d became less prominent with decreasing f. For f smaller than 0.0567, H/d did not affect $\overline{Nu}$ significantly in the range $1 \leq H/d \leq 8$. The fractional area, f, for the present study was 0.00128. Thus the trend observed in $\overline{Nu}$ as a function of H/d spacing would seem to be due to the small value of f (large impingement area).

Both Nu_o and $\overline{Nu}$ are substantially larger for the cooling jets than for the heating jets. In Section 4.2, the large differences between Nu for the heating and cooling jets sides were attributed to the effects of the ambient air. The much smaller differences between the heating and cooling values of Nu_o cannot be attributed to this effect;

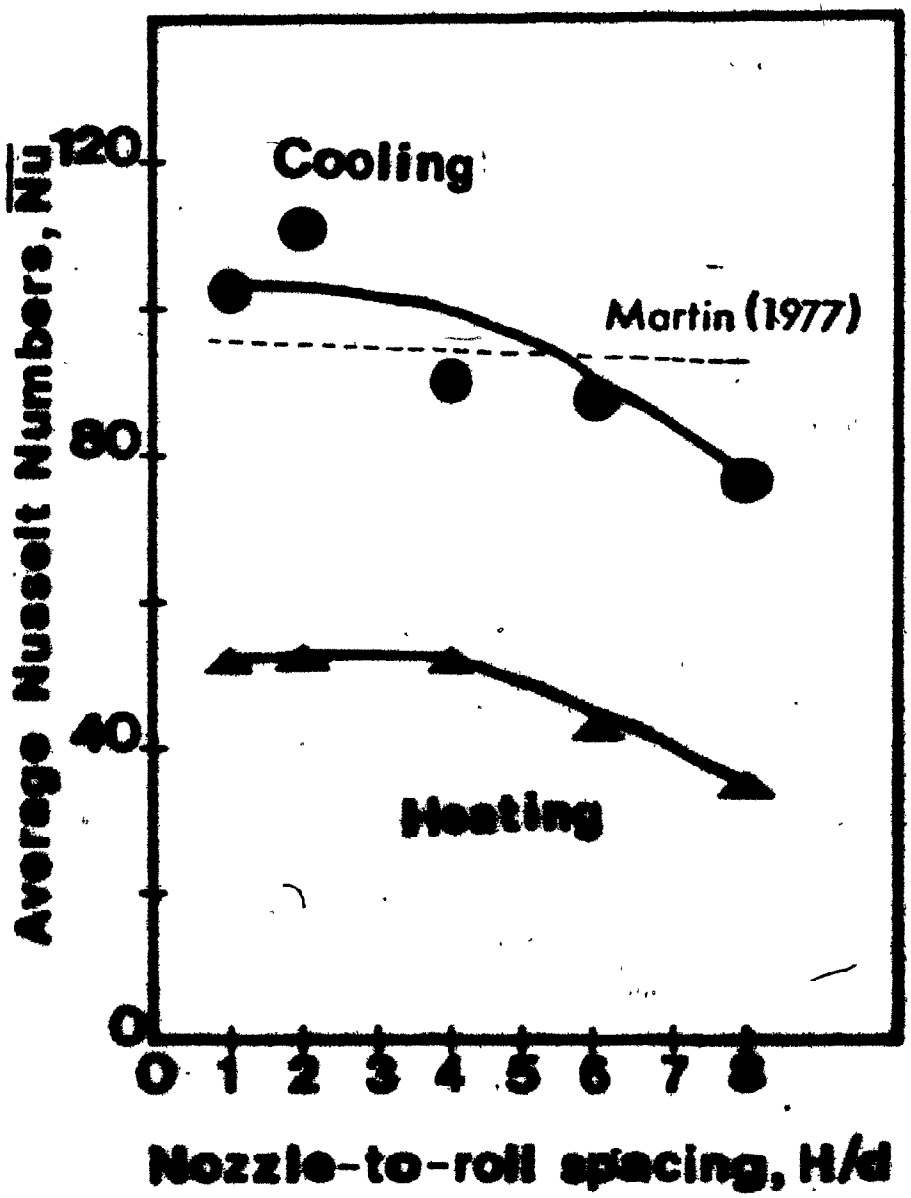

Figure 4.4.7 Effect of nozzle-to-roll spacing on average Nusselt numbers.

particularly at small H/d spacings. The only plausible explanation found for this difference was the effect of Reynolds number, which accounts for only 10% of the difference in Nu_o.

4.5 Effect of Cylinder Circumferential Angle

The effect of the circumferential position of the nozzle around the middle roll was studied by displacing the nozzles ±30° from the neutral position. Measurements were made with nozzles at θ_H = 60° and 120° on the heating jets side and at θ_C = 240° and 300° on the cooling jets side. The nozzle-to-roll spacing was maintained at H/d = 4 and the nozzles were positioned normal to the surface of the roll (ϕ = 0°) as in the neutral position.

The local Nusselt number distributions for the two circumferential angles (±30° from the neutral position) are presented in Figures 4.5.1 and 4.5.2. These two distributions along with the neutral position are shown superimposed in Figure 4.5.3. The positions of the curves are displaced by ±30° from the neutral position but their shape has not changed significantly.

On the heating side, the curves are essentially coincident for the initial 45°, where the small leakage of cool air through the bottom nip to the heating jets side produced negative heat transfer coefficients. This region has not been affected at all by the displacement of the nozzles about the circumference. On the cooling jets side,

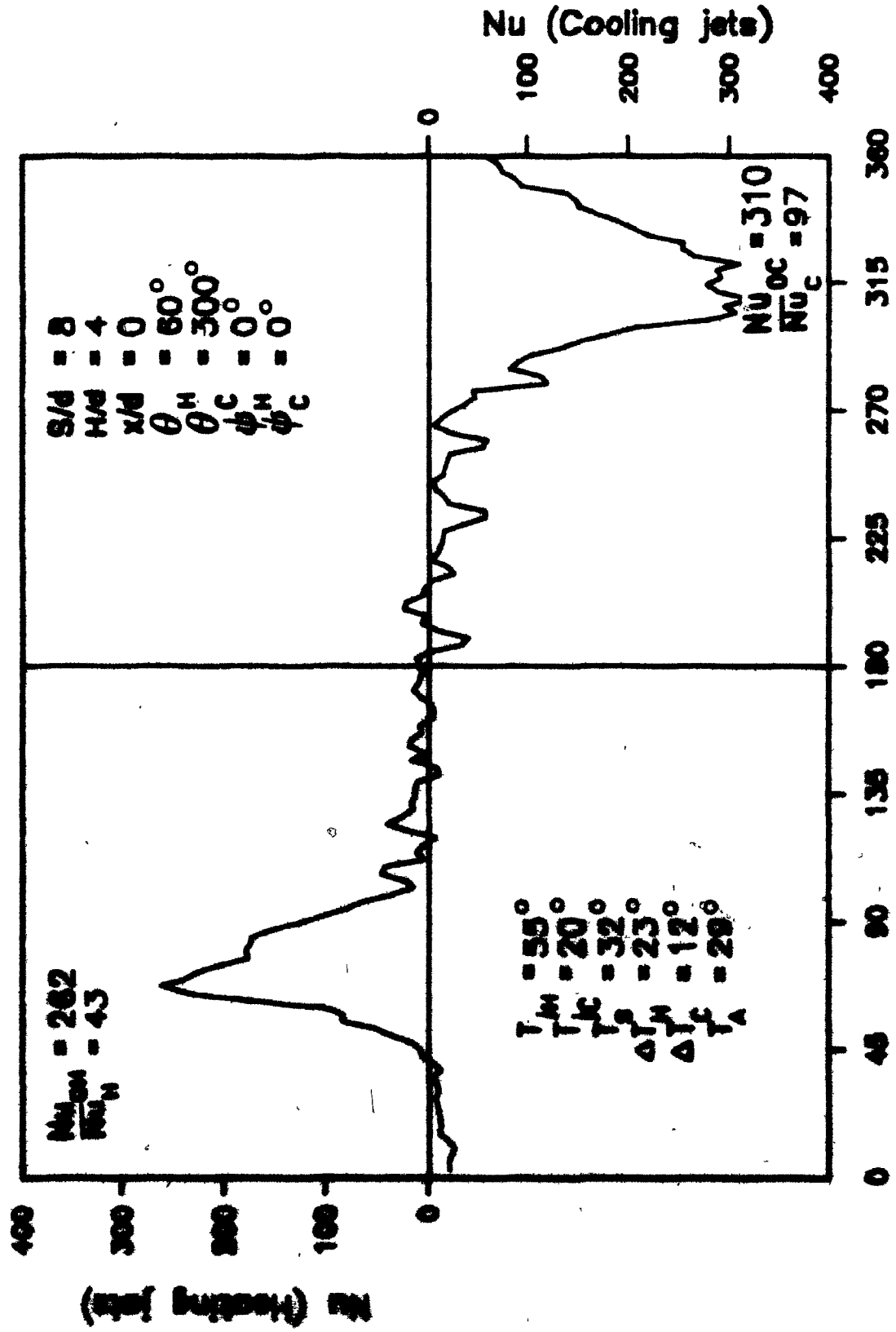

Figure 4.5.1 Circumferential Nusselt number distributions for θ_H = 60° and θ_C = 300° (Expt. 19).

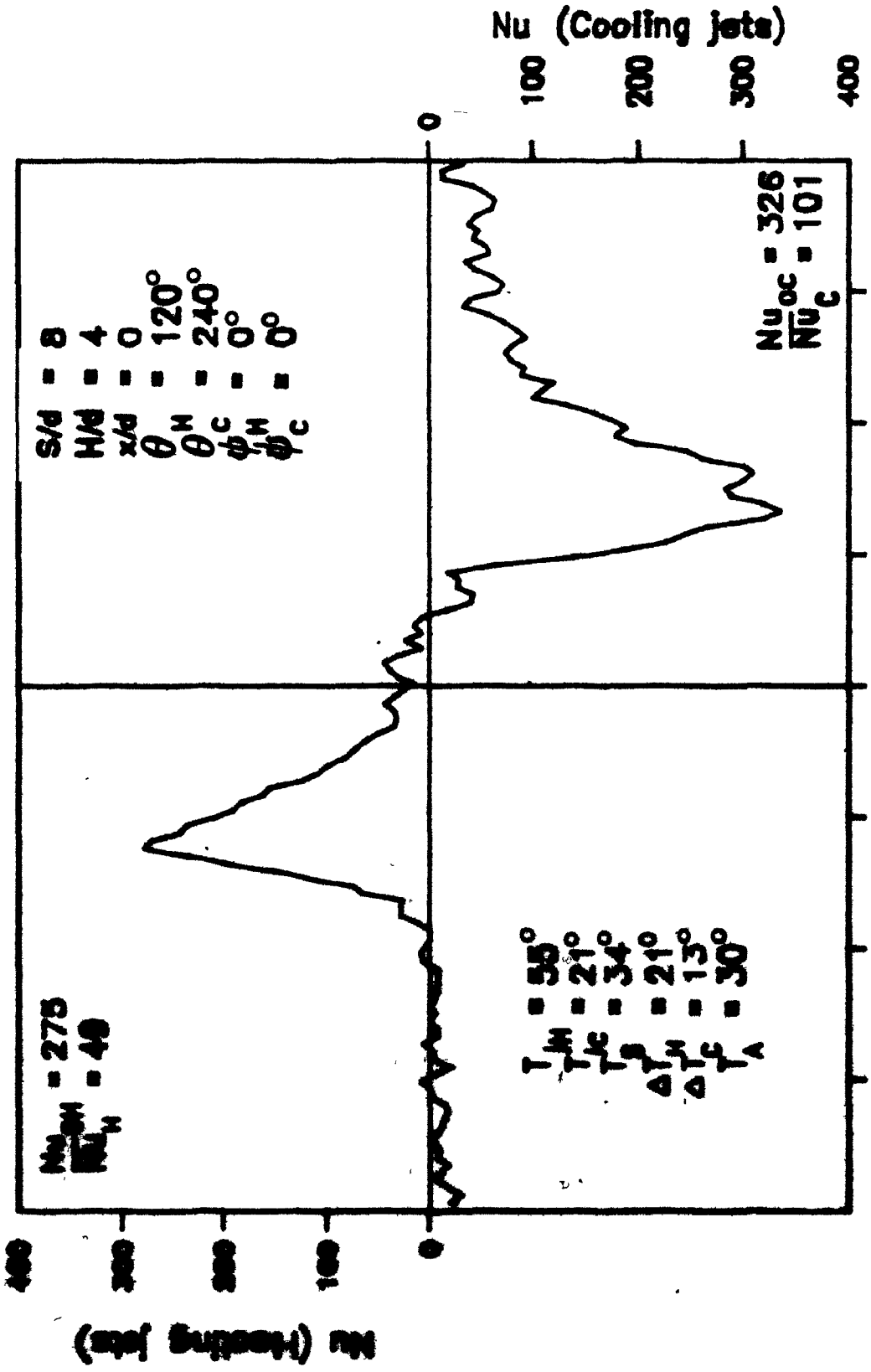

CIRCUMFERENTIAL POSITION

Figure 4.5.2 Circumferential Nusselt number distributions for θ_H = 120° and θ_C = 240° (Expt. 20).

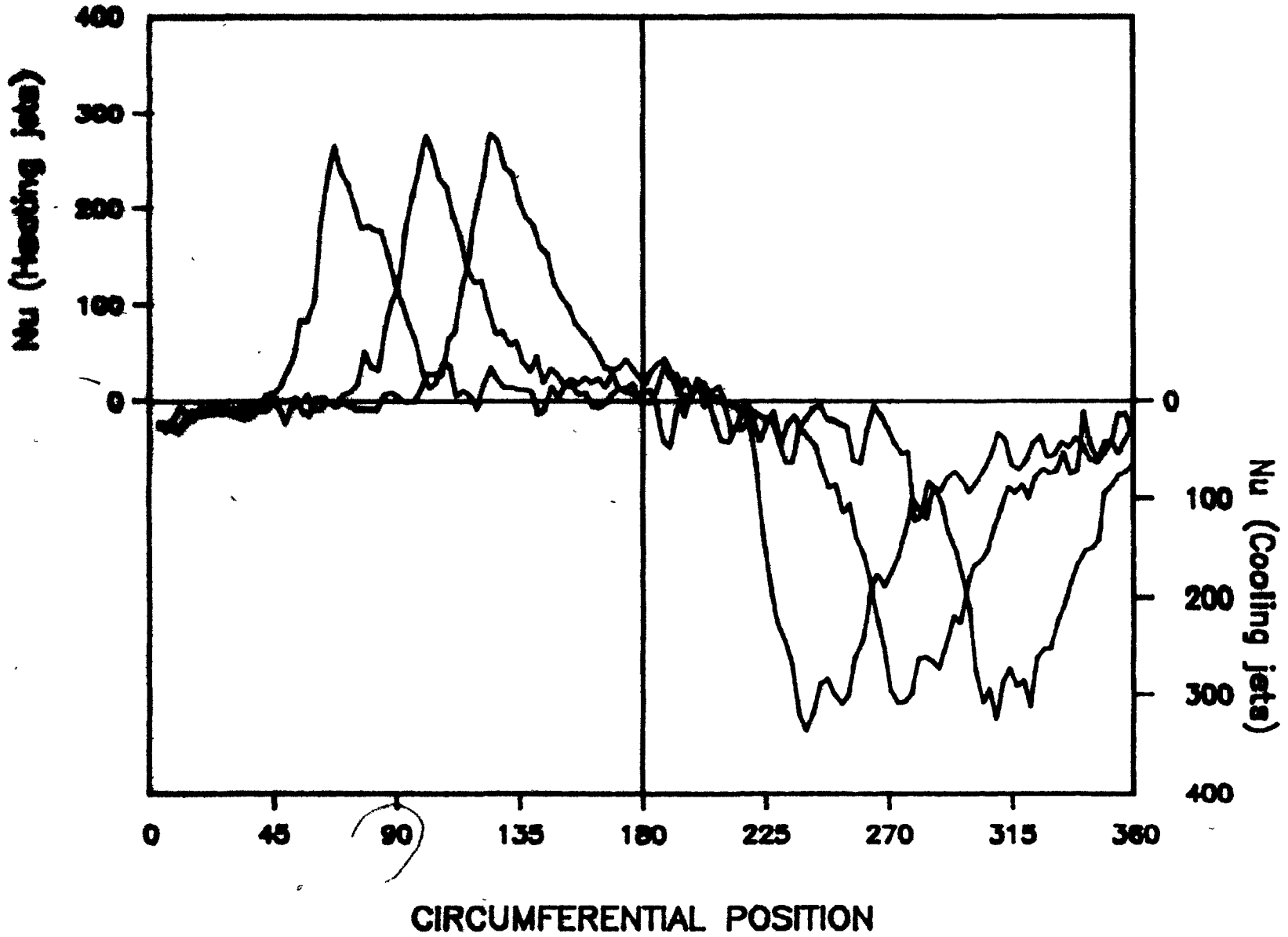

Figure 4.5.3 Circumferential Nusselt number distributions shown for 3 circumferential nozzle positions.

the results over the first 45° show a little more scatter, which can be attributed to the amount of hot air leaking through the top nip. When the heating nozzles were positioned closest to the top nip (θ_H = 120°), more air was forced through the top nip than when they were placed further away from the top nip (θ_C = 60°).

The Nusselt numbers near the converging nips did show a slight increase as the nozzles were shifted towards these nips (θ_H = 120° and θ_C = 300°). However, the nozzles at these circumferential angles are not yet close enough to the converging nips to affect significantly the regions of high heat transfer. The regions of high heat transfer extend approximately 45° or 7 nozzles diameters on either side of the stagnation points.

Neither the shape nor the magnitude of the Nusselt number distributions in Figure 4.5.3 were affected significantly by shifting the stagnation point ±30° around the circumference of the roll. The effect of circumferential nozzle position on the stagnation point and circumferentially averaged Nusselt numbers is shown in Figures 4.5.4 and 4.5.5 respectively. The total variations for either Nu_o or $\overline{Nu}$ are less than 10%, which in view of the accuracy of these measurements (± 5%) cannot be considered significant. Hence, it can be concluded that circumferential displacement of these nozzles by ±30° did not have any significant effect on the overall heat transfer to the middle roll.

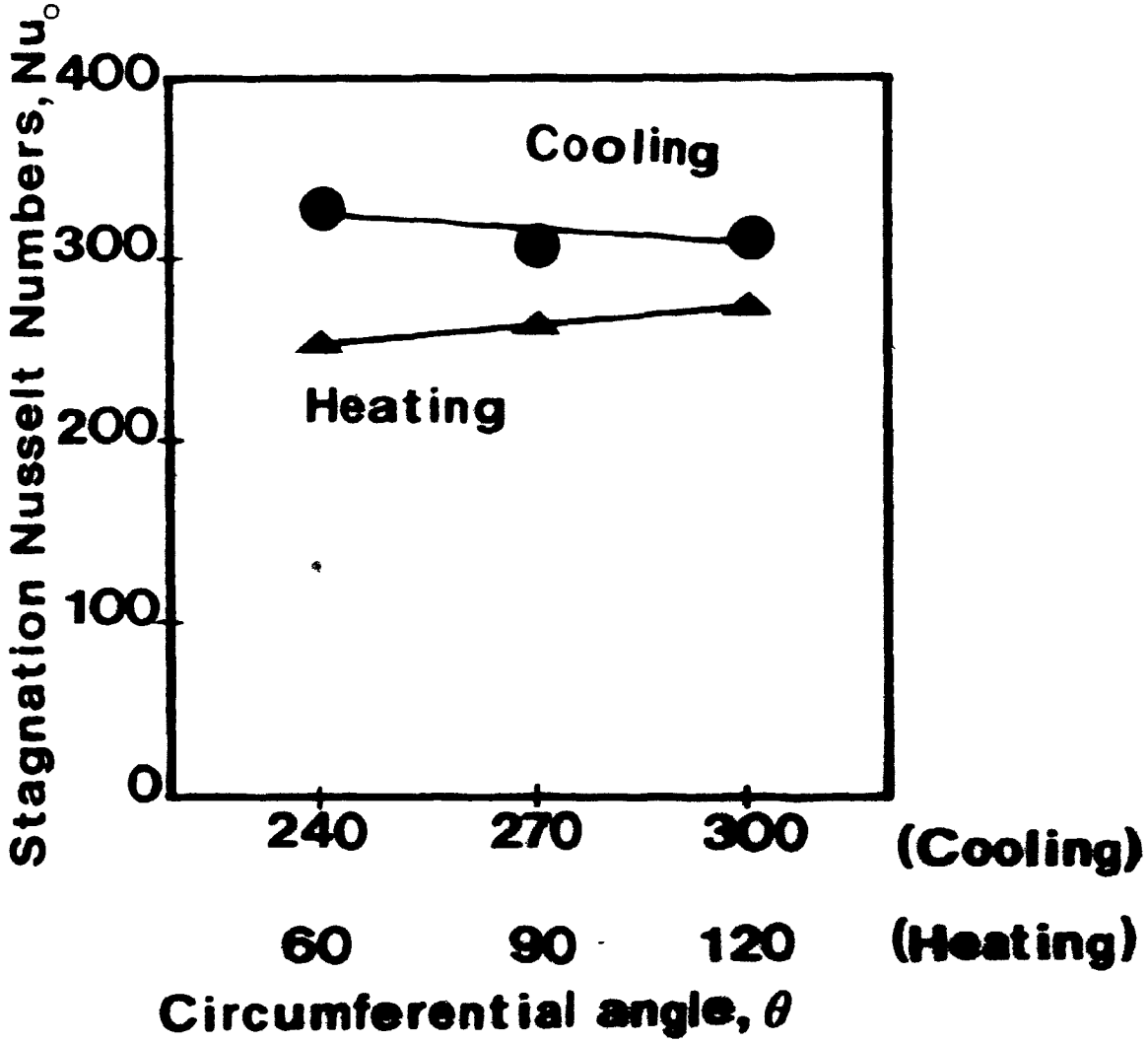

Figure 4.5.4 Effect of circumferential angle on stagnation Nusselt numbers.

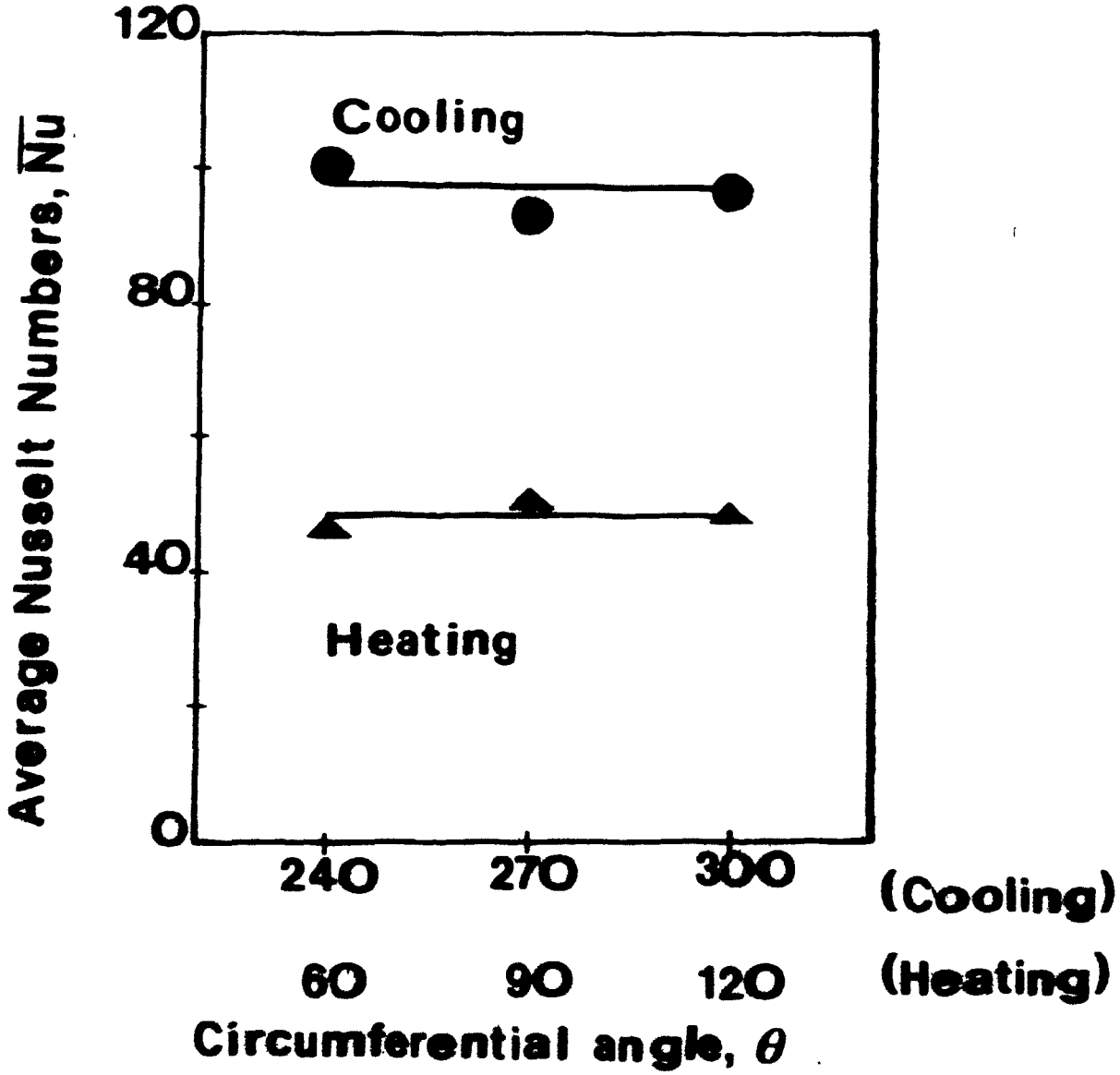

Figure 4.5.5 Effect of circumferential angle on average Nusselt numbers.

Judging by the Nusselt number distributions in Figure 4.5.3, it would appear that a further displacement of the nozzles by 30° towards the diverging nip (in the direction of smaller values of θ) would have little effect on the heat transfer. A further displacement towards the converging nip however might lead to reduced heat transfer to the roll onto which the jets are impinging. In terms of nozzle diameters, it appears that the diverging nip can be approached to within approximately 5 nozzle diameters and the converging nip within 10 nozzle diameters without affecting the heat transfer to the roll significantly. This conclusion needs to be confirmed with measurements made with nozzles having different diameters.

4.6 Effect of Deflection Angle

The deflection angle, ϕ , was varied from the neutral position at $\phi = 0°$ to $\phi = \pm 30°$ (experiment numbers 21 and 23) and to $\phi = \pm 45°$ (experiment numbers 22 and 24). The nozzle-to-roll spacing of H/d=4 and the circumferential positions of $\theta = 90°$ and 270° on the heating and cooling sides, respectively, were maintained throughout these experiments. In the neutral position, the nozzles were normal to the surface of the roll. The sign convention adopted was that for a positive ϕ , the jets were orientated in the direction of rotation of the middle roll, while with a negative ϕ , the jets were positioned to oppose the rotation of this roll.

The local Nusselt number distribution at the axial position, x/d=0, for $\phi = \pm 30°$ and $\pm 45°$ are presented in Figures 4.6.1 to 4.6.4. These Nusselt number distributions exhibit the same features noted earlier in Section 4.2; the lack of symmetry about the stagnation point and the occurance of secondary peaks as the roll recedes from the cooling jets. However, the size and shape of the distribution curves were altered significantly by the deflection angle, ϕ .

The stagnation point Nusselt number, Nu_o, are plotted in Figure 4.6.5 as a function of ϕ for the heating and cooling jets. Both curves exhibit the same trends in Nu_o; the Nu_o increase steadily with decreasing ϕ to a maximum at $\phi = -30°$ and then decrease at $\phi = -45°$.

One effect of deflection angle, ϕ, on the local Nusselt number distribution was to shift the profiles somewhat, either in or against the direction of motion of the middle roll, with respect to the corresponding profile for $\phi = 0°$ (neutral position). The extent by which the profiles are shifted, expressed in terms of nozzle diameter, d, is plotted in Figure 4.6.6. Both the stagnation point Nusselt numbers and the extent of shift exhibit the same trend in deflection angle.

As the deflection angle is changed towards the positive direction from the neutral position, the jet arrives at the impingement surface with an orientation more nearly parallel to the surface, and flowing in the same

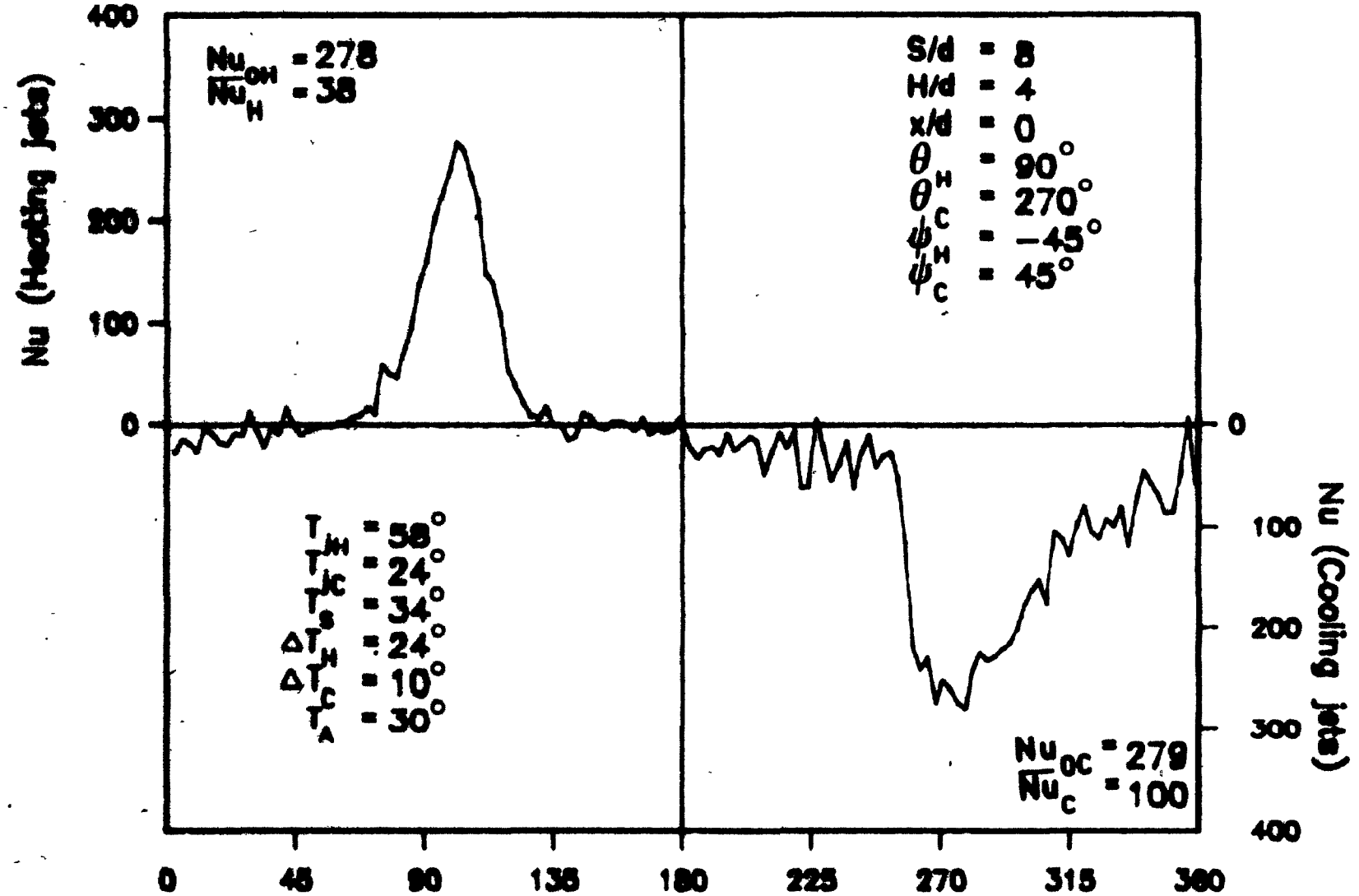

Figure 4.6.1 Circumferential Nusselt number distributions for ϕ_H = -45° and ϕ_C = 45° (Expt. 22).

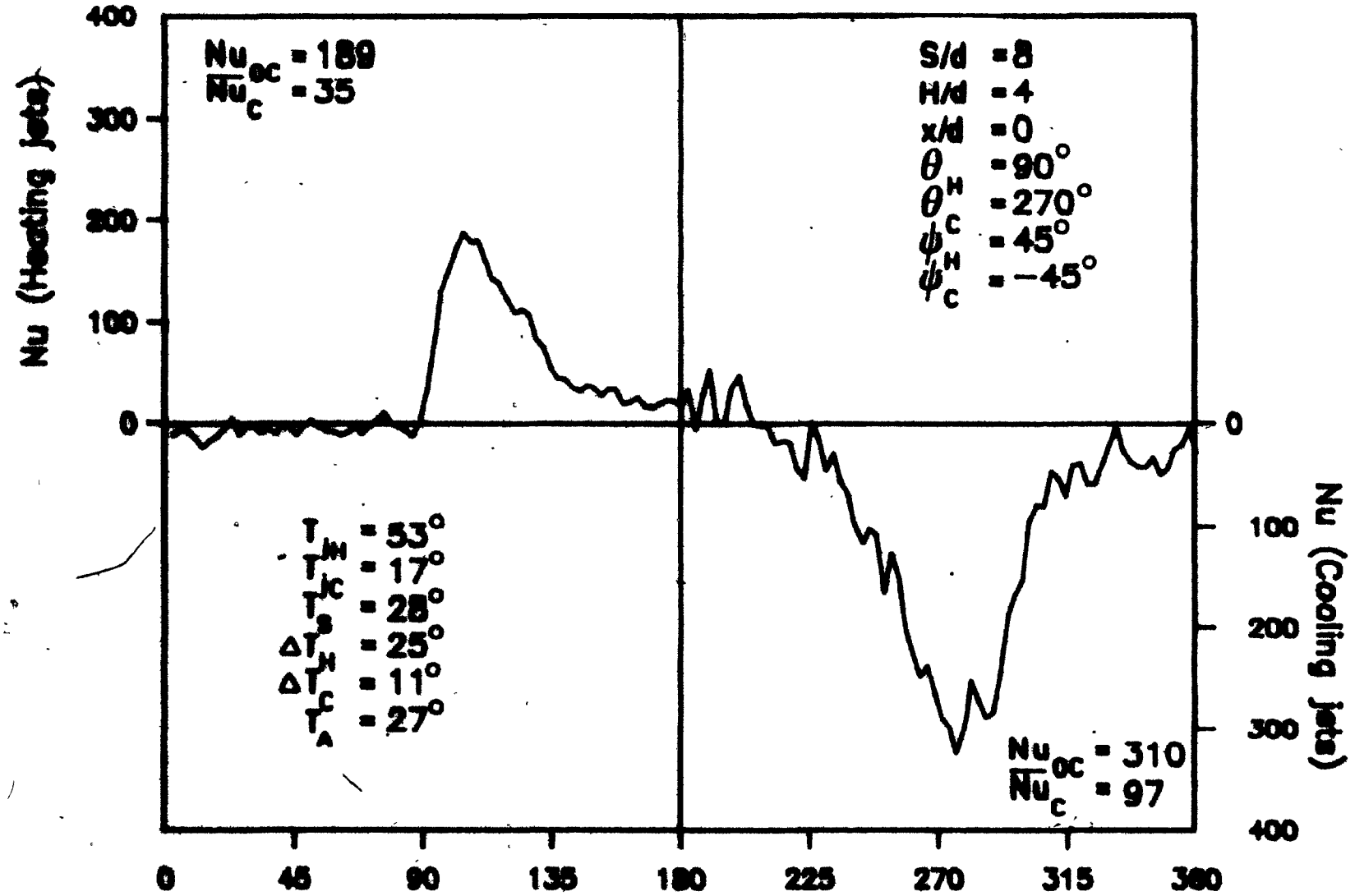

Figure 4.6.2 Circumferential Nusselt number distributions for ϕ_H = 45° and ϕ_C = −45° (Expt. 24).

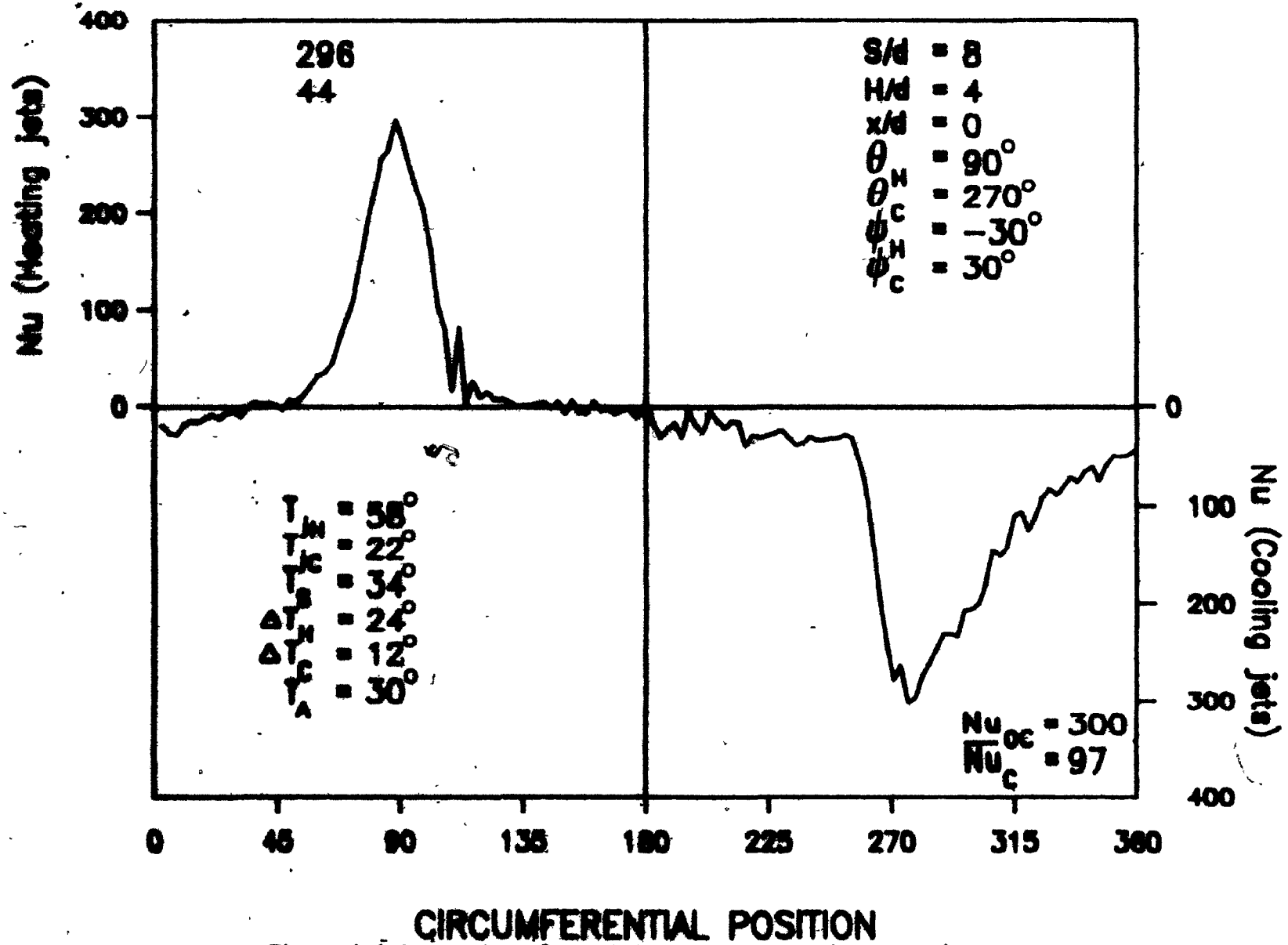

Figure 4.6.3 Circumferential Nusselt number distributions for ϕ_H = -30° and ϕ_C = 30° (Expt. 21).

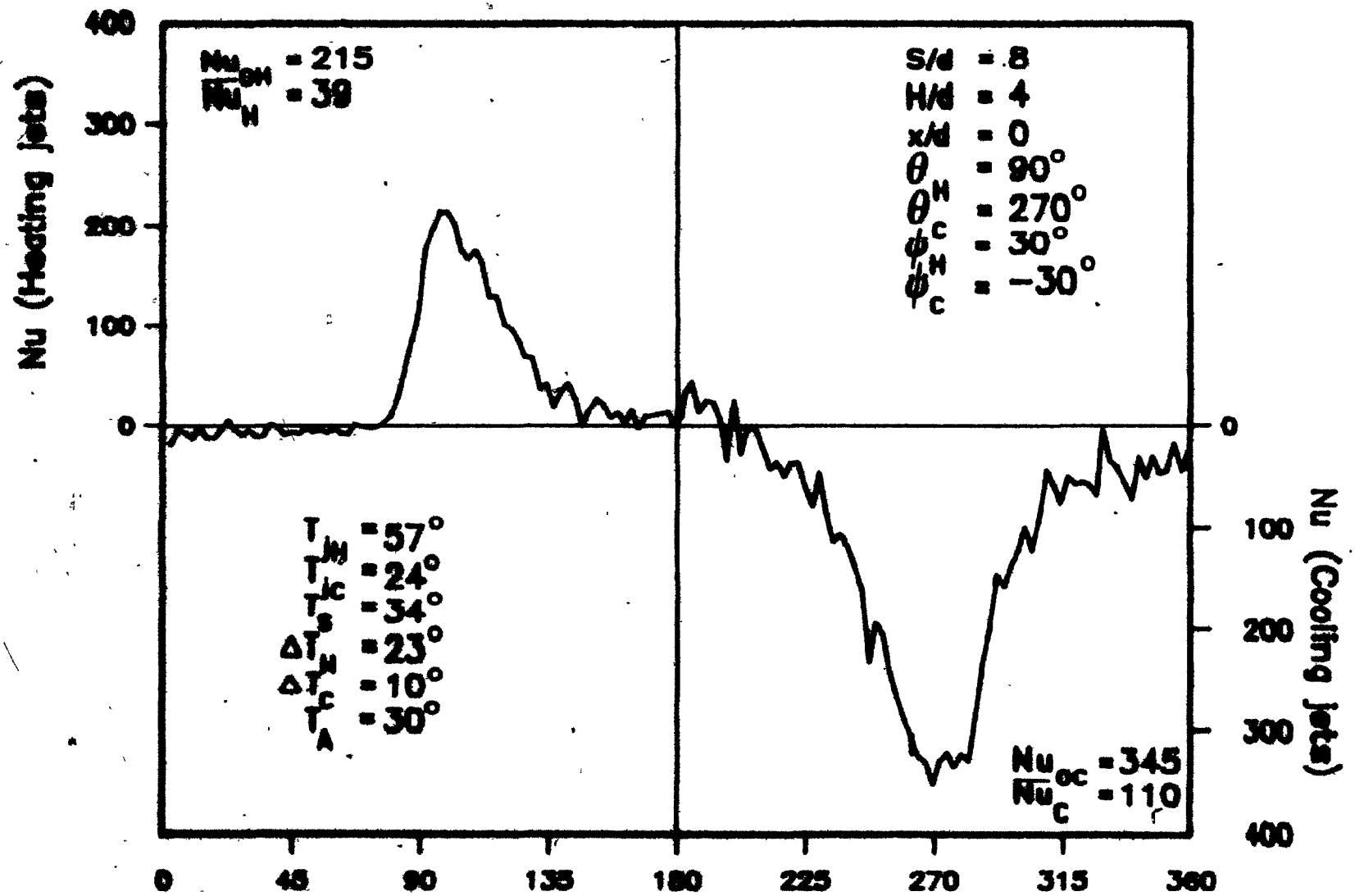

Figure 4.6.4 Circumferential Nusselt number distributions for ϕ_H = 30° and ϕ_c = −30° (Expt. 23).

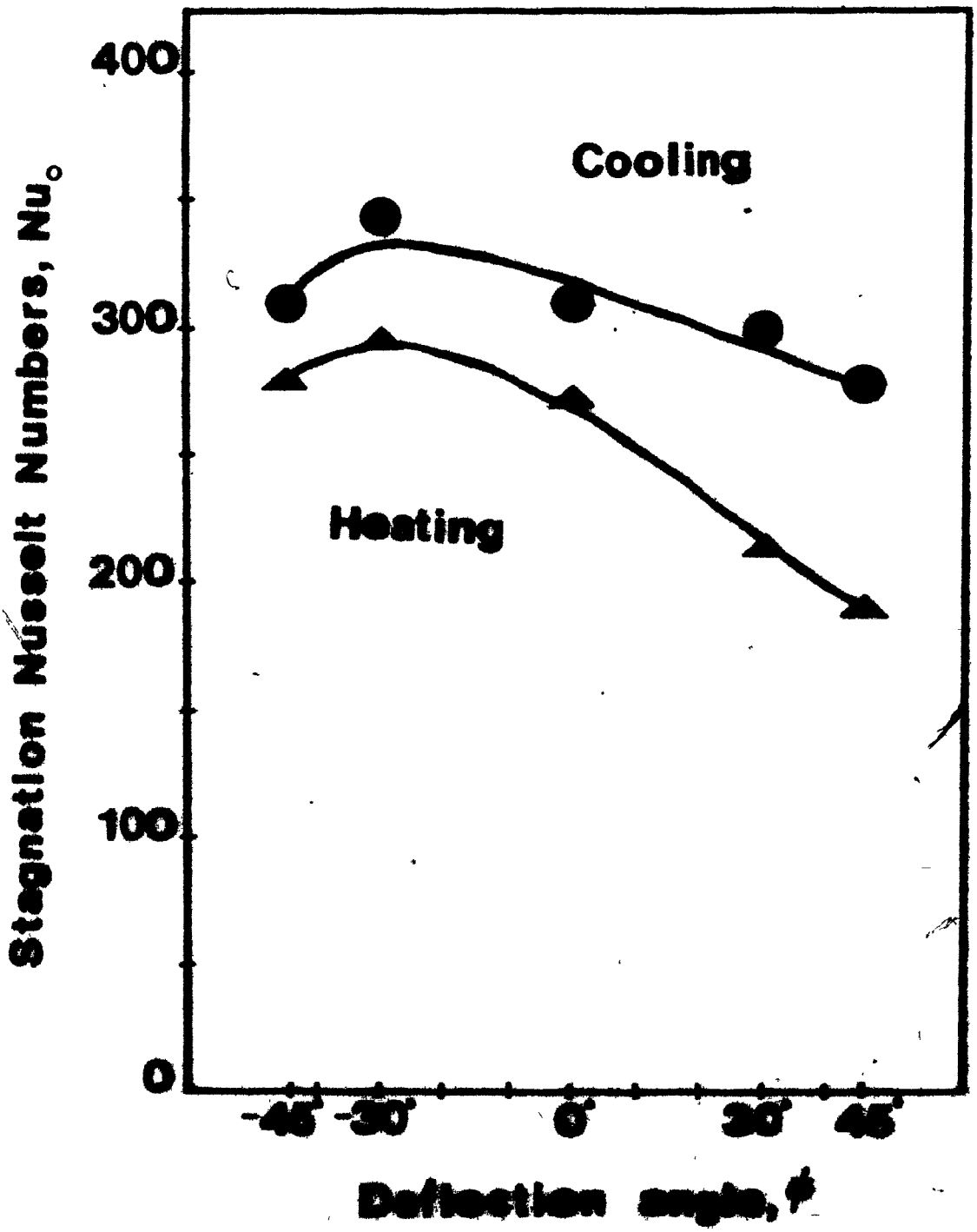

Figure 4.6.5 Effect of deflection angle on stagnation Nusselt numbers.

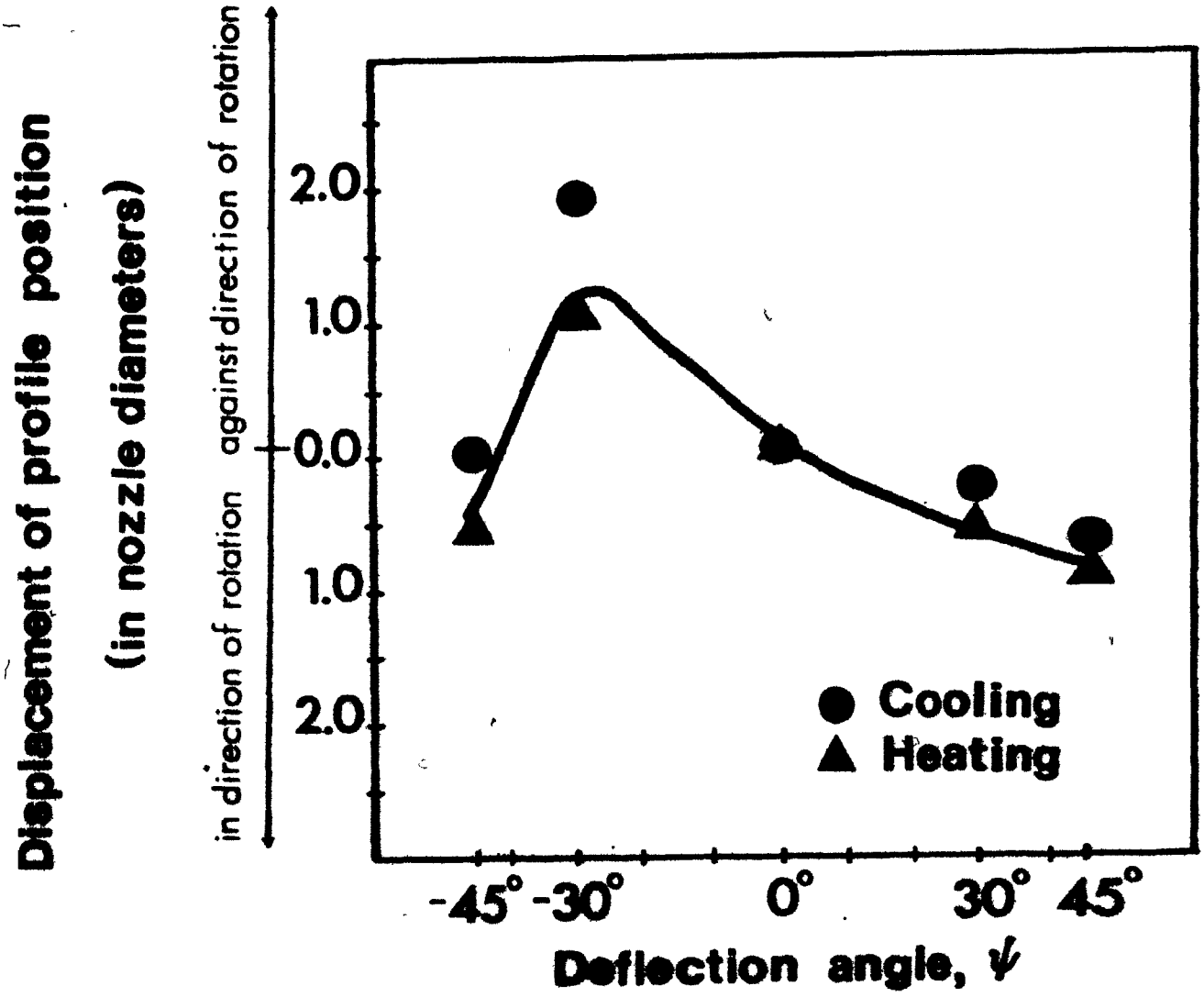

Figure 4.6.6 Effect of deflection angle on the position of the circumferential Nu profile.

direction as the surface motion. In the limit, i.e. ϕ =90°, the jet would arrive tangent to the surface and moving with the surface. The high values of heat transfer coefficients for impinging jets derive from the high velocity gradients and thin boundary layer in the impingement region. Thus as is increased in the positive direction, an increasing fraction of the nozzle discharge flows with the impingement surface on the leaving side of the stagnation point, and flows in a condition similar to a flow parallel to a surface.

Thus, with increasingly positive values of nozzle deflection angle, ϕ , the progressive loss of the impingement flow characteristics, which give the high heat transfer coefficients associated with impinging jets, causes heat transfer coefficients to decrease, as is seen on Figure 4.6.5. A corresponding trend is evident in Figure 4.6.6 in that, as ϕ increases from the neutral position of =0°, the Nusselt number profiles also shift toward the direction of motion of the impingement surface, i.e. the profiles occur slightly later, relative to the neutral position profile. The extent of shift of profile is however not large, with the heating and cooling jet profiles shifting an average of 0.75d (or 5°) in the direction of surface motion for both measured cases, ϕ =30° and ϕ =45°.

For small changes in deflection angle in the negative direction, the consequences of increasingly positive values of ϕ , described above, continue to apply but now to the

opposite effect. Thus as this angle is changed from the neutral position to ϕ =-30°, the profiles now shift earlier, in this case by an average of 1.5d (or 10°), and the values of Nu_o increase by 7 to 10%. However, as the nozzle deflection angle is increased still further in this direction, to ϕ =-45°, thus directing the nozzle exit flow more strongly in the direction opposite to the surface motion, Figures 4.6.5 and 4.6.6 indicate that both of these measured effects reverse. Thus, by ϕ =-45°, the shift of the profiles reduces to an amount now averaging 0.5d (or 3°), and the values of Nu_o drops to about the same as exist for the deflection angle of ϕ =0°. With the nozzles inclined at negative values of ϕ, a larger fraction of the nozzle discharge is directed towards the region of impingement surface approaching the stagnation point, i.e. to a region of opposed flow. In this region the impingement surface drags fluid towards the stagnation point, i.e. in a direction opposed to the jet flow. One effect of this condition of opposed flow is that the wall jet thereby expands more rapidly, thus causing the wall jet velocity to drop more rapidly, which in turn leads to a reduction in heat transfer coefficient in the region from wall jet to stagnation point on the side of the jets where surface motion approaches the stagnation point. Thus it is not surprising that by increasing ϕ from 0° to -45°, it is demonstrated that for some values of ϕ around -30° there occurs a maximum in Nu_o as well as a maximum in the shift of

the profiles in the direction opposite to surface motion.

The circumferentially averaged Nusselt numbers, $\overline{Nu}$, which are plotted as a function of deflection angle, ϕ, in Figure 4.6.7 for both the heating and cooling jets, do not show the same trend in $\overline{Nu}$. Furthermore the results for the heating and cooling jets are distinctly different. The heating jets produced a maximum $\overline{Nu}$ at $\phi = 0°$ with small reductions in $\overline{Nu}$ as ϕ was varied in either the positive or negative direction. The cooling jets showed an increase in $\overline{Nu}$ with increasing ϕ, with the exception of the result at $\phi = -30°$. At $\phi = -30°$, $\overline{Nu}$ is 20% higher than the trend shown by the other four data points. This maximum does coincide with the maximum in $\overline{Nu}$ for both the cooling and heating results, but not with the maximum of the $\overline{Nu}$ heating curve.

The different shapes of the Nu_o heating and cooling curves are most likely a consequence of the complex interactions of the flow fields of the jets and those associated with the calender rolls. The change in these flow conditions will affect the heat transfer to the roll and the heat losses to different extents. Since the ratio of the heat lost to the heat transferred is much higher for the heating curves than for the cooling curves, it follows that these curves should be affected differently. For the Nu_o curves, heat losses are not important, and the shapes of the cooling and heating curves are quite similar.

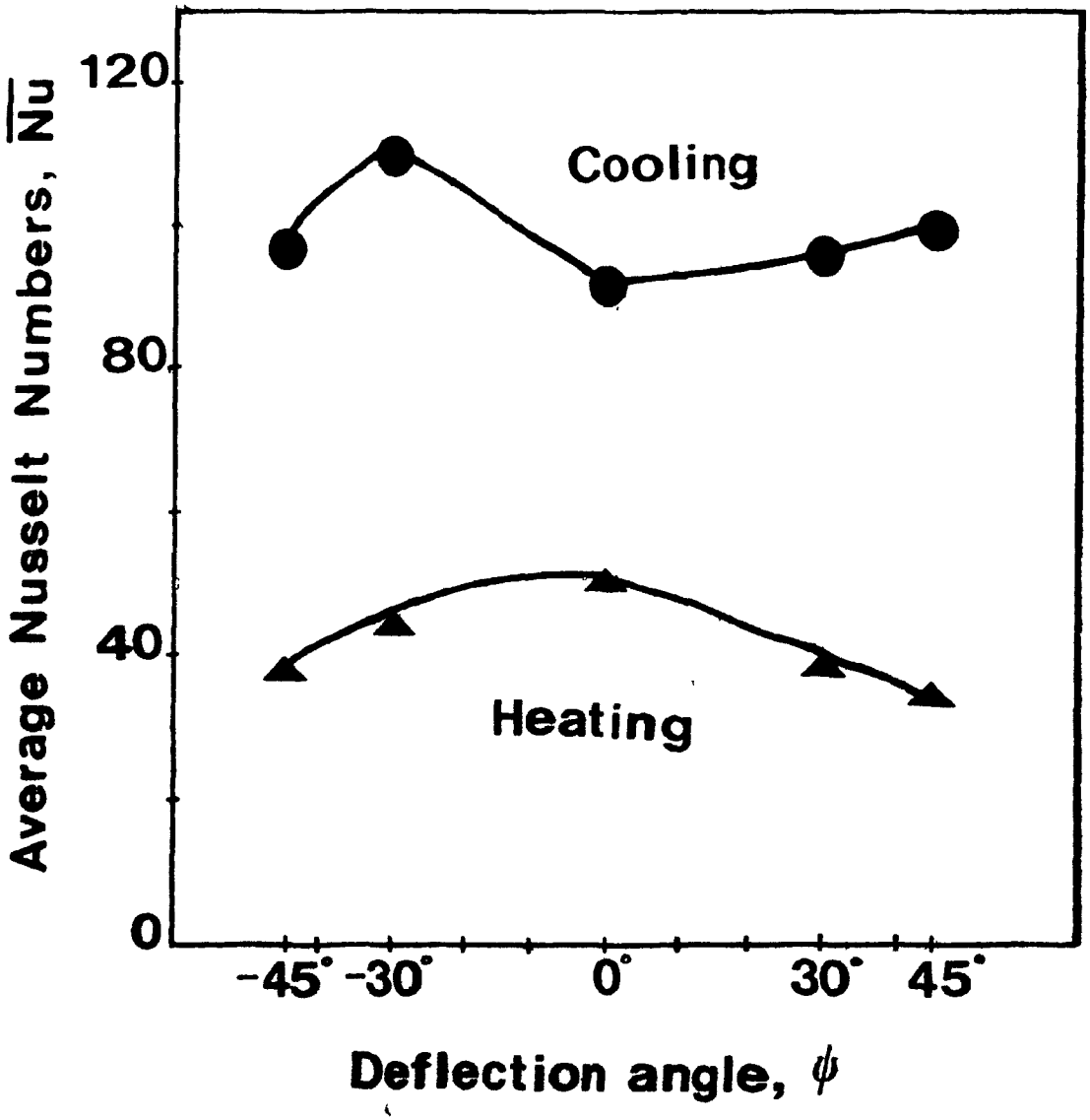

Figure 4.6.7 Effect of deflection angle on average Nusselt numbers.

5. SUMMARY AND CONCLUSIONS

The effect of nozzle position on local and average heat transfer rates for a row of round jets impinging on a rotating cylinder was investigated experimentally. The cylinder was the middle roll in a vertical stack of three driven rolls, each 457 mm in diameter which were set up to simulate the conditions in a paper machine calender. The rolls were driven at a constant surface speed of 16.7 m/s, and air was blown from 25 mm diameter circular commercial calender cooling nozzles with a nozzle exit velocity of 70 m/s, which was equivalent to a Reynolds number range from 100,000 to 120,000. Both heating and cooling of the roll were studied with nozzle exit temperatures in the range 15 to 22°C and 55 to 62°C and roll surface temperatures in the range 28 to 38°C. The following range of nozzle positions was investigated:

Nozzle-to-roll spacing, H/d, 1 to 8

Nozzle-to-nozzle spacing, S/d, 4 and 8

Axial locations, x/d, -4 to 4 for S/d=8

-2 to 2 for S/d=4

Circumferential angle, θ_H, 60°, 90°, and 120°

and θ_C, 240°, 270°, and 300°

Deflection angle, ϕ, -45° to +45°.

1) The temperature of the ambient air, which was entrained by the jet flow, was found to have a very pronounced effect on the average heat transfer rates to the roll. Heat

exchange between the jet and the surrounding air reduced the temperature driving force between the jet and the roll surface. For heating jets, the ratio of temperature differences $(T_j - T_s)/(T_j - T_A)$ was much larger than for the cooling jets. Consequently, the heat exchanged with the surroundings relative to the heat exchanged with the roll surface was smaller for the cooling jets, and the average Nusselt number, which was measured with reference to the temperature difference $T_j - T_s$, was larger for the cooling jets than for the heating jets.

2) The nozzle-to-nozzle spacing of S/d = 4 was found to produce a 17% higher and more uniform heat transfer along the length of the roll than the S/d = 8 spacing. The higher heat transfer is a consequence of using twice the number of nozzles and therefore twice the amount of air. Nozzles spaced at S/d = 8 actually transfered 50% more heat per nozzle than those spaced at the S/d = 4. Two rows of nozzles, placed on the same roll, each with S/d = 8 but staggered along the axis by x/d = 4 and positioned 51° apart on the circumference will transfer 50% more heat than one row of nozzles with a spacing of S/d = 4.

3) The circumferentially averaged Nusselt numbers decrease with increasing H/d. This effect becomes less pronounced for H/d=4.

4) The position of the nozzles around the circumference of the roll, θ, has no significant effect on the average heat transfer, provided the stagnation point is at least 10

nozzle diameters away from the nip.

5) The stagnation point Nusselt numbers, Nu_o, showed a maximum for both the heating and cooling jets when they were inclined by $\phi = -30°$ in the direction opposing the rotation of the roll surface. The circumferentially averaged Nusselt number showed a maximum for $\phi = -30°$ for the cooling jets and a maximum at $\phi = 0°$ for the heating jets.

References

Brdlik, P.M. and V.K. Savin (1965): Heat transfer between an axisymmetric jet and a plate normal to the flow, J. Eng. Physics, Vol. 8, p. 91.

Bryan, W.P. (1972): How to get more cooling from calender cooling systems, Paper Trade Journal, January 10, p. 36-37.

Crotogino, R.H., G.R. Weiss, J. Visentin and L. Dudas (1982): State of the art in CD calender control, EUCEPA Symp. Control Systems Pulp Paper Ind (Stockholm) Proc., p. 220-228.

Das, D. (1983): Convective heat transfer under a turbulent impinging slot jet at large temperature differences, M. Eng. thesis, Chem. Eng. Dept., McGill University.

den Ouden, C. and C.J. Hoogendoorn (1974): Local convective heat transfer coefficients for jets impinging on a plate, experiments using liquid crystal technique, Int. Heat Transfer Conf., Tokyo, Paper NA.2.5.

Fechner, G. (1971): Warmeubertragung bei senkrencht auf treffendem Strahl an der Platte und am Rohr, Dissertation T.U. München.

Fjeld, M. and W.P. Hickey (1984): Die Querprofilregelung am Kalander: Praxisbezogene Betrachtungen uber den Einstaz von Luftdusen, Das Papier, Volume 38, No. 1, p. 4-13.

Gardon, R. and J. Cobonpue (1962): Heat transfer between a flat plate and jets of air impinging on it, Proc. 2nd Int. Heat Transfer Conf., ASME, p. 454-460.

Gardon, R. and J.C. Akfirat (1965): The role of turbulence in determining the heat transfer characteristics of impinging jets, Int. J. Heat and Mass Transfer, Vol. 8, p. 1261-1272.

Gardon, R. and J.C. Akfirat (1966): Heat transfer characteristics of impinging two-dimensional air jets, J. Heat Transfer, Vol. 88, No. 1, p. 101-108.

Kahoun, J.B., W. Zurowitch, and L. Newby (1965): System for on-machine measurements and control of paper caliper, Tappi, Vol. 48, No. 7, p. 60A-65A.

Kataoka, K. and T. Mizushina (1974): Local enhancement

of the rate of heat transfer in an impinging round jet by free-stream turbulence, Int. Heat Transfer Conf., PC 8.3, p. 305-309.

Koopman, R.N. and E.M. Sparrow (1976): Local and average transfer coefficients due to an impinging row of jets, Int. J. Heat and Mass Transfer, Vol. 19, p. 673-683.

Korger, M. and F. Krizek (1972): Verfahrenstechnik (Maine) 6, p. 223-228.

Kumada, M., I. Mabuchi and Y. Kawashima (1972): Mass transfer on a cylinder in the potential core region of a two-dimensional jet, Trans. Japan Soc. Mech. Engrs., Vol. 38, p. 315.

Kumada, M., I. Mabuchi, Y. Kawashima and M. Hirati (1976): Mass transfer on a cylinder in developed region of a two-dimensional jet, Heat Transfer, Japanese Research, Vol. 5, No. 3.

Lyne, M.B., L. Haglund and H. Bjelkhagen (1976): Control of machine calender roll diameter with air showers - An experimental investigation, Svensk Papperstidning, Vol. 79, No. 8, p. 251-258.

Martin, H. (1977): Heat and mass transfer between impinging gas jets and solid surfaces, Advances in Heat Transfer, Vol. 13, Academic Press.

Mitchell, J.G. and D.K. Sheahan (1978): The control of reel building with calender stack air showers, CPPA Tech. Sect., Spring Conf. (Jasper, Alberta).

Murray, B.C. and T.D. Patten (1978): Heat transfer under an array of impinging jets, 6th Int. Heat Transfer Conf., Toronto. .Nakatogawa, T., N. Nishiwaki, M. Kirati and K. Torii (1970):
Heat transfer of round jets impinging normally on a flat plate, Int. Heat Transfer Conf., Paris, Paper PC.5.2.

Obot, N.T. (1980): Flow and heat transfer for round turbulent jets impinging on permeable and impermeable surfaces, Ph.D. thesis, Chem. Eng. Dept., McGill University.

Perry, K.P. (1954): Heat transfer by convection from a hot gas to a plane surface, Proc. Instn. Mech. Engrs., Vol. 168, No. 30, p. 775.

Polat, S., A.S. Mujumdar and W.J.M. Douglas (1984): Heat transfer distribution under a turbulent

impinging jet - a numerical study, to be published in Drying Technology.

Poreh, M. and J.E. Cermak (1959): Flow characteristics of a circular submerged jet impinging normally on a smooth boundary, 6th Mid-Western Conf. on Fluid Mechanics, Univ. of Texas, p. 198.

Saad, N.R. (1981): Flow and heat transfer for multiple turbulent impinging slot jets, Ph.D. thesis, Chem. Eng. Dept., McGill University.

Schlünder, E.U. and V. Gnielinski (1967): Wärme-und Stoffübertragung zwishen Gut und aufprallendem Düsenstrahl, Chemie-Ingenieur-Technik, Vol. 39, 9/10, p. 578-584.

Subba Raju, K. and E.U. Schlunder (1977): Heat transfer between an impinging jet and a continuously moving flat surface, Warme-und Stoffubertragung, Thermo- and Fluid Dynamics, Vol. 10, p. 131-136.

Tani, J. and Y. Komatsu (1966): Impingement of a round jet on a flat surface, 11th Int. Conf. on Applied Mech., p. 672.

van Heiningen, A.R.P. (1982): Heat transfer under an impinging slot jet, Ph.D. thesis, Chem. Eng. Dept., McGill University.

Walz, D.R. (1964): Spot cooling and heating surfaces with high velocity impinging air jets, part 2, circular jets on plane and curved surfaces, slot jets on curved surfaces, TR461, Stanford Univ.

Wedel, G.L. (1980): Air impingement heat transfer, Tappi, Vol. 63, No. 8, p. 89-92.

Appendix

For each rotation of the roll, the surface temperature distribution, which is illustrated in Figure A-1, is used to calculate the local heat flux distribution according to the procedure outlined in Section 3.5.1. The local heat flux distribution, for one rotation, is shown in Figure A-2.

The local heat flux distribution was calculated for 100 rotations and was averaged point-wise over the 100 rotations. The resulting heat flux distribution is shown in Figure A-3. The heat flux distribution was then converted to Nusselt number distribution by the definitions shown on page 68, Section 3.5.2.

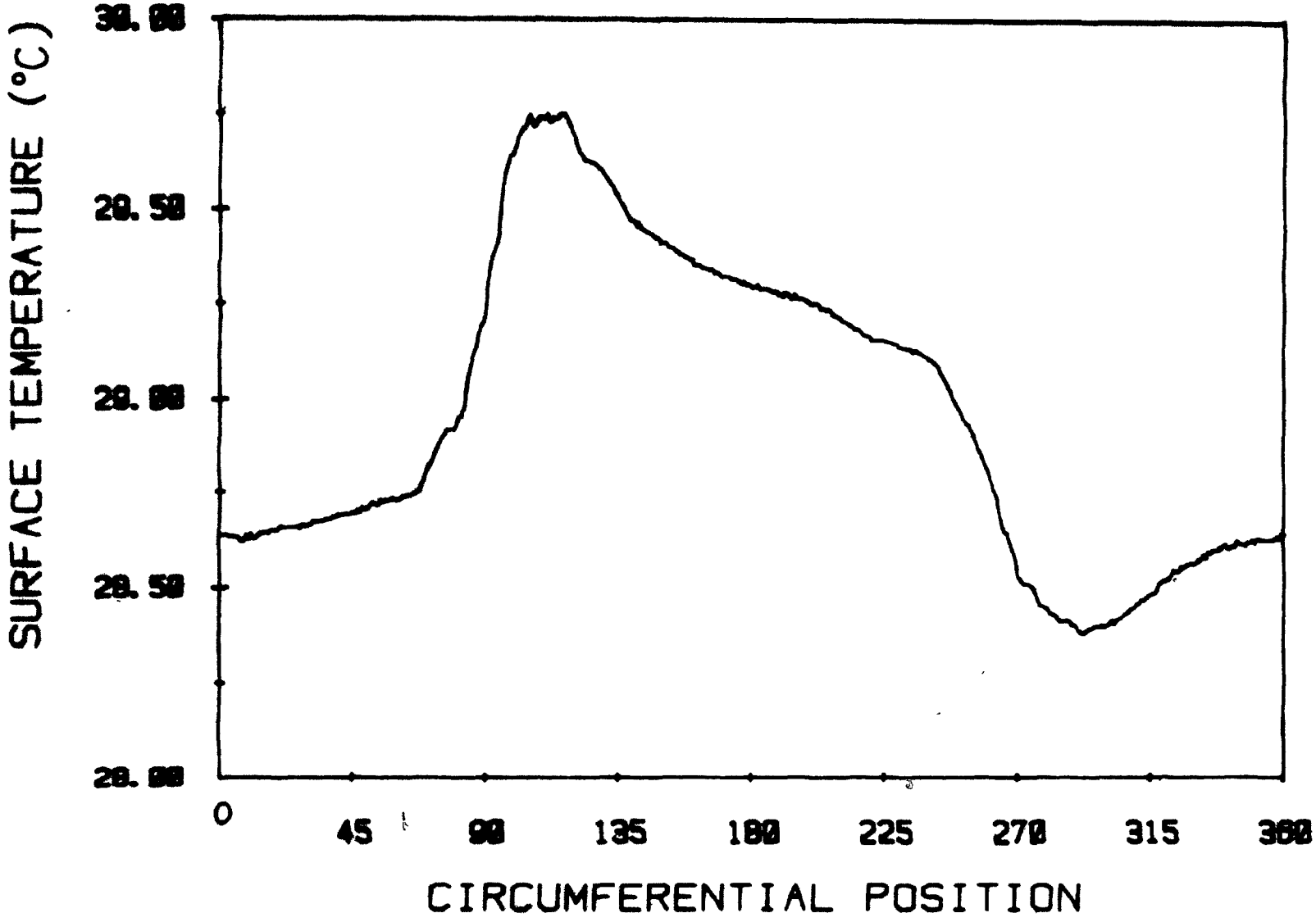

Figure A-1 Local surface temperature distribution for one rotation.

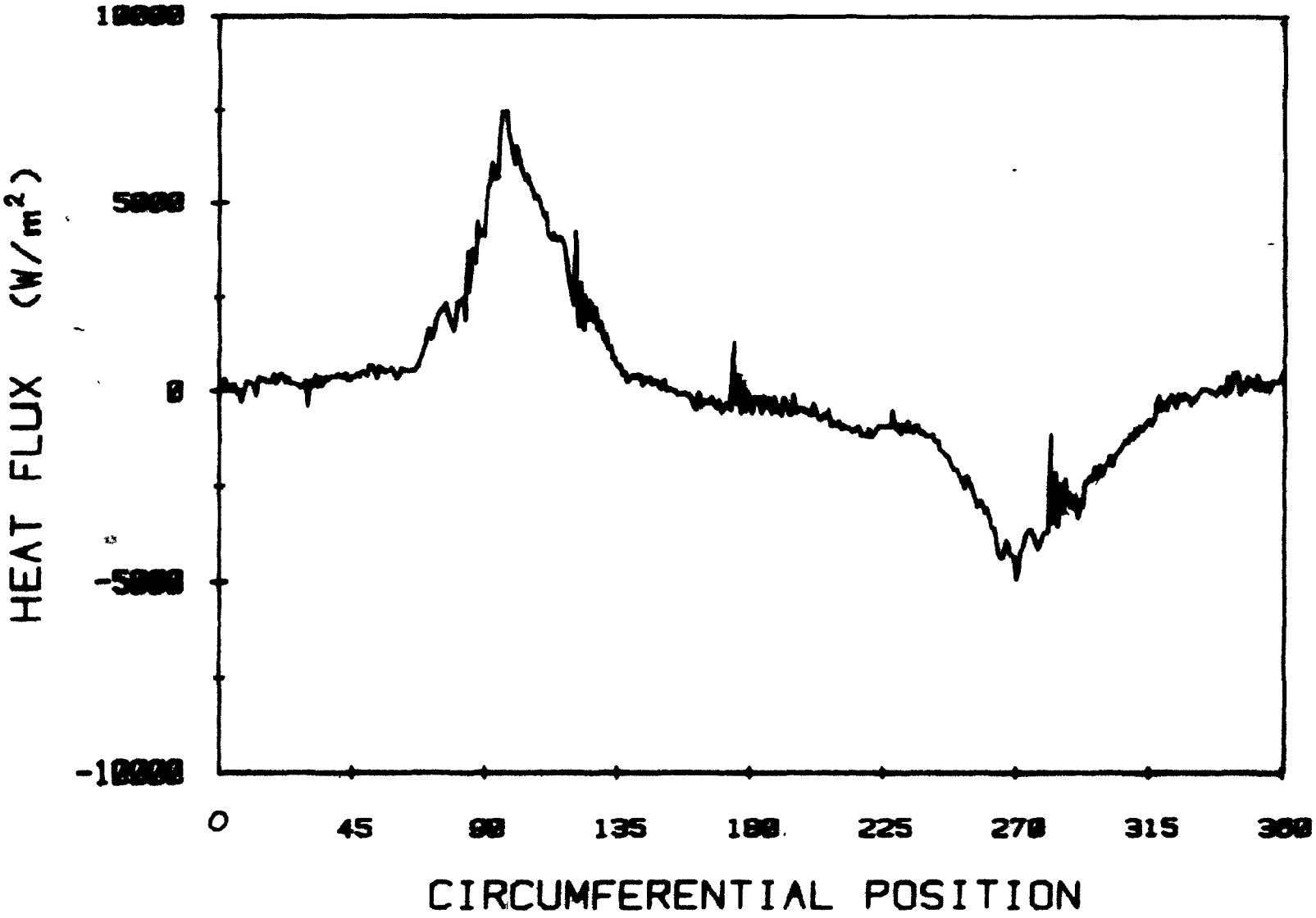

Figure A-2 Local heat flux distribution for one rotation.

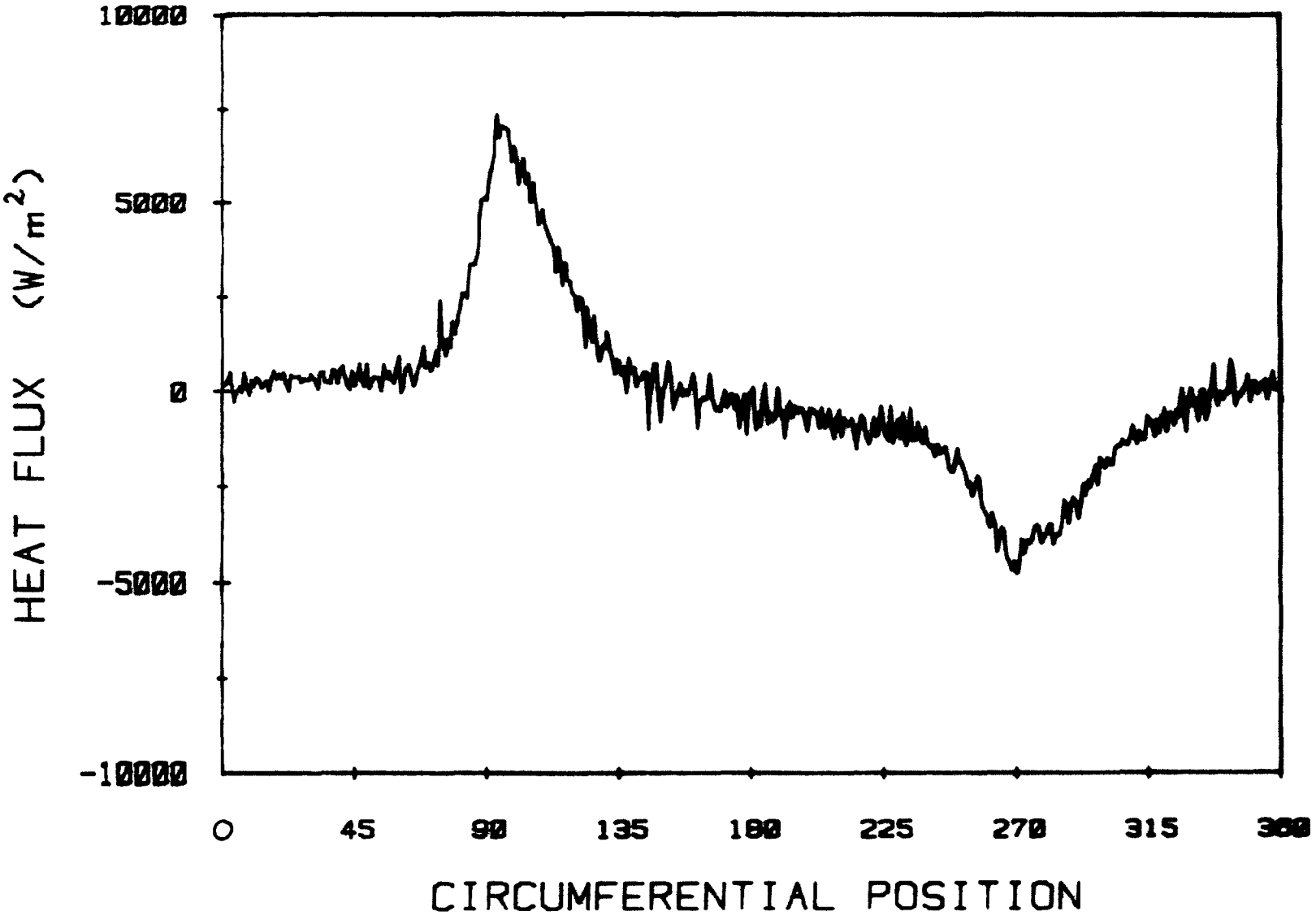

Figure A-3 Heat flux distribution averaged over 100 rotations.